UNIVERSITY OF OKLAHOMA
GRADUATE COLLEGE

ROBUST OPTICAL WIRELESS LINKS OVER TURBULENT MEDIA USING DIVERSITY SOLUTIONS

A DISSERTATION

SUBMITTED TO THE GRADUATE COLLEDGE

In partial fulfillment of the requirements for the

Degree of

DOCTOR OF PHILOSOPHY

By

HASSAN MORADI
Norman, Oklahoma
2011

ROBUST OPTICAL WIRELESS LINKS OVER TURBULENT MEDIA USING DIVERSITY SOLUTIONS

A DISSERTATION APPROVED FOR THE
SCHOOL OF ELECTRICAL AND COMPUTER ENGINEERING

BY

Dr. Hazem Refai, Chair

Dr. Curt Adams

Dr. James J. Sluss, Jr.

Dr. Thordur Runolfsson

Dr. Peter G. LoPresti

Acknowledgments

Many thanks are extended to my advisor, Dr. Hazem Refai, whose vision, support, and technical guidance throughout my work have been invaluable. I am tremendously appreciative for his support, patience, opportunity to learn and advance, and for his faith in me.

To the members of my doctoral committee—Dr. Curt Adams, Dr. James J. Sluss, Dr. Thordur Runolfsson, and Dr. Peter LoPresti—I express my gratitude for their advice and suggestions throughout the stages of my PhD degree. Additionally, I acknowledge Dr. Mohammed Atiquzzaman for his support toward the accomplishment of this work. Particular thanks are given to Dr. LoPresti and his group members at the University of Tulsa. This work has been funded by National Science Foundation (NSF).

I am grateful for the opportunity to have worked with incredibly smart, talented, and supportive researchers and students, especially Dr. Yahia Tachwali. I extend a big "thank you" to Dr. Ali Akbar Zarezadeh, Samer Rajab, Ahmad Othman, Nathanael Ngbondo, Ben Akunne, and Asaad Kaadan. Many thanks to Michelle Farabough, the editor and Sandra Arnett the assistant for our group. To members of the OU Super-Computing Center for Education and Research (OSCER) and the technical support at Samtec, Inc., who provided experimental parts free of charge, I will forever be indebted.

Most importantly, I would like to express my gratitude to my lovely wife Roja, whom without I would be an entirely different person than I am today and such success would have been impossible. Finally, for my beloved family and that of my wife, I extend my gratitude for their endless love and support. They remain a great source of friendship and inspiration, and continue to encourage excellence. This dissertation is dedicated to them.

Table of Contents

List of Tables

List of Figures

Abstract

Free-space optic (FSO) technology, i.e., optical wireless communication (OWC), is widely recognized as superior to radio frequency (RF) in many aspects. Visible and invisible optical wireless links solve first/last mile connectivity problems and provide secure, jam-free communication. FSO is license-free and delivers high-speed data rates in the order of Gigabits. Its advantages have fostered significant research efforts aimed at utilizing optical wireless communication, e.g. visible light communication (VLC), for high-speed, secure, indoor communication under the IEEE 802.15.7 standard. However, conventional optical wireless links demand precise optical alignment and suffer from atmospheric turbulence. When compared with RF, they suffer a low degree of reliability and lack robustness. Pointing errors cause optical transceiver misalignment, adversely affecting system reliability. Furthermore, atmospheric turbulence causes irradiance fluctuations and beam broadening of transmitted light. Innovative solutions to overcome limitations on the exploitation of high-speed optical wireless links are greatly needed.

Spatial diversity is known to improve RF wireless communication systems. Similar diversity approaches can be adapted for FSO systems to improve its reliability and robustness; however, careful diversity design is needed since FSO apertures typically remain unbalanced as a result of FSO system sensitivity to misalignment. Conventional diversity combining schemes require persistent aperture monitoring and repetitive switching, thus increasing FSO implementation complexities. Furthermore, current RF diversity combining schemes may not be optimized to address the issue of unbalanced FSO receiving apertures.

This dissertation investigates two efficient diversity combining schemes for multi-receiving FSO systems: *switched diversity combining* and *generalized selection combining*. Both can be exploited to reduce complexity and improve combining efficiency. Unlike maximum ratio combing, equal gain combining, and selective combining, switched diversity simplifies receiver design by avoiding unnecessary switching among receiving apertures. The most significant advantage of generalized combining is its ability to exclude apertures with low quality that could potentially affect the resultant output signal performance.

This dissertation also investigates mobile FSO by considering a multi-receiving system in which all receiving FSO apertures are circularly placed on a platform. System mobility and performance are analyzed. Performance results confirm improvements when using angular diversity and generalized selection combining.

The précis of this dissertation establishes the foundation of reliable FSO communications using efficient diversity-based solutions. Performance parameters are analyzed mathematically, and then evaluated using computer simulations. A testbed prototype is developed to facilitate the evaluation of optical wireless links via lab experiments.

1. Introduction

This chapter details the motivation behind the dissertation research presented herein. Factors such as misalignment and atmospheric turbulence that contribute the poor of optical wireless communication are addressed, and solutions are proposed. Research scope is defined, and a list of achieved objectives is provided. The chapter also includes a summary of contributions offered the FSO research community. A dissertation outline is provided at the end of the chapter.

1.1 Motivation

Free space optic (FSO) communication is cost-effective and provides high-bandwidth access. The technology has been welcomed with growing attention and has recently experienced commercial success. When compared with its radio frequency (RF) counterpart, FSO is considered far superior. Transmission data rate achieves Gigabit per second—several fold higher than current RF wireless systems. FSO links are simple to deploy and have high capacity, making them suitable for backbones in last mile applications. FSO technology offers increased security and is immune to Electromagnetic interference. Deployment is inexpensive and license-free.

FSO communication provides a possible solution for the popular Gig Ethernet network or Ethernet-Passive Optical Network (E-PON) infrastructure, particularly in areas where optical fiber use is not practical. Aligned FSO link deployment minimizes implementation complexities, e.g., first mile and last mile problems, and lessens costly developments associated with other communication methods. FSOs are favored in disaster recovery efforts where high-speed data rate for real-time streaming of video may necessary. Optical wireless systems have been found to function well in a number of environments previously typified with exposure to severe RF noise conditions, e.g., military campaigns, where RF spectrum management cannot be fully coordinated.

Secure connectivity is one of the exceptional properties of narrow optical beams. They are highly secure, difficult to detect or hack, and immune to unintentional and intentional interference, i.e., jamming. These features are crucial for developing open, lucrative applications for FSO in commercial, military, and space applications that require satellite and inter-stellar communication.

Several efforts have aimed to standardize optical wireless link utilization for high-speed applications. The IEEE Standard Association has recently developed the IEEE 802.15.7 standard [1] to facilitate visible-light communication (VLC) for short-range applications that use intensity modulating optical sources, such as light emitting diodes (LEDs) and laser diodes (LDs). This standard describes VLC (380nm to 780nm) utilization for wireless personal area networks (WPAN) and covers topics that include network topologies, addressing, collision avoidance, acknowledgement, performance quality indication, dimming support, visibility support, colored status indication, and color-stabilization. The standard defines PHY and MAC layer protocols for short-range

optical wireless communications using visible light in optically transparent media. The IEEE 802.15.7 standard delivers data rates sufficient for supporting audio and video multimedia services, while also considering visible link mobility, visible-light infrastructure compatibility, and impairments due to noise and interference from sources like ambient light.

Despite such exceptional advantages, FSO links suffer from possible vulnerabilities, including line of sight, physical obstruction, or loosing alignment due to building sway. Furthermore, FSO is susceptible to atmospheric conditions. The possibility of integrating an FSO link with an RF link as a redundant backup link has previously been explored for communication networks and resulted in a network that provides increased reliability and quality of service.

Spatial diversity strategies—categorized in single-input multiple-output (SIMO) and multiple-input multiple-output (MIMO) fashions—can alternatively assist connectivity robustness. An angular diversity scenario can aid in resolving incompatibility issues with optical wireless node movement and misalignment. Asymmetrically unbalanced transceiver apertures with intentional misalignment are installed to establish node mobility while maintaining connection. Such a design eliminates the need for a complicated traditional pointing, acquisition, and tracking (PAT) solution. FSO-based mobile nodes could potentially be used in a mobile ad hoc network (MANET).

Placing emphasis on introducing mobility to optical wireless nodes can extend the range of FSO network applications and lead to increased availability and reliability of optical wireless services—and ultimately the successful implementation of spatial diversity.

1.2 Scope

A number of spatial diversity studies that offer a variety of designs and applications are currently available for FSO turbulent channels. The scope of this dissertation includes design solutions for the practical development of diversity combining with the enhancements to processing resources and movement capabilities. While the proposed combining methods improve the processing computation loaded to the combiner, conventional combining methods are not preferred. They are unbalanced and deliver high processing load and low combining efficiency when the receivers are misaligned. The proposed combining techniques feature low processing complexity, making them suitable for unbalanced multi-receiving apertures—a desirable characteristic for high data rates of FSO communications. The communication media is considered as a turbulence-induced fading channel, namely scintillation. Nonrandom effects of the atmosphere are of less interest in this dissertation.

1.3 Objectives

A section of PHY foundation for developing fundamental diversity-based solutions in practical FSO systems, namely efficient combining schemes and a mobile FSO approach, is offered for consideration. Given this context, the objectives of this dissertation are presented in two parts:

- Efficient diversity combining schemes, including
    - The design of a pilot-assisted channel estimation mechanism for practical FSO communication over atmospheric turbulence;
    - A lab test-bed design for potential implementation and evaluation of FSO algorithms, techniques, solutions, and features;

- The utilization of temporal diversity when channel state information (CSI) is unavailable at the receiver side;
- A demonstration of the performance of available multi-receiving, spatial combining schemes under the availability of CSI from a turbulent channel, with focus on processing load and combining efficiency in high speed optical links;
- The realization of efficiently applicable combining schemes, namely switched diversity combining methods, for FSO receivers under SIMO topology, as well as a performance evaluation using mathematical and simulation analyses;
- Optimization of the available switched diversity schemes toward an innovative, more efficient scheme, namely switch-to-dominant combining (SDC).

- Mobile FSO design, including
  - The theoretical design of a multi-receiving structure based on a simple circular node configuration;
  - Mathematical, analytical, and simulation analyses of the mobile FSO under SIMO and MIMO topologies over a turbulent channel; (The achievement of bit error rate (BER) performance and processing load are of utmost importance in the analyses.)
  - The utilization of efficient diversity combining solutions for the multi-receiving node, as well as the examination of combining performance through mathematical analyses and computer simulations.

1.4 Method

This study employs a mathematical analysis, computer simulations, and limited implementation to prove improvements achieved by the proposed schemes. The processing stages of the proposed solutions are analyzed mathematically to identify performance parameters. Computer simulations using the OU Super-Computing Center resources are conducted to test the numerical performance evaluation under a variety of wireless channel conditions.

The development of the FSO testbed for channel estimation uses system-level design tools to explore optimal detection requirements for transceiver stage and to identify appropriate partitions for the field-programmable gate arrays (FPGA). The system-level design tools used in this work include: MATLAB®, System Generator for DSP by Xilinx ®, and Xilinx® Embedded Development Kit.

1.5 Research Contribution

The contributions of this work are summarized as follows:

1- Design and simulation of a practical channel estimation mechanism for an FSO transceiver over weak turbulence-induced fading channel.

2- Limited implementation of the channel estimation mechanism.

3- Design of an optimal detector under CSI unavailability through the utilization of temporal diversity.

4- Evaluation of available combining schemes under a spatial diversity setup for BER performance improvement of the optical connection.

5- Mathematical analysis of the techniques under optical fading channel conditions.

6- Proposed diversity combining schemes for further performance improvement of the optical link.
7- Mathematical characterization of the proposed techniques.
8- Introduction to the limited mobility of the optical node using angular diversity for a multi-receiving circular node structure.
9- Mathematical and simulation analyses of the mobile FSO node under a MIMO configuration.

1.6 Dissertation Organization

This dissertation is comprised of seven chapters and is summarized as follows:

Chapter 2 provides a necessary foundational background. Initially, the system model of a typical FSO system is defined. The model comprises three major parts of a point-to-point communication link: modulation formats, channel effect, and noise model. A brief, but useful, list of characteristics for each part is provided. Detailed analysis on turbulence-induced fading, which serves as the focus of this dissertation, is then presented. A number of available research studies focusing on the design and implementation of optical wireless links are briefly reviewed; these are limited to modulation techniques, optimal detection approaches, and diversity techniques.

Chapter 3 presents the optimal detection of the received FSO signal when instantaneous channel information is unavailable at the receiver. Noise and channel model/statistics, including turbulence model, are known. A practical estimation approach based on pilot-assisted symbols for noise and channel statistics is also provided. Using such pilot symbols, the chapter proposes an alternative optimal detection technique for when the channel coefficients are correlated in a time domain.

Chapter 4 explores the use of two efficient diversity schemes for a dual branch FSO system under SIMO topology. First, important factors under a diversity combining point of view are briefly reviewed, and secondly the deployed schemes, namely switch-and-stay and switch-and-examine, are designed based on available trends of switched diversity. Mathematical analysis on the performance evaluation is reported. Simulation results conclude the chapter.

In Chapter 5, a new switched diversity-based technique, i.e., switch-to-dominant combining, is proposed, and the appropriate switching strategy is described. The chapter extends the analysis to mathematical characterization and simulation to evaluate the combining efficiency delivered by the scheme under a multi-receiving SIMO topology. The analysis outlines performance boundaries in terms of the probability of error and outage.

Chapter 6 focuses on the inclusion of limited mobility to the optical node. A circular, multi-receiving MIMO structure as an angular diversity is proposed to combat the sensitivity of the line-of-sight optical beams to movement and misalignment. A MIMO link based on transmit selection combining with feedback and received generalized selection combining is employed. Theoretical and simulation discussions demonstrate node connectivity performance in terms of bit error.

The research concludes in Chapter 7, and future research is proposed.

2. Background

This chapter outlines basic concepts of optical wireless communications. System model of noise and atmosphere turbulence are presented, and related aspects and studies in literature are discussed.

2.1 Free Space Optical Technology

FSO communication is a cost-effective, high-bandwidth access technique with growing attention and recent commercial success. FSO links are simple to deploy and have high capacity, making them suitable for backbones in last mile applications. FSO technology offers high data rate (Gigabits range), increased security, and immunity to electromagnetic interference, as well as inexpensive and license-free deployment. The earliest wireless infrared communication systems [2] research conducted by IBM in Zurich focused on exploring wireless LANs covering entire office spaces using access points. This then-novel idea has led to growing interest in using optical signals in free space and has inspired related research and development [3].

Because of their desirable characteristics, FSO links are now considered an alternative to optical fibers for deployment in Metropolitan Area Networks (MANs) [4].

While FSO technology is a redundant solution to high-speed wireless, it is also point-to-point (P2P) and line-of-sight (LoS) communication that can achieve data rates comparable with fiber optics without exorbitant costs or time-consuming installation [5]. The technology is often suitable for LAN-to-LAN connections and ad hoc networks when optical fiber installation is impractical. Although RF links are more reliable and can be deployed as easily as FSO links, they are not considered for backbone networks due to low capacity and security [6]. FSO applications in disaster areas [7], [8] and for indoor communications have been theoretically and experimentally evaluated in [9], [10], [11]; however, FSO suffers major drawbacks due to LoS property of the connection link and high attenuation in fog and snow. Both adversely disrupt traffic flow through affected links. For these reasons, the deployment of FSO communication systems has been investigated for issues related to availability [12], [13]. Subsequently, the unreliability and directionality of optical links present challenges to such network operations [14].

2.2 Hybrid FSO/RF Technology

Fiber is expensive and time-consuming to deploy, creating significant drawbacks to FSO and RF links. For this reason, hybrid FSO/RF networks with reliable, high-capacity and easy to backbone deployment [6] have gained attention. In a hybrid FSO/RF system like the one shown in Figure 2-1, the FSO link serves as the primary link, and the RF link is the secondary (backup) link [15]. In the event that an FSO link becomes obscured in a hybrid FSO/RF ad hoc network, the system switches to a reliable RF to maintain communication. This scheme is referred to as *reconfiguration* [16], characterized when the delivered signal quality decreases below a preset threshold. Accordingly, switching can be accomplished by rerouting traffic via an alternate optical link, and the RF link is

then employed to maintain the traffic flow. In such hybrid networks, the immediate switching from FSO to RF leads to suboptimal utilization of the FSO network. Of note is that the FSO link switches from the RF to an FSO link after quality recovers from suboptimal conditions. The capacity of the hybrid link as the upper bound of the limiting information rate is highly dependent on channel condition. Thus, a higher capacity exhibits a more reliable transmission link.

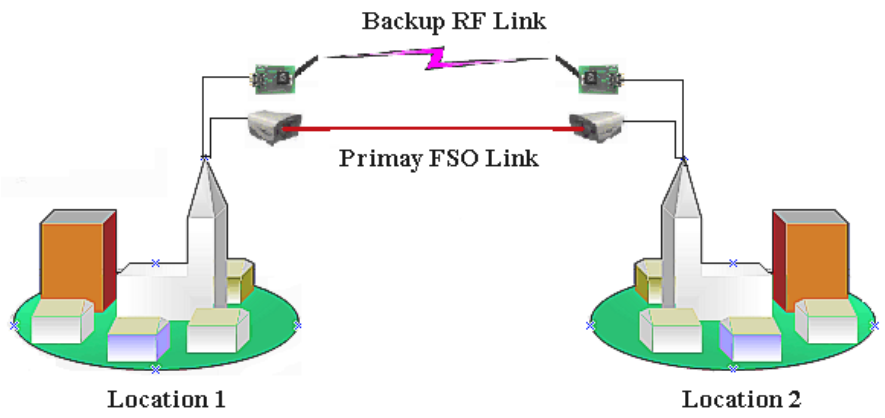

Figure 2-1: Conceptual configuration of a two-node hybrid FSO/RF network

Three approaches for utilizing a hybrid RF link in conjunction with an FSO link are available. One is based on data duplication on the RF providing data recovery. This is useful if a spatial diversity mechanism is used. The remarkable difference between radio and optical data rates makes diversity not applicable unless an adaptive rate algorithm is used on the FSO channel [17]. One may consider the case when an individual RF link yields the same transmission rate as an FSO link. In [18], a combined FSO with E-band RF link is considered so the capacity is numerically evaluated, mostly assuming nonrandom channels. In a second approach, user data is sent over a hybridized link in which FSO and RF links dynamically interact with each other to achieve a combined

transmission link. Maximum reliability and throughput for hybrid channels is achieved in terms of outage probability [19] and comes with more bandwidth utilization at the expense of increased transceiver design complexity. A third approach uses an RF link as a backup wherein user data is not transferred on the RF link while the FSO link is in active status. Thus, RF is used primarily for control signals and data transfer while FSO is unavailable [16]. Lower bandwidth and a less complicated transceiver design are utilized.

Many studies—from theoretical analyses to experimental solutions—on hybrid FSO/RF systems have been reported in literature. Gurumani [15] proposed a hybrid FSO/RF network where each node in the network of hybrid nodes is equipped with multiple transceivers and has multiple associations with other network nodes. As proof of concept, a hardware testbed was constructed using four hybrid nodes and multiple infrared (IR) transceivers to establish optical links. Dynamic path reconfiguration in the optical domain was demonstrated by blocking various node transceivers in the testbed. End-to-end delay along different FSO paths and path reconfiguration were measured. An RF link is intended as a backup network to improve reliability and assumed always available. An RF channel is used for control signals and data only in the event of a complete FSO network outage. This example serves as a relatively simple, practical research approach for establishing a hybrid FSO/RF communication. Additional general methods can be found in [20].

A research group headed by Drs. Christopher C. Davis and Stuart D. Milner at the University of Maryland [21], [22], [23] has designed and developed gimbal-mounted, hybrid FSO/RF nodes with combined apertures for a joint PAT operation. This

reconfiguration occurs physically via PAT and logically using autonomous reconfiguration algorithms and heuristics. Davis and Milner describe these hybrid nodes and their performance as hybrid network simulations that are re-configurable in a network testbed for high data-rate video transmission. Using OPNET and MATLAB, the performance of directional broadband hybrid FSO/RF networks has been analyzed using simulation and modeling techniques.

The capacity of RF links is much less than that for backbone traffic demand. As such, routing consideration remains an issue in hybrid FSO/RF networks. Limited research has investigated system routing and traffic engineering. Kashyap and Shayman [4], [6] introduced the concept of criticality index for traffic profile entries and provided optimal algorithms for use when traffic can be split over multiple paths. The aforementioned research provides a framework for modeling FSO link failures and formulating a routing problem to compute backup paths for the FSO topology traffic flow on FSO topology. Cited research suggests that algorithms are shown to have a performance gain even when either FSO topology is optimized for current traffic or if grid failure probabilities are non-uniform. Jahir *et al.* [24], [8] developed a routing protocol for ad hoc networks consisting of *hybrid* nodes using FSO and RF links, in which the FSO is the primary link and RF is backup. The routing protocol, namely Ad hoc On demand Distance Vector *hybrid* (AODVH), computes multiple "FSO-only" paths to ensure high data rate communication and uses "hybrid paths" of FSO and RF links as backups.

Hybrid channel coding designs specifically for hybrid FSO/RF have been extensively proposed. Vangala and Pishro-nik [5], [19] recommended a non-uniform and rate-compatible low density parity check (LDPC) code for hybrid FSO/RF networks. In works

similar to those by Tapse and Borah [25], hybrid codes focus on the behavior of LDPC codes in hybrid FSO/RF channels. Coded bits are randomly sent to the RF and FSO link, although the majority are transmitted through the FSO link and only a fraction by the RF link. Reliability is increased using optimized and rate-adaptive codes, resulting in higher overall system throughput. The authors believe that complexity reduction by eliminating switching between the FSO and RF channel, avoiding duplication, and providing higher security, are significant advantages of hybrid-channel coding. However, sending traffic simultaneously on both FSO and RF links initiates an amount of hardware complexities. Extensive efforts by researchers to build hybrid coding have extended coding characteristics by incorporating intelligence and learning capabilities in proposed techniques.

The capacity of a hybrid link as the upper bound of a limited information rate is highly dependent on channel condition, i.e. the higher the capacity the more reliable the transmission link. In [26], authors model the channel as a time-varying fading channel, and then address link capacity based on the *Shannon–Hartley* theorem. Goldsmith and Varaiya [27] previously evaluated the effect of fading on wireless channel capacity, and their published definitions have been used in [26] to find closed-form capacity expressions for a hybrid link. The improvement level of Shannon-based capacity is demonstrated when a lognormal optical fading channel model is applied.

2.3 FSO System Model

Like any wireless communication link, a P2P FSO connection link is affected by channel attenuation and additive noise. The received signal $r[k]$ at discrete time k can be expressed by

$$r[k] = h[k]s[k] + v[k] \quad 2\text{-}1$$

where $s[k]$ is the modulated transmitted signal; $h[k] > 0$ is the normalized time-varying and ergodic channel coefficient due to atmospheric attenuation and/or turbulence; and $v[k]$ is total additive Gaussian noise. Assuming a discrete-time sampling, the term time $[k]$ may be neglected in the analysis presented.

2.4 Modulation of Transmitted Signal

User data bits need to be modulated before they are sent to the FSO transmitter. *Intensity modulation* (IM) is the conventional modulation scheme in optical communication [28]. In IM, information is used to modulate the intensity. Various types of IM exist, the simplest of which is referred to On-Off Keying (OOK) where $s[k] \in \{0,1\}$. The OOK on-condition corresponds to symbol '1', and the off-condition corresponds to symbol '0'. At the end of a symbol period, the receiver's output is compared to a set threshold value I_D, and a decision on the transmitted symbol is made. This proves a major drawback, as finding an optimal threshold adds complexities to the receiver design. Nonetheless, OOK has been widely used in literature for designing receivers with optimal detection [29], [30], [31], [32].

A common representation of non-OOK intensity modulation encoding is Pulse Position Modulation (M-PPM), in which M user data bits are mapped, i.e. modulated, to 2^M possible cases. PPM is a popular way to bypass the need to estimate the receiver's required parameters. If the simplest case M=2 is assumed, the modulation is referred to as Binary PPM (BPPM), or so-called Manchester coding. The system uses pulse signaling where the pulse time is one half the bit interval—a shorter time interval than for the OOK system [28](Sec. 6.3). This is considered a return-to-zero (RZ) transmission format.

Theoretically, it provides comparable performance to OOK [28], [33], [34]; however, it does not require channel estimation, nor does it meet estimation error. Rather it encounters a duplication of the available bandwidth and a more complex aperture design. FSO links are a suitable example of using PPM due to the insensitivity of link performance to multipath interference. Several works have been published on the use of PPM modulation in FSO links. Letzepis *et al.* [35] used QPPM modulation when analyzing diversity gain using an optimal detection. Safari and Uysal [36] and Lee and Chan [37] applied BPPM for their diversity systems, and Bayaki *et al.* [38] evaluated various representations of PPM for the evaluation of BER in a MIMO-based combiner.

Digital carrier modulation methods in RF are also applicable in wireless optics. Binary phase shift keying (BPSK) [39], [40], [41], quadrature phase shift keying (QPSK) [42], and frequency modulation (FM or FSK) [28] are among the most common FSO communication modulation techniques. However, [43](Sec. 6.5) demonstrates that in a Gaussian FSO channel, BPSK exhibits a superior BER performance when compared to FSK. Such modulations are named Radio-over-FSO (RoFSO) in literature [44], [45]. The concept indicates to first modulate the data onto an electrical subcarrier whose frequency is analogous to symbol rate using the standard I/Q modulation formats, such as multilevel phase-shift keying (*M*-PSK) or multilevel quadrature amplitude modulation (*M*-QAM). A direct current (DC) bias is added to make the modulated signal nonnegative prior to directly modulating the light source [46].

Subcarrier Intensity Modulation (SIM) is often used for digital carrier modulation in optical transmission [39], [40], [46], [47], [48]. Note that the local carrier is applied to the received signal after optical-to-electrical conversion. SIM is used to vary the

irradiance/intensity of an optical source using a modulating subcarrier. For instance, for a single subcarrier the baseband signal of a modulating subcarrier is defined by [43](Sec. 4.5)

$$m(t) \triangleq C\big(1 + d(t)\big)\sin(\omega_{sc}t) \qquad 2\text{-}2$$

where ω_{sc} is the frequency of subcarrier; $d(t)$ is the information signal (e.g., for BPSK, $d(t) \in \{-1,1\}$); and $C < 0.5$ is the transmitter gain. In such definitions, the intensity of a basedband signal at the transmitter side is [43](Sec. 4.1)

$$I(t) \triangleq I_0(1 + \beta m(t)) \qquad 2\text{-}3$$

where I_0 is average transmitted intensity, and $\beta \leq 1$ is a fraction of intensity. Interested readers can refer to [28](Fig. 4.2) for more details.

Similarly, multiple subcarrier modulation (MSM) can be applied to provide a bandwidth efficiency by transmitting *M* parallel subcarriers at *M* separated frequencies $\omega_{sc,n}$; $n = 1, \dots, M$. Many studies [42], [39], [49] have reported the employment of MSM in wireless optical communications. Ohtsuki [42] presented the basic transceiver design of a multiple subcarrier modulation system with QPSK. Ghassemlooy *et al.* [39] completed research that looks at the analysis of multiple subcarrier intensity modulation when considering a MIMO diversity combiner.

SIM and MSM modulations are categorized as intensity modulation. A major advantage of a subcarrier technique is that various modulation methods other than BPSK can also be used [39], resulting in higher bandwidth efficiency. Another advantage is the ability to find a threshold value for optimal detection as it is fixed at the zero. This is important for a subcarrier technique, as threshold calculation complexities—those

associated with an increase of modulator design hardware complexity at the transmitter—have been eliminated. In general, the chief drawbacks of intensity modulation/direct detection (IM/DD) MSM systems are the average optical power inefficiency due to the large added DC bias, as well as distortions due to the LD and optical channel nonlinearity [44]. These factors introduce a complex situation on the linearity of the optical devices to avoid excessive distortion and maintain adequate performance.

Using multiple subcarrier modulation facilitates the feasibility of orthogonal frequency division multiplexing (OFDM)-based signals over free space optics links. OFDM has previously been implemented in optical fiber communications. In fact, a recently published book [50] details OFDM applications (including FSO) in optical communications. OFDM design outperforms traditional-based modulation schemes (i.e., OOK) with a reported receiver sensitivity improvement of 3 dB at the BER of 10^{-3}, translating to a 41% increase in FSO link distance at 50% lower bandwidth occupancy [51]. OFDM exhibit graceful BER degradation in the presence of stochastic turbulence, effectively increasing system robustness to adverse atmospheric conditions. In this way, OFDM proves an effective solution for next generation FSO systems [44] and introduces an analytical model for the transmission of OFDM-based signals over FSO links. Experimental results have been provided in literature. Cvijetic *et al.* [52] first provided experimental demonstration of 10Gb/s using OFDM over FSO links. OFDM-based FSO systems using LDPC codes have been analyzed by Djordjevic *et al.* in [51]. The work shows that for weak turbulence the coding gain improvement of LDPC coded FSO-OFDM system with 64 subcarriers over the LDPC encoded FSO OOK system is 8.47 dB for QPSK and 9.66 dB for BPSK at the BER of 10^{-5}. More details are available in [51].

2.4.1 Noise Model

In general, wireless communication channels are interfered by shot noise, usually modeled as Gaussian noise additive to the signal. Various types of undesired shot noises in optical wireless channels adversely affect the BER performance of a communication link. Shot noise can be a result of background signal noise, thermal noise, dark noise, or laser noise, which affects the performance of optical wireless communication. This sub-section briefly reviews the formulation of an FSO channel affected by additive Gaussian noise for a p-i-n photodetector. The dependency of the noise on signal power and bit rate is also characterized.

A receiver's signal-to-noise ratio is generally limited by shot noise caused by ambient light and/or by thermal noise in the electronics after photodetector identification. Two parameters—σ_1 and σ_0—are considered as standard deviations of the noise for symbols '1' and '0', respectively. Since various noise currents are not correlated, σ_1 and σ_0 can be expressed as the sum of two Gaussian additive noises, namely *shot noise* and *thermal noise* [53]. When using a p-i-n photodetector [28], [34]

$$\sigma_1 = \left(2qB_{eq}\left[RP_1 + RP_{back} + I_{dark}\right] + \sigma_n^2\right)^{1/2}$$

$$\sigma_0 = \left(2qB_{eq}\left[RP_0 + RP_{back} + I_{dark}\right] + \sigma_n^2\right)^{1/2} \qquad 2\text{-}4$$

where P_1 and P_0 are the received powers for symbols '1' and '0', respectively. Also, I_1 and I_0 are the means of total generated currents, defined as

$$I_1 = RP_1 + RP_{back} + I_{dark}$$

$$I_0 = RP_0 + RP_{back} + I_{dark} \qquad 2\text{-}5$$

Equations (2-4) and (2-5) imply a signal-dependent Gaussian noise model. Note that if P_0=0 then P_1=2P_t, where P_t is the average optical power as in the equations above; q is electron charge constant (C); B_{eq} is noise equivalent bandwidth (NEBW) (Hz); R is the receiver's responsivity (A/W); P_1 and P_0 are in (W); P_{back} is background power received by the receiver (W); I_{dark} is dark noise current (A); and σ_n is Gaussian noise current standard deviation due to thermal noise (A). Assuming an OOK modulation, $P_0 \le P_1$, thus, $I_0 \le I_D \le I_1$. The average electrical signal to noise ratio (SNR) of an FSO link is defined by

$$\bar{\gamma} \triangleq \frac{4R^2 P_t^2}{(\sigma_1 + \sigma_0)^2} \qquad \text{2-6}$$

Independent of the optical signal, dark current noise results from the current that continues to flow in the photodiode when there is no incident light. Also, σ_n as the standard deviation of the Gaussian noise current due to thermal noise can be expressed as [53]

$$\sigma_n^2 = \frac{4kTF_n B_{eq}}{R_L} \qquad \text{2-7}$$

where k is Boltzmann's constant (J/°K); T is absolute thermal temperature (°K); F_n is detector excess noise factor; and R_L is transimpedance or load equivalent resistance of the receiver that adds thermal noise to the signal (Ω). F_n, or the detector excess noise factor (also called amplifier noise equivalent factor) is an indication of the randomness photomultiplication due to excited electrons during photodetection [28]. Also, laser noise —Relative Intensity Noise (RIN) — may affect the signal received by the photodtector,

which is dependent on the detector parameters, e.g. responsivity, and equivalent bandwidth. The laser noise (or timing jitter noise)—the time deviation between the expected occurrence of a signal edge and the time the edge actually occurs (phase variation)—can be described by a Gaussian probability distribution function (PDF). It is important to note that responsivity may be given as the optical-to-electrical conversion coefficient in ampere/watt. This can be theoretically determined by $R = \eta q / hv = \eta \lambda_0 / 1.24$, where η is the detector efficiency (or quantum efficiency) formally defined as [43]:

$$\eta = \frac{Detected\ field\ power}{Incident\ field\ power} \qquad 2\text{-}8$$

where hf is photon energy in watts; h is Planck's constant; f is the impinging field frequency; and λ_0 is the light wavelength in micron. Table 2-1 lists sample values of noise-related parameters in FSO channels.

Table 2-1: Sample values related to noise statistics

Parameter	Symbol	Value
Electronic charge	q	1.6×10^{-19} C
Boltzmann Constant	k	1.38×10^{-23} J/°K
Responsivity	R	0.7 A/W
Temperature	T	300°K
Excess noise factor	F_n	2
Dark current	I_{dark}	2 nA
Background optical power	P_{back}	80 nW
Transimpedance (load) resistance	R_L	50 kΩ

Equations (2-4) and (2-7) represent the dependency of noise variances on NEBW. When using the non-return-to-zero (NRZ) scheme, the NEBW of an OOK signal is limited by the available bandwidth of the transmitted signal, found using $B_{eq} = bit\ rate / 2$ [54]. Evaluating numerically, Figure 2-2 demonstrates the effect of bit rate on FSO SNR

performance. SNR can be improved in 5dB of magnitude when the data rate decreases from 40Mbps to 5Mbps, at P_t =-50dBm.

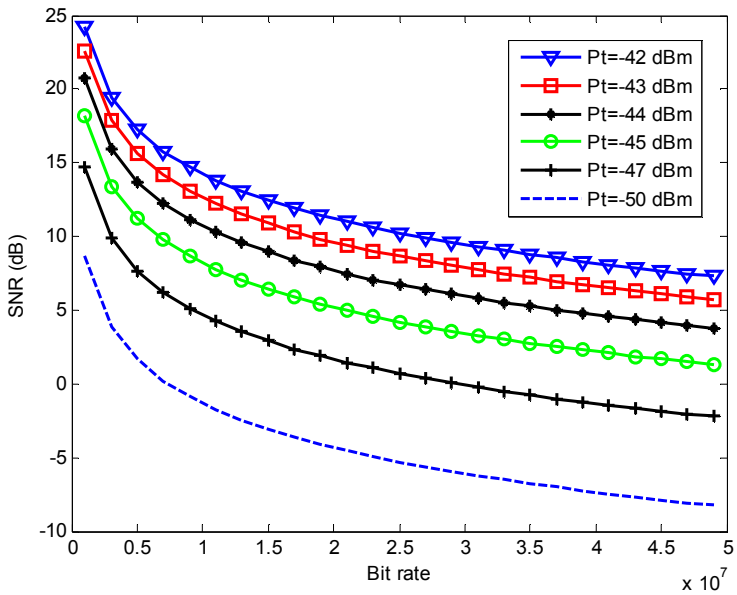

Figure 2-2: The effect of bit rate on the SNR of OOK FSO signal

The dependency of noise variance on the transmit power can be investigated using Eq. (2-4). The equation indicates that the parameters σ_1 and σ_0 are mathematically identical in OOK modulation:

$$\sigma_1 \approx \sigma_0 \qquad 2\text{-}9$$

The result is numerically plotted in Figure 2-3 using the information given in Table 2-1. The fluctuation of noise variance versus changes in P_t based on the information in Table 2-1 is negligible, particularly for low values of received power. The biggest difference is 1dBm for a relatively high received power of -35dBm. This can be subsequently withdrawn.

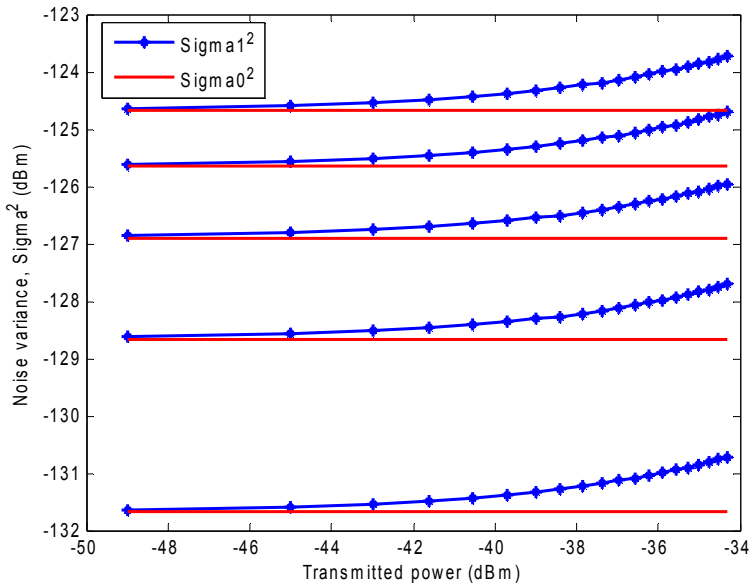

Figure 2-3: Effect of transmit power on σ_1^2 for a p-i-n photodetector with IM/DD in Gaussian channel with different values of bit rate using given information in Table 2-1

2.4.2 Channel Model

FSO communication is a possible solution for network traffic connectivity; however, misalignment and atmospheric conditions, e.g., diffraction, scattering, absorption, and fading turbulence, highly affect network availability performance. These same conditions can be modeled in the analysis even though optical links become totally obscured by external objects. In such case a channel state model can be defined to represent the influence of atmosphere, as included in Eq. (2-1).

Channel state is considered a product of two random factors, namely $h = h_a\, h_b$ where h_a is the attenuation due to atmospheric turbulence, and h_b is the attenuation due to geometric spread and pointing errors [55]. Among the atmospheric conditions, diffraction, scattering, and absorption are categorized as deterministic effects of degradation on the transmitted signal. The chief effect of absorption and scattering is

laser beam attenuation caused by reducing free space transmittance. The expanding profile of a laser beam in free space is explained by diffraction theory. Actually, the propagation of light can be visualized by considering every point on the wavefront as a point source for a secondary radial wave. The subsequent propagation is built as the contribution of all new wavefronts when added together. Various analytical models can be used, including the Fraunhofer diffraction equation for the far field and the Fresnel Diffraction equation for the near field [56].

Absorption occurs when photons are absorbed by gaseous molecules where they are converted into kinetic energy. The wavelength-dependent nature of absorption gives rise to atmospheric windows in which FSO transmission is possible. Likewise, scattering is a wavelength-dependent phenomenon occurring in the atmosphere—either a redirection or redistribution of light leading to a significant reduction in the intensity of light at the receiver of an FSO communications link. Two types of scattering are prevalent in FSO communications, namely Rayleigh and Mie. Rayleigh scattering occurs due to particles, such as air molecules and haze, which are small compared to the wavelength of the incident light [57].

Atmospheric turbulence causes irradiance fluctuations and beam broadening of the transmitted light. Despite scattering, absorption, and diffraction, turbulence is a random property of propagation medium. Turbulence is usually characterized as fading in statistical analysis. As such, it does not initiate from the multipath effect of propagation; rather it comes from small random variation in the refractive index heterogeneousity of air. Links may experience fading even in clear sky conditions. The importance of

atmosphere turbulence as it relates to the work presented herein warrants the description of corresponding properties of fading for optical wireless communications.

2.4.3 Misalignment and Mobile FSO

Misalignment is a major cause for FSO performance degradation. Additionally, an appropriate pointing task is further complicated by pointing system vibration attributable to tracking noise and mechanical impacts. In such cases, a PAT system may be conventionally designed to address the pointing task against misalignment problem. Several studies have mathematically modeled the misalignment and pointing task onto FSO transceiver aperture design for both ground and satellite FSO transmission systems. Arnon *et al.* [58] derive mathematical performance models for digital communication satellite networks as a function of system parameters, number of satellites, and vibration amplitude. The optical intersatellite network model under consideration includes a transmitter satellite, regenerative satellites, and a receiver satellite network. Pointing system vibration effects on the performance of optical communication satellite networks have been examined. Extensive mathematical analyses have been conducted, as well, when the bit error probability and the azimuth pointing-error angle are statistically related.

PAT tool design, feasibility, and implementation of optical links in system alignment have been extensively studied in literature. As aforementioned, a research group headed by Davis and Milner [21] has practically designed and developed gimbal-mounted for PAT operation. The prototype for an exclusive real-time PAT system capable of controlling multiple transceivers with a single sensor detecting candidate links and reducing pointing error into the milliradian range is briefly described [59]. In it the use of

GPS to facilitate necessary alignment is under consideration. In [60], a pointing technique utilizes Real-Time Kinematic GPS coordinates, local angular sensors, and a reference baseline, to retrieve accurate navigation information (e.g., roll, pitch, yaw) of the mobile or static platform carrying an optical transceiver.

The work in [61] introduces an experimental study on the design of an automatic alignment system that maintains an LoS connection for any FSO transceiver system. A complete transceiver system includes a position-sensing detector (PSD) to receive the signal; a laser to transmit the signal; a gimbal to move the transceiver to maintain alignment; and a computer to coordinate the necessary movements during motion. Also, the system demonstrated in [62] examines the capability to add mobility to FSO technology with high precision at considerable speeds.

Optical communications can be employed in MANET networks [63]. The use of PAT becomes more critical when an optical mobile platform (e.g., ad hoc network) is under development. While the vehicle carrying the optical instrumentation is in motion, a PAT system is required to compensate for vibrations applied to the optical platform through the proper application of advanced control laws. In a work by Sofka *et al.* [64], *a feedforward vibration rejection* control system interacting with an optical tracking system is presented to successfully perform the PAT task. By employing a Kalman filter and fusing the data collected from an inertial measurement unit consisting of a 3-axis accelerometer, it was found that a 3-axis magnetic sensor and a 3-axis gyroscope provided experimental results. Among others, *cone tracking* can be an attractive method to optimize transmit beam pointing in an FSO communication system [65]. Using this scheme, the transmit beam is scanned in a circle at high speed (a minimum of a few

hundred Hz), and then the phase difference between the scan and power modulation detected on the receiver is measured. Using this method, receiver position information is provided, thus correcting transmit beam pointing accordingly. A theoretical mobile structure of a multi-element optical node design is proposed in [66], [67], [68]. It uses spherical surfaces covered with transmitter and receiver modules while maintaining optical links—even when nodes are in relative motion. Work reported in [62], [69], and [70] is part of an ongoing investigation on mobile FSO networks, including the design of efficient protocols that allow mobile sensor nodes to function as a mesh network and permit information exchange among nodes directly and possibly through an intermediate node.

To slightly improve the FSO node mobility capability and maximize both misalignment tolerance and optical power collected, a novel approach to experimental design and measurement using a lens array coupled to an array of large-core fibers has been provided by Spaunhorst *et al.* [71]. At transmitter side, a control algorithm by Zhou *et al.* [72] investigates various FSO transmitter designs for mobile networks. Similarly, fiber bundles are utilized so that the beam deflection properties of a lens can be exploited to affect beam steering.

2.5 Atmosphere Turbulence

Long-distance outdoor FSO links are highly vulnerable to degrading effects of atmospheric turbulence (fading) that severely impair link performance. Atmospheric turbulence results from variations in the refractive index caused by inhomogeneties in temperature and changes in pressure. This negatively influences received signal intensity, resulting in a BER performance. Like any wireless communication link, the FSO channel

faces signal fading due to propagation in free space. Fading is a result of atmosphere induced turbulence, which is different than visibility considerations due to fog and Mie scattering signal attenuation previously investigated in [12], [57] and [73].

2.5.1 Physics of Turbulence

The model for turbulent flow physics in a fluid is based on dissipation of kinetic energy of eddies and viscosity of the fluid. Kolmogorov [74] first studied this phenomenon in 1941 and found that turbulent flow in atmosphere comes from temperature, the rapid variation of pressure, and various sizes of eddies (scale length). The smallest ℓ_0 and the largest L_0 are defined as the inner and outer scales of turbulence, respectively. ℓ_0 is typically on the order of few millimeters, and L_0 ranges from tens to hundreds of meters in diameter [75]. Mathematical modeling expressions for these two parameters can be found in [75] and [76]. Turbulence energy from large-scale structures cascades to smaller scales until it is converted to heat as a result of viscous dissipation. This time- and space-dependent, large-scale phenomenon causes a small variation in the refractive index of air. The light beam suffers deflection, which is different from atmospheric absorption and light scattering, i.e., *scintillation*, due to the random fluctuation in the air temperature.

The mathematical model for expressing refractive index can be found in literature, e.g., [76] and [77]. For an optical beam in the air, the fluctuation in the refractive index $n(r,t)$ changes slightly with time and place. The single most important parameter in turbulence analysis is the *refractive index structure coefficient*, C_n—a measure of fluctuation of the refractive index that determines turbulence strength based on the difference between points separated by a scalar distance $d = |r_1 - r_2|$. Physically,

fluctuation in the refractive index structure coefficient can be expressed only in terms of fluctuation in temperature, while fluctuation due to pressure can be neglected. Using Kolmogorov theory for $\ell_0 \leq d \leq L_0$, C_n is a function of temperature change

$$C_n \propto \Delta T \qquad 2\text{-}10$$

C_n (in $m^{-1/3}$) is typically in the order of 10^{-8} for strong turbulence and 10^{-6} for weak turbulence and decreases with altitude change in pressure and temperature. The higher the value for C_n, the stronger the channel turbulence. A fundamental result from Kolmogorov analysis, this phenomenon is addressed by [75], [76] and [77]:

$$D_n(z,d) = C_n^2(z)d^{2/3} \qquad \ell_0 \ll d \ll L_0 \qquad 2\text{-}11$$

For equations, z dimension as the value of altitude is usually considered in analysis. No unique mathematical description of $C_n(z)$ versus altitude z is available; however, Hufnagle-Valleyl [76](Eq. (1.5)) and [77](Eq. (2.39)) provide commonly used models. A simple model for refractive index structure coefficient, $C_n(z)$ in terms of altitude [78], [79] is expressed as

$$C_n^2(z) = K_0 z^{-1/3} \exp\left(\frac{-z}{z_0}\right) \qquad 2\text{-}12$$

where K_0 is the parameter describing the strength of the turbulence and z_0 is the effective height of the turbulent atmosphere. In general, C_n also changes along the propagation path. However, uniform versus the path is usually assumed for ground-to-ground communication in the literature because of homogeneity assumption.

Channel fading due to atmosphere turbulence results from the scintillation effect of the transmission media. Thus, *scintillation index,* S.I., and *Rytov parameter*, σ_χ, are

usually defined to represent the effect of turbulence [80]. A relation between turbulence strength and the refractive index structure coefficient, C_n, is always present. For the Rytov parameter assuming plane wave, the relation is given by [43] and [79]

$$\sigma_\chi^2 = 0.56\left(\frac{2\pi}{\lambda}\right)^{7/6}\int_0^L C_n^2(x)(L-x)^{5/6}dx \quad \text{(for plane wave)} \qquad 2\text{-}13$$

and for spherical wave,

$$\sigma_\chi^2 = 0.56\left(\frac{2\pi}{\lambda}\right)^{7/6}\int_0^L C_n^2(x)\left(\frac{x}{L}\right)^{5/6}(L-x)^{5/6}dx \quad \text{(for spherical wave)} \qquad 2\text{-}14$$

In the equations above, λ is the light wavelength, and L is the propagation path. This equation is important, as it also relates turbulence to wavelength. A lower wavelength provides stronger fading and vice versa. It can be assumed that C_n is constant through the path, which gives the closed-form expression [81]

$$\sigma_\chi^2 = 0.124\left(\frac{2\pi}{\lambda}\right)^{7/6} C_n^2\, L^{11/6} \qquad 2\text{-}15$$

By assuming a wavelength of 529 nm and propagation distances of a kilometer, σ_χ are shown to vary from 10^{-2} to 1 for different values of C_n^2 [79]. Moreover, the fading strength through σ_χ^2 is 3.5 times improved when using a wavelength of 1550nm instead of 529nm.

2.5.2 Fading Distribution Model

In wireless RF communications, fading usually denotes the multipath effect of the propagation medium. Fading can also be present in optical wireless communication due to turbulence, which is different than multipath in RF domain. Refractive index fluctuation causes scintillation from temperature variation, pressure, and eddies velocity in the atmosphere. This behavior is modeled as a random atmospheric reaction to

transmitted light. Fluctuation includes both log-amplitude and phase fluctuation. However, when propagation distance is long, log-amplitude fluctuations become significant [79]. Consider the propagation of light through a large number of atmospheric elements, each causing an independent, identically distributed phase delay and scattering. By the Central Limit Theorem, the marginal distribution of the log-amplitude is Gaussian [79]:

$$f_\chi(\chi) = \frac{1}{\sqrt{2\pi}\sigma_\chi} \exp\left(-\frac{(\chi-\mu_\chi)^2}{2\sigma_\chi^2}\right) \qquad 2\text{-}16$$

where χ is called log-amplitude fluctuation of the wave, i.e., an identically distributed normal random variable with mean μ_x and standard deviation σ_x. The channel coefficient in Eq. (2-1), which models the channel between the transmit aperture and the receive aperture, is given by

$$h = \frac{I}{I_m} = e^{2X} \qquad 2\text{-}17$$

where I_m and I are the signal light intensities at the transmitter (without turbulence) and receiver (with turbulence), respectively. In scintillation fading, the average power loss due to atmospheric fading normalized is considered such that fading does not, on average, attenuate or amplify optical power. It is explicitly chosen that

$$\mu_I = E[h] = 1 \qquad 2\text{-}18$$

leads to $\mu_x = -\sigma_x^2$ [82], [83]. Finally, the marginal distribution of channel coefficient has a PDF of the form

$$f_I(h) = \frac{1}{\sqrt{8\pi}h\sigma_\chi} \exp\left(-\frac{(\ln(h)+2\sigma_\chi^2)^2}{8\sigma_\chi^2}\right) \qquad 2\text{-}19$$

where $h \geq 0$ from (2-17), and σ_x is defined as $\sigma_x = \sqrt{\ln(S.I.+1)}/2$. This expression represents a *lognormal distribution* for h and is the dominant fading model for weak turbulence regime of free space links. Additional distribution models for atmosphere turbulence can be found in literature. Gamma-Gamma [13], [31], [38], [44], [84], [85] and K-Distribution [32], [40] [55], [86], [87], and [88] are among the valid models for every turbulence and strong turbulence regimes, respectively.

The instantaneous electrical SNR of an FSO link is defined by

$$\gamma \triangleq \frac{4h^2 R^2 P_t^2}{(\sigma_1 + \sigma_0)^2} \qquad \text{2-20}$$

For simplicity, it can be assumed that $2P_t R = 1$ in the analyses. The distribution probability of γ for a lognormal distribution then yields

$$f_\gamma(\gamma) = \frac{1}{\sqrt{32\pi}\gamma\sigma_\chi} exp\left(-\frac{\left(\ln(\gamma/\overline{\gamma})+4\sigma_\chi^2\right)^2}{32\sigma_\chi^2}\right) \qquad \text{2-21}$$

2.5.3 Coherence Time and Coherence Length

In practical models of turbulence, channel fading coefficients resulting from fluctuation of light intensity are temporally and spatially correlated for different samples. Both have been previously proposed and modeled in literature.

Time dependency is initiated due to the fact that the data-sampling rate is much higher than the time-variant channel fluctuation. The dependency level depends on channel coherence time, τ_c. Fading coefficients are more dependent for longer channel coherence times. In FSO communication, the fading process has a coherence time in the

order of milliseconds, which is slow compared to typical symbol rates for FSO systems. A value of $T_b/\tau_c \leq 0.001$ is applicable in FSO application simulations.

Coherence time τ_c is assumed long when compared to bit interval, assuming fading coefficients are constant for thousands of symbol durations. This condition allows the receiver to effectively estimate coefficients as CSI estimation. Additionally, the temporal correlativeness may help performance of an optimal receiver by taking advantage of a correlation between time samples [83] and [89]. This type of receiver will be briefly introduced in the following section.

Without loss of generality, the covariance of any two individual symbols transmitted at time samples n_1 and n_2 through the channel having log-amplitude PDFs can be formulated as coefficient between processes $h[n_1]$ and $h[n_2]$, also defined as

$$\rho_{n_1,n_2} = \frac{E[(h[n_1]-\mu_h)(h[n_2]-\mu_h)]}{\sigma_h^2} = \frac{C_{n_1,n_2}}{\sigma_h^2} \qquad 2\text{-}22$$

where σ_h^2 and μ_h are the variance and mean of channel gain (coefficient), respectively, and C_{n_1,n_2} is the covariance coefficient. Such covariance coefficient of any two individual symbols transmitted at time samples n_1 and n_2 through a channel with log-amplitude PDFs can be formulated as [89], [90]

$$C_{n_1,n_2} = \sigma_x^2 \exp\left[-\left(\frac{T_{n_1,n_2}}{\tau_c}\right)^{5/3}\right] \qquad 2\text{-}23$$

where σ_x^2 is the variance of log-amplitude, and T_{n_1,n_2} is the time difference between the symbols $T_{n_1,n_2} = T_b|n_1 - n_2|$, where T_b is the bit interval. Consequently, C_{n_1,n_2} is not dependent on time but rather on time interval, and $C_{n_1,n_2} = C_{n_2,n_1}$. The calculation is

nearly zero for $T_{n_1,n_2}/\tau_c \geq 3$, which indicates channel coefficients are completely independent. The coherence time, also known as correlation time, can then be considered as the root for equation $C_{n_1,n_2}(\tau)\big|_{\tau=\tau_c} = e^{-1}$.

Coherence length (or correlation length) proves another important factor when discussing the correlation between spatial samples, especially when investigating spatial diversity for FSO systems. Extensive and valuable analyses are provided in [75], [76](Sec. 6.4) regarding the characterizing mathematical model for the coherence length of various wavefront shapes, including plane, spherical, and Gaussian waves.

Channel coefficients are basically correlated in space domain due to atmospheric eddies movement. Temporal correlativeness may affect optimal detection performance even when investigating a single-input single-output (SISO) system. Special correlativeness, on the other hand, requires consideration when a spatial-based diversity system proving superior detection performance is used. The important parameter coherence length, d_0, in particular, represents the time-varying fading channel variation in the space domain and is analogous to the coherence time that emerges from the same physics theory. These may be formulated by Taylor Hypothesis of frozen turbulence as $\tau_c = d_0/u_\perp$ [79], where $u_\perp$ is the perpendicular component of the wind velocity vector to the propagation direction. Using an alternate perspective [79], temporal correlation from varying bit samples in a SISO regime can be modeled as a virtual SIMO spatial correlation by $d_{ij} = |i-j|T_b u_\perp$.

2.5.4 Detection of FSO Signal

As discussed earlier, user information is transmitted as an intensity-modulated signal through the atmosphere. At the receiver side, a noncoherent detection process is one in

which the detector directly converts the received signal power to an electric signal. For this reason, detection is sometimes referred to as direct detection, and modulation/detection process is so called IM/DD.

Using a different approach, coherent detection is characterized when a local light is projected with a received signal onto the photodetector and then aligned with a mirror and lens [28]. In this way, optical to electric conversion is accomplished for the combined filed and local signal. Additional details will follow in later subsections.

Optimal detection is an important concept, as it denotes criterion for equally likely transmitted bits '0' and '1' where error probabilities are both identical. Of note is that if CSI is not available, more than one optimal detection method may be available for detecting a specific signal. In this case, varying BER performances are possible, although both are referred to as optimal detection. All “detection” notations in this dissertation indicate optimal detection. Consequently, numerous optimal detection schemes are available for a given signal. The following section provides a review of the most popular detection techniques toward optimal detection of FSO signals.

2.5.5 Noncoherent Detection

Noncoherent detection is first explained in terms of on-off keying signal detection. For OOK with IM/DD, receiver output is compared to a noise-dependent threshold value I_D at the end of a symbol (bit) period. Subsequently, a decision regarding transmitted symbol is made. For antipodal signal sets, the decision threshold is always zero; therefore, an accurate setting is uncomplicated. However, for OOK modulation, the decision threshold related to noise statistics must often be set dynamically.

2.5.5.1 Detection with no Turbulence

In this subsection, the effect of channel turbulence fading is neglected. Thus, for a non-fading channel with Gaussian additive noise, the optimum decision metric for the received current i_p may be expressed as [28] and [34]

$$i_p \underset{0}{\overset{1}{\gtrless}} \frac{\sigma_0 I_1 + \sigma_1 I_0}{\sigma_0 + \sigma_1} \qquad 2\text{-}24$$

and by assuming $\sigma_1 \approx \sigma_0$ from Eq. (2-9), it can be seen that the detection metric converts to $i_p \underset{0}{\overset{1}{\gtrless}} 0.5$. A recently published work [34] outlines a simple pilot-aided method as a multi slot averaging (MSA) estimation technique to approximate the values of parameters required at the noncoherent detector.

2.5.5.2 Detection with Perfect CSI

Channel State Information (CSI) indicates information about the instantaneous knowledge of the channel coefficient h at the receiver side. The availability of CSI makes the design of the optimal detector—even for MIMO systems—quite simple. Assuming a normalized received power for a working receiver based on optimal detection, threshold value using a Maximum Likelihood (ML) metric is found by

$$I_{D,\,With\text{-}CSI}[k] = I_v + \frac{h[k]}{2} \qquad 2\text{-}25$$

where $h[k]$ is the CSI of the channel at discrete time k. Accordingly, the detection metric of any received signal $r_n[k]$ is expressed as $r_n[k] \underset{0}{\overset{1}{\gtrless}} I_{D,\mathrm{With}-CSI}[k]$.

2.5.5.3 Detection without CSI Availability

The unavailability of CSI causes increased complexities in the combiner design. Additionally, when compared to detection using perfect CSI, the unavailability of CSI contributes to BER performance loss. Assuming basic conditional probabilities and neglecting sampling time k for the sake of simplicity in notation, ML decision criteria is determined as

$$\Lambda(r_n) = \frac{p(r_n|1)}{p(r_n|0)} \underset{0}{\overset{1}{\gtrless}} 1 \qquad 2\text{-}26$$

where r_n is the instantaneously received signal of the selected branch. In order to develop a symbol-by-symbol (S-by-S) detection [79] in this case, the conditional probabilities are

$$p(r_n|0) = \frac{1}{\sqrt{2\pi}\sigma_v} \exp\left(-\frac{(r_n - I_0)^2}{2\sigma_v^2}\right) \qquad 2\text{-}27$$

where it is assumed $\sigma_1 = \sigma_0 = \sigma_v$. Similarly for the symbol '1'

$$p(r_n|1) = \frac{1}{\sqrt{2\pi}\sigma_v} \int_0^\infty f_\gamma(\gamma) \exp\left(-\frac{(r_n - I_0 - 2\sigma_v\sqrt{\gamma})^2}{2\sigma_v^2}\right) d\gamma \qquad 2\text{-}28$$

where $f_\gamma(\gamma)$ is the PDF of the received electrical SNR.

Symbol-by-symbol (S-by-S) detection is the most basic optimal detection scheme when CSI is unavailable. It is categorized as the conventional method for noncoherent detection [29]. However, in terms of performance loss, the method introduces the least efficient technique. Subsequently, extensive studies have been conducted to address new optimal detection schemes with performance improvement when compared to S-by-S. This subsection offers a brief review of popular schemes addressing CSI unavailability.

One possible scheme is *multiple–symbol detection* (MSD) [29], [30] in which block–wise decisions are made using an observation window of several bit intervals. A decision is made based on an N-symbol block–wise basis wherein the noncoherent receiver utilizes more sample data to implicitly account for unknown instantaneous fading. This method has been found to partially recover performance loss associated with S-by-S detection. Consequently, all symbols within a given block are detected simultaneously. The N–dimensional PDF of the block is required to build the MSD metric associated with noncoherent maximum likelihood block detection (BD). In this case, an exhaustive search with sequential computations of size 2^N is needed to complete the detection process. A larger value of the observation window N yields a receiver with a significantly superior BER performance. As analytically demonstrated in [29], when N increases, the performance of MSD approaches results with CSI detection. However, a wide observation window causes difficulties in practice, as computational load is logarithmically dependent on N. With a goal of reducing the computational complexity of MSD, Riediger *et al.* [29] developed a fast decoding algorithm for MSD to significantly reduce the size of the search set for a large N.

Decision–feedback detection (DFD) [91] is an alternate optimal noncoherent detection that potentially exhibits BER performance improvement when compared to S-by-S. Similar to MSD, the method is based on an observation window of length N [91]. The DFD receiver makes a decision on the N-th symbol assuming previous N-1 decisions are correct. A maximum likelihood function of the binary DFD rule is defined for detection of N-th received symbol. Thus, the DFD receiver has an overall complexity

independent of N, corresponding to a significant reduction relative to the complexity of a block detection search.

The correlativeness between channel coefficients may help detect optical signal improvement. In this case, information from a partially correlated channel aids optimal detection by finding a more accurate ML. The new likelihood function takes advantage of the correlation between a received symbol and a known received pilot symbol. A previously published work by Zhu and Kahn [89] suggests that when channel coefficients at variable times are temporally correlated, a pilot symbol-assisted modulation (PSAM)-based method, rather than symbol-by-symbol method, optimizes the likelihood function, thus improving the performance in terms of bit error rate. The mathematical analysis and simulation results offered in [83] are provided in the following chapter.

The receiver design for a high-speed FSO signal is necessarily highly complex when channel state information is not available. The S-by-S detector requires integral computations for ML function for each received bit, causing a receiver design that is difficult to implement. In fact, a numerical calculation of integral equations, i.e., likelihood function $\Lambda(i_d)$ for any individual received symbol (bit) i_d, is required. Hence, detection is based on metric $\Lambda(i_d) \underset{0}{\overset{1}{\gtrless}} 1$. This method imposes excessive load at the receiver, making currently proposed techniques for most applications difficult to implement. Because the method appears uncomplicated, claims of achieving BER performance improvements have been made. In [83], the authors detail a method to alter the detection scheme by optimally calculating a threshold value, I_D, applied to a given

period. The detection rule is thus changed to $i_d \underset{0}{\overset{1}{\gtrless}} I_D$, and, quite simply, I_D is optimally computed by numerically solving an integral equation; it remains unchanged during an observation interval. In practice, I_D is affected only by received signal strength, noise, and fading statistics, which are not dependent on time for stationary channels. A lookup table accessible by the receiver can facilitate greater receiver design simplicity. The computational load, then, of numerical computations for any individually received symbol at the receiver is avoided. Authors in [83] and [91] suggest using this technique to efficiently improve the performance of detector by reducing computational load. Details of such threshold-based detection are extensively discussed in the next chapter.

2.5.6 Coherent Detection

With coherent detection, user information can be sent via amplitude, frequency, and signal phase, in multiplexing techniques (SCM, OFDM, CDMA, ...) in particular. A local optical carrier is needed for signal demodulation before conversion from optical-to-electrical. A heterodyne SNR is of interest when compared to the corresponding result for noncoherent detection, as it is likewise more efficient in terms of bandwidth use [28]. When comparing SNR to the noncoherent detection receiver, the SNR for the heterodyne case is 3dB higher [92]. However, a more complex design with electronic or optical synchronization parts is required. Strict polarization control of an optical local oscillator in an optical source using coherent detection in FSO communication also proves a challenge. Noncoherent detection is often applied to simplify receiver implementation complexities. This is more applicable when data is not sent in the phase of signal frequency.

Two types of coherent detection, namely heterodyne and homodyne, are inherent in optical receivers. A coherent optical receiver includes a polarization beam splitter for dividing an optical signal into an optical signal with horizontal polarization and an optical signal with vertical polarization. Optical couplers combine two optical signals of two polarized components with two optical local signals. Signals are then nearly matched therewith in both polarization and in a state with each other. The photodiode current output is a signal with IF frequency $\omega_{IF} = \omega_s - \omega_{Lo}$, where ω_s is the frequency of the received signal, and ω_{Lo} is the frequency of the local oscillator. ω_{IF} has a value of approximately 0.1–5 Grad/s for heterodyne detection. Given that IF maintains $\omega_{IF} = 0$, IF will have a homodyne receiver. Polarization and synchronization procedures in coherent homodyne detectors are therefore more complicated than heterodyne. That is, the coherent receiver will need half the power that a noncoherent receiver needs to achieve the same SNR performance. Also, the SNR of the homodyne is four times as large as that of the noncoherent receiver [92]. Thus, the SNR of a homodyne receiver is twice that of one for heterodyne and four times more sensitive than a noncoherent detector.

2.6 Diversity for FSO

The use of diversity is merely a promising solution for improving FSO communication performance experiencing background radiation, thermal noise, fading, and attenuation caused by atmospheric conditions. By using multiple apertures at the transmitter and receiver and then communicating at different frequencies and/or paths (spaces), the inherent redundancy of diversity has the potential to significantly enhance performance. To model the diversity, the cumulative probability of received signal

distribution is calculated for *M*-branch through combining diversity receivers by the mean of both space and time diversities.

Time diversity in free space communications can be developed by employing channel coding and interleaving. By considering burst-mode data transmission with a large data frame length compared to a large channel coherence time, time diversity can be exploited [93].

2.6.1 Theoretical Studies on Diversity

In space diversity the signal is transferred over several propagation paths. The use of space diversity in FSO systems was first proposed in [94], and several publications have focused on the same. Single/Multiple-Input Single/Multiple Output (SISO, SIMO, MISO, and MIMO) systems are developed from spatial diversity techniques. Tsiftsis *et al.* [32] have discussed diversity deployment of the transmitter and receiver and investigated bit error probability of a MIMO-based spatial diversity system that uses equal gain combining (EGC), optimal combining (OC, or Maximum Ratio Combining (MRC)), and selection combining (SC) in a *K*-distribution turbulence model. Results have been numerically compared to SISO, SIMO and MISO systems. Navidpour *et al*. [31] have mathematically studied BER performance of MIMO FSO links for both independent and correlated log-normal atmospheric turbulence channels.

Performance analysis of outage probability and diversity gain as an adapted performance parameter, so-called asymptotical relative diversity order (ARDO), is briefly evaluated in [36]. The system is assumed to be MIMO. Also, two decode-and-forward (DF) and relay-assisted systems based on either serial (multi-hop transmission) or parallel (cooperative diversity) configurations are included in the conclusion of the theoretical

analysis. In [95], Puryear has investigated the use of spatial diversity with wavefront predistortion based on feedback from the receiver and coherent detection to overcome turbulence-induced outages, mitigate interference, and prevent eavesdropping. He has also shown the performance of an optical system under a sparse aperture system with imperfect (delayed, noisy, and distorted) knowledge of CSI.

The effect of turbulence can be reduced by performing aperture averaging and/or employing spatial diversity at the receiver [33], [96]. Aperture averaging may be considered a simple form of spatial diversity when the receiver lens aperture is larger than the fading correlation length. Khalighi *et al.* [33] provide a synthesis and comparison of the effectiveness in terms of telecommunication for aperture averaging and spatial diversity when under different atmospheric turbulence conditions. In [97] an experimental observation of the aperture averaging effect on a given FSO signal intensity is analyzed.

Different atmospheric turbulence and modulation models show dissimilar performances of spatial variety on the diversity system. Bayaki *et al.* [38] presented an approach to performance analysis of SISO and MIMO FSO systems in Gamma–Gamma fading. A parameterization of Gamma–Gamma fading via a generalized power series representation of a modified Bessel function is provided. This approach is also applicable for high SNR where the first few series terms suffice for accurate results. Closed–form expressions for average pairwise error probabilities (PEP), BER, and diversity gain have been provided for SISO and MIMO under EGC and MRC combining schemes.

Wavelength diversity is a branch of space diversity that can be adopted for FSO applications. In such systems, the source signal is transmitted in multiple light

wavelengths. Atmospheric conditions, e.g., fog, cause a variety of influences on the transmitted signal for different wavelengths. Hence, the level of atmosphere attenuation is dependent on the wavelength of light. Harris *et al.* [57] proposed the use of multiple wavelengths to increase the redundancy of the received power. The work investigated the performance of a slantpath, wavelength-diversified FSO link between a ground station and an unmanned aerial vehicle in the presence of radiation fog. The FSO link is configured to operate using the simultaneous transmission of three wavelengths—0.85, 1.55, and 10 μm—connecting a ground station to an unmanned aerial vehicle operating at either a 4- or 8-km altitude. The link is analyzed by combining multiple carrier wavelengths into either an EGC or SC scheme. Results demonstrate that an SC diversity scheme has a received power approximately three times greater than that of EGC. The work does not, however, consider turbulence-induced fading in the analysis; rather the effect of atmosphere is modeled as the attenuation due to scattering.

Angle diversity is a potential solution to mitigate the effect on performance resulting from misalignment. Optical wireless sensor network (WSN) [69] and MANET are among the practical applications of angle diversity, since the transceiver structure is unbalanced. Using LED transmitters, Ghosh *et al.* [69], [70] demonstrated the design and initial experimental results of a wireless sensor node network realizing mobile FSO nodes with the goal to provide nodes that may have limited mobility.

Cooperative diversity and relaying, originally offered for RF communication, can also be adapted for free space communication and serve as an alternative way to realize spatial diversity advantages for FSO. Theoretical studies for FSO channels are found in literature and focus on feasibility and modeling for various cooperative modes. Authors in [81]

study both serial (multi-hop transmission) and parallel (cooperative diversity) relaying coupled with amplify-and-forward and decode-and-forward modes. Both are considered path-loss and turbulence-induced, log-normal fading in their relay-assisted model. Results show an improvement in end-to-end outage probability, which is a performance evaluation factor. A brief study of BER performance has been investigated [98]; authors consider a 3-way FSO communication setup to achieve cooperative-based spatial diversity.

2.6.2 Experimental Studies on Diversity

Feasibility of diversity is of interest to experimental researchers, as well. Field measurements demonstrated the effectiveness of spatial diversity [99] at the MIT Lincoln Laboratory, where noncoherent summing of the partially uncorrelated photocurrents of four spatially separated receivers was tested to mitigate the effect of fading-induced turbulence on the optical signal. Both spatial and temporal diversity are considered in the system. Only one transmitter in the architecture resulted in a SIMO spatial diversity solution. Four receptive apertures separated by a distance greater than the coherence diameter were used to capture a single transmit beam and achieve spatial diversity. Temporal diversity was achieved using symbol interleaving combined with forward error correction coding (FEC) and interleaver spans of up to 2s. Small, 12mm apertures were used, which facilitated pointing, tracking, and coupling into single-mode fiber.

Other experimental works have contributed to FSO communication diversity. A receiver hardware module has been experimentally designed [100] to realize the diversity approach. The work presents a low-power, imaging diversity, front-end receiver employing the MRC combining algorithm for FSO communication. It consists of seven

signal channels and an output stage; each channel has a front-end transimpedance amplifier, a SNR estimator, and a variable gain amplifier (VGA).

The power gain of using diversity systems is found to be substantial [37]. Theoretical analysis on the power gain is presented for a SIMO *N*-branch combiner with BPPM modulation in a lognormal turbulence model. An experimental outage probability for a dual-branch (dual) receiver system that uses combining schemes is also presented.

Power gain is defined in a diversity system as the fractional decrease in required transmitted power when compared with a nondiversity system to achieve a similar specified outage probability. Power gain affects the performance factor directly from outage probability. In [37] power gain of EGC performance is found to be nearly as good as OC. Consequently, choice of diversity scheme does not greatly contribute to power gain performance. By contrast, BER performance is highly dependent on diversity method selection.

3. Detection with no CSI Availability

This chapter focuses on the optimal detection of the FSO signal under turbulent media when CSI is not available at the receiver side. Basically, when the random fluctuation of the channel fading is comparable to the data rate of the transmitted data, the receiver will not be able to estimate channel coefficients. In such a case, computations are required to optimally detect any individually received symbol. Several detection approaches based under the unavailability of the CSI are presented in chapter 2. The objectives of this chapter are limited to the utilizing thresholding-based detection to reduce the processing load within the optimal detection, as presented in part in [83]. Based on the thresholding-based suggestion, rather than regular likelihood ratio, the threshold value is calculated and applied for an interval, thus facilitating a less complex receiver design. Two schemes—Likelihood Thresholding Detection (LTD) and PSAM-based Thresholding Detection (PTD)—are proposed. PTD is designed based on time diversity utilization.

3.1 Introduction

The receiver design for a high-speed FSO signal is necessarily highly complex when CSI is not available. Currently, though most approaches provide high detection

performance in terms of bit error, receiver design is difficult to implement. This chapter proposes two practical thresholding-based detection schemes. Both offer significant improvement to receiver throughput on a computational load basis when CSI is not available. However, the receiver knows channel model, fading distribution, and fading correlation. The first is based on a simple ML function where BER is the same as conventional symbol-by-symbol detection. This method, however, causes a loss of BER performance. The second uses the aid of PSAM to modify the ML function when channel coefficients are temporally correlated. While numerical analysis based on this method shows that BER performance in a lognormally distributed fading channel is very close to detection achieved with perfect CSI, the receiver suffers from increased complexity. If random processes for fading and noise are assumed as stationary and given that the detection threshold is quickly calculated and applied during a given period, such complexity of PASM-based and symbol-by-symbol detection methods can be reduced.

The balance of this chapter is organized as follow: in Section 2 related works are reviewd. Section 3 focuses on the channel model review and Section 4 addresses the method for estimating channel fading statistics (including instantaneous CSI) in practice. The scheme initially introduced, namely LTD, is presented in Section 5, and Section 6 describes the proposed PSAM-based detection scheme: PTD. Section 7 demonstrates simulation results obtained from numerical analysis, and finally, Section 8 offers a brief conclusion.

3.2 Related Works

FSO signal suffers from turbulence-induced fading, which degrades communication link performance. In theoretical analysis, time-varying channel fading can be modeled as

scintillation with lognormal distribution; however, it is also affected by additive Gaussian noise. Given that channel fading is not assumed in the system model [34] or that instantaneous CSI is assumed known at the receiver side [35], [101], the design of an optimal detector would be quite simple. In both cases, the receiver merely requires computation of a simple mathematical expression, and BER remains at a minimal value.

Finding the decision metric for optimal detection of a faded FSO signal without CSI availability imposes receiver complexity [102]. In fact, a numerical calculation of integral equations, i.e., likelihood function $\Lambda(i_d)$ for any individual received symbol (i.e., bit) i_d, is required. Hence, detection would be based on metric $\Lambda(i_d) \underset{0}{\overset{1}{\gtrless}} 1$. This method imposes excessive load at the receiver, making currently proposed techniques for most applications difficult to implement. Because this method appears uncomplicated, claims of achieving BER performance improvements have been made. This chapter details a method to alter the detection scheme by optimally calculating a threshold value, I_D, applied on a given period. The detection rule is thus changed to $i_d \underset{0}{\overset{1}{\gtrless}} I_D$, and, quite simply, I_D is optimally computed by numerically solving an integral equation and kept unchanged during an observation interval. In practice, I_D is affected only by received signal strength, noise, and fading statistics. Thus, a lookup table accessible by the receiver can facilitate greater receiver design simplicity. As a result, the computational load of numerical computations for any individually received symbol at the receiver is avoided. This chapter first proposes *likelihood thresholding detection,* i.e., LTD, based on this concept, resulting in a less complex receiver aperture and higher throughput of the hardware when

compared to conventional methods, e.g. conventional symbol-by-symbol detection [79]; differential thresholding detection [103]; decision-feedback detection [91]; and block and multiple symbol detection [29]. Although LTD removes a significant amount of processing load for repetitive calculation of $\Lambda(i_d)$, it still provides a BER performance similar to symbol-by-symbol detection.

A published work by Zhu and Kahn [89] suggested that when channel coefficients at different times are mutually correlated, a PSAM-based scheme, rather than a symbol-by-symbol method, optimizes the likelihood function, thus improving the performance in terms of BER. In this case, information from partially temporal correlated channel fading aids optimal detection by finding a more accurate ML. The new likelihood function takes advantage of the correlation between a received symbol i_d to a known received pilot symbol i_p. Data is transmitted in slots, each containing a small number of pilot symbols ($N_p \geq 1$) and many data symbols. However, such computations for the likelihood function $\Lambda(i_d, i_p)$ basically overflow receiver throughput, thus causing an efficiency loss. Such analysis is a reasonable argument when the effect of the processing load for calculation of $\Lambda(i_d, i_p)$ is neglected. This chapter proposes a simpler scheme than that proposed by Zhu and Kahn. Specifically, the scheme is introduced as *PSAM-based Correlative Detection,* i.e., PCD. Consequently, a *PSAM-based Thresholding Detection,* i.e., PTD, solution is introduced in this chapter. In addition to cutting the processing load, the proposed scheme results in a greater performance loss reduction than that realized by LTD. Improvement is achieved through a significantly more accurate ML function $\Lambda(i_d, i_p)$ if the channel coefficients for bits i_d and i_p are mutually correlated. If no correlation exists, BER performance provided by PTD degrades to that achieved by LTD.

3.3 System Model Review

This chapter assumes OOK modulation of the optical signal with direct (noncoherent) detection at the receiver. The channel fading is modeled as a lognormal distribution without consideration of inter-symbol interference (ISI).

3.3.1 Additive Noise

The received signal $i_d[n]$ can be expressed in any discrete time n by

$$i_d[n] = h[n]s[n] + i_n[n] \qquad 3\text{-}1$$

where $s(t)$ is the transmitted signal; $h[n]$ is the normalized time-varying channel fading due to atmospheric turbulence and considered to be constant over a large number of transmitted bits; and $i_n[n]$ is total additive noise. For simplicity in notation, the time index $[n]$ is neglected in the analysis presented herein. Although non-random attenuation due to propagation and scattering can also be included in the model [12], [57], these do not affect the results when communication is stochastically analyzed. Assuming the channel is not affected by turbulence-induced fading, i_n will be the only random variable used in the model. The averaged ML-based BER for such a Gaussian channel with equally likely transmitted bits is expressed in terms of noise and signal parameters. The minimal error probability is provided by the ML-based decision threshold expressed by [34]

$$I_{D,G} = \frac{\sigma_0 I_1 + \sigma_1 I_0}{\sigma_0 + \sigma_1}, \qquad \text{(no turbulence)} \qquad 3\text{-}2$$

where σ_1 and σ_0 are the standard deviations of the noise currents for symbols '1' and '0', respectively; $I_1 (= I_0 + 2P_t R)$ and I_0 are averages of the generated currents at the receiver for symbols '1' and '0', respectively—all of which were introduced in section 2.4.1. The

threshold value $I_{D,G}$ can be assumed constant for a given observation period if Gaussian noise is assumed to be *stationary*. Note that for an FSO channel with only additive Gaussian noise, the average SNR can be expressed by [28]

$$\gamma_G = \frac{4R^2 P_t^2}{(\sigma_1 + \sigma_0)^2} \qquad \text{(Gaussian noise)} \qquad 3\text{-}3$$

3.3.2 Turbulence Model

As a review from section 2.4.2, the fading channel coefficient, which models the channel between the transmit aperture and the receive aperture, is given by Eq. (2-17) for a lognormal channel. Since log-amplitude variable X is Gaussian, the expected value of the channel coefficient h is equal to Gaussian *moment-generating function* (MGF) evaluated at X=2:

$$\mu_I = E[h] = \mathcal{M}_x(2) = e^{(2\mu_x + 2\sigma_x^2)} \qquad 3\text{-}4$$

Assuming channel coefficients at different times are independent, the variance of h can be calculated as

$$\sigma_I^2 = E[h^2] - E[h]^2 = \mathcal{M}_x(4) - \left(\mathcal{M}_x(2)\right)^2 = e^{(4\mu_x + 4\sigma_x^2)}\left(e^{4\sigma_x^2} - 1\right) \qquad 3\text{-}5$$

In scintillation fading, the average power loss due to atmospheric fading is normalized, such that the fading does not, on average, attenuate or amplify the optical power. It explicitly leads to $\mu_I = E[h] = 1$ that leads us to $\mu_x = -\sigma_x^2$. Thus, the variance will be equal to

$$\sigma_I^2 = e^{4\sigma_x^2} - 1 \qquad 3\text{-}6$$

This parameter is so called *scintillation index*, i.e., S.I., which was discussed in sections 2.5.1 and 2.5.2. It can be seen from (3-6) that the parameter σ_x is different from the standard deviation of fading process. The parameter is occasionally referred to as *fading strength*. Finally, the lognormal distribution will be given by a PDF of

$$f_I(h) = \frac{1}{\sqrt{8\pi}\, h\sigma_x} \exp\left(-\frac{\left[\ln(h) + 2\sigma_x^2\right]^2}{8\sigma_x^2} \right), \qquad 3\text{-}7$$

where $h \geq 0$ and σ_x is defined as

$$\sigma_x = \frac{\sqrt{\ln(S.I.+1)}}{2} \qquad 3\text{-}8$$

Note that for a lognormal channel with additive Gaussian noise, the instantaneous SNR from (3-3) will be converted to Eq. (2-20). The averaged value of SNR can be defined from (11) by

$$\bar{\gamma} \triangleq \frac{4R^2 P_t^2}{(\sigma_1 + \sigma_0)^2}, \qquad 3\text{-}9$$

which is defined as the same expression in Eq. (3-3).

3.3.3 Channel State Information (CSI)

CSI is the *instantaneous* fading state, i.e., fading coefficients h, at each symbol period. Some investigations assume perfect availability of CSI at the receiver [32], [35]. This assumption enables the design of the optimal detector in its simplest form so that the ML-based decision threshold is simply defined as

$$I_{D,\,With-CSI} = \frac{\sigma_0 (I_0 + 2P_t R h) + \sigma_1 I_0}{\sigma_0 + \sigma_1} \qquad 3\text{-}10$$

when h is somehow known at the receiver side. Detection takes place by the computation of (3-10) for metric $i_d \underset{0}{\overset{1}{\gtrless}} I_{D,With-CSI}$ regarding any individually received symbol i_d. Such detection for a lognormal fading channel maintains BER at the lower bound [101]

$$P_{e,L}(\gamma_G, \sigma_x) = \frac{1}{2} - \frac{1}{\sqrt{\pi}} e^{-\sigma_x/2} \sum_{k=0}^{K} \frac{(-1)^k \gamma_G^{(2k+1)/2}}{2^{(2k+1)/2}(2k+1)k!} \exp\left(\frac{(4k+1)\sigma_x}{\sqrt{2}}\right)^2 , \quad 3\text{-}11$$

where K is a sufficiently large integer. Above equations were achieved with the assumption that the receiver knows the channel model, fading distribution, fading correlation, and noise statistics. Also, instantaneous CSI is assumed to be available. This type of detection provides the most minimal BER for the system. In practice, however, channel CSI is not easily available at the receiver. In this case, BER performance of the system degrades. Specifically, the level of such degradation is highly dependent on the method chosen for detection. In the following sections, an alternate solution is provided to bypass the complexity of CSI measurement while achieving BER performance close to (3-11). First, a discussion regarding a practical method for noise and fading parameters is presented, noting that the definition of channel estimation in this work does not merely refer to CSI estimation, but also includes the statistics of noise and turbulence. However, CSI estimation is not a goal in this chapter, as it is assumed inaccessible due to rapid turbulence fluctuation.

3.4 A Practical Channel Estimation

The threshold level I_D derived in (3-2) is a function of noise statistics parameters, i.e., I_0, σ_0 and σ_1. The next section demonstrates that channel fading statistics, i.e., σ_x, are also required when considering a fading model. The receiver requires knowledge about

such parameters before integral calculation takes place. This section briefly analyzes the practical measurement for parameter estimation through a simple multi-slot averaging (MSA) method. The method uses the help of PSAM in the signal, where known symbols '1' and '0' are periodically inserted into the information slots at the transmitter side. The received pilot symbols are decoded for estimating noise and fading statistics.

3.4.1 Noise and Fading Statistics

The receiver integrates the signal from the photocurrent for each symbol interval. Different symbols face different noise and fading components. Based on Eq. (3-1), the receiver's output photocurrent is calculated by

$$i_p = 2P_t Rh + i_n \qquad \text{3-12}$$

The transmitted power for symbol '0' is zero, then $i_{p,0} = i_n$ for this symbol. I_0 and σ_0 are the average and standard deviation of the received samples of symbol '0', respectively. This can easily be estimated by averaging the received pilot signals. For an ideal estimation, the number of samples should extend to infinity, which is impossible in practical applications. However, a limited number of samples may provide a good approximation as a result of *temporal averaging* (TA).

The noise analysis for symbol '1' is not without complexity. The random process $i_{p,1}$ is the sum of two ergodic, independent Gaussian and lognormal variables, i_n and h. For noise i_n with Gaussian distribution $f_n(X)$, mean I_0, and variance σ_1, the distribution of the received signal will be the convolution of PDF's for the following two variables

$$f_{p,1}(X) = f_I(X) * f_n(X)$$
$$= \frac{1}{4\pi\sigma_x\sigma_1}\int_0^\infty \frac{1}{h}\exp\left(-\frac{\left[\ln(h)+2\sigma_x^2\right]^2}{8\sigma_x^2}\right)\exp\left(-\frac{(h-I_0-X)^2}{2\sigma_1^2}\right)dh \qquad 3\text{-}13$$

Although the integral shown above may be calculated only by numerical integration, there are expressions for mean and variance of the photocurrent signal. Assuming that the turbulence-induced fading coefficients are uncorrelated, the statistics of a received symbol '1' is equal to

$$\mu_{p,1} = \mu_I + I_0 = 1 + I_0 \qquad 3\text{-}14$$

and

$$\sigma_{p,1}^2 = \sigma_I^2 + \sigma_1^2 = e^{4\sigma_x^2} + \sigma_1^2 - 1 \ . \qquad 3\text{-}15$$

In practice, noise standard deviations σ_0 and σ_1 are very close and can be assumed identical by approximation [34]

$$\sigma_1 \approx \sigma_0 \qquad 3\text{-}16$$

Thus, the estimator of fading standard deviation will be presented from (3-15) by

$$\hat{\sigma}_x \approx \frac{1}{2}\sqrt{\ln[\hat{\sigma}_{p,1}^2 - \hat{\sigma}_0^2 + 1]} \ , \qquad 3\text{-}17$$

where $\hat{\sigma}_{p,1}$ and $\hat{\sigma}_0$ are the estimated values of standard deviations for received symbols '0' and '1', respectively, using the pilot signals, as shown in Figure 3-1. Since noise is assumed to be a stationary random process, parameters $\hat{\sigma}_{p,1}$ and $\hat{\sigma}_0$ can be calculated by the TA method due to the ergodicity of the random processes $i_{p,1}$ and i_n. Also, the

estimated mean value can be practically calculated using the TA method from both symbols '1' and '0' in pilot signal [104](Eq. 17.25).

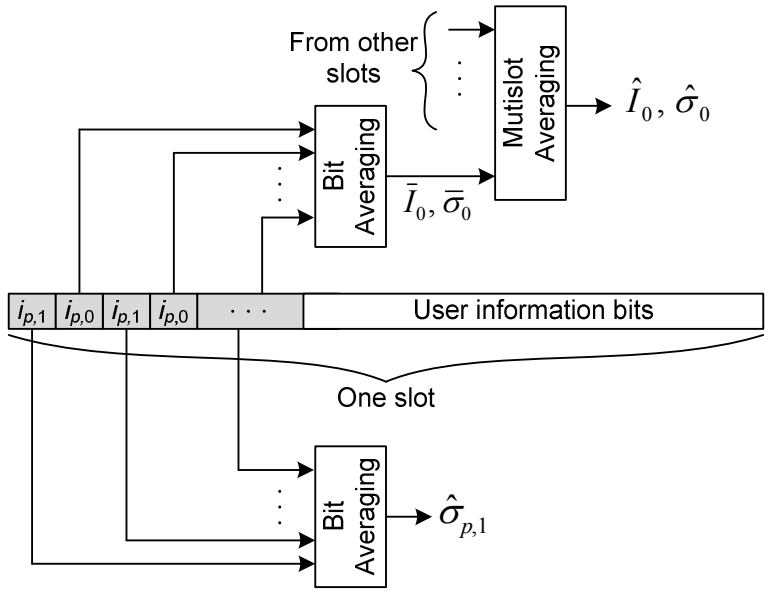

Figure 3-1: MSA estimator

3.4.2 Fading Random Process

By demonstrating the relation between noise and fading standard deviations, estimator in Eq. (3-17) is applicable when an independency between fading samples has been assumed. However, in practical models, channel fading coefficients due to fluctuation of light intensity are correlated for different samples. The level of dependency is contingent on the channel coherence time, τ_c. Fading coefficients show more dependency for longer channel coherence times. It is assumed that in FSO communications, fading process has a coherence time on the order of milliseconds, which is slow compared to typical symbol rates of FSO systems [35].

The time-varying channel is modeled as a joint log-normal channel with PDF $f_I(h[1], h[2], \dots, h[N_h])$ for N_h different samples. Each symbol has a different fading

statistic and is dependent on fading of other symbols at different times. Assuming a constant light intensity at the receiver during bit interval T_b, the covariance matrix of the log-amplitude $\mathrm{X} = \{X_1, X_2, \dots, X_{n_1}, \dots, X_{n_2}, \dots, X_{N_h}\}$ is defined by

$$\mathbb{C}_x = \begin{bmatrix} \sigma_x^2 & C_{1,2} & \cdots & C_{1,N_h} \\ C_{2,1} & \sigma_x^2 & \cdots & C_{2,N_h} \\ \vdots & \vdots & \ddots & \vdots \\ C_{N_h,1} & C_{N_h,2} & \cdots & \sigma_x^2 \end{bmatrix}_{N_h \times N_h} \qquad 3\text{-}18$$

Without loss of generality, the log-amplitude PDFs of two individual symbols transmitted at time samples n_1 and n_2 are Gaussian, and the temporal covariance can be formulated as [89]

$$C_{n_1,n_2} = \sigma_x^2 \exp\left[-\left(\frac{T_{n_1,n_2}}{\tau_c}\right)^{5/3}\right], \qquad 3\text{-}19$$

where σ_x^2 is the variance of log-amplitude and T_{n_1,n_2} is the time difference between the symbols: $\tau = T_{n_1,n_2} = T_b|n_1 - n_2|$. Consequently, the covariance function C_{n_1,n_2} is not dependent on time but rather on time interval and $C_{n_1,n_2} = C_{n_2,n_1}$. The covariance coefficient between processes h_1 and h_2 is also defined as

$$\rho_{n_1,n_2} = \frac{E[(h[n_1]-\mu_I)(h[n_2]-\mu_I)]}{\sigma_I^2} = \frac{C_{n_1,n_2}}{\sigma_I^2}, \qquad 3\text{-}20$$

where σ_I^2 is defined by (3-6). This coefficient at $T_{n_1,n_2} = \tau_c$ is equal to $0.3679\sigma_x^2 / e^{4\sigma_x^2} - 1$. Hence, coherence time is defined as the time over which the covariance coefficient between channel coefficients is above $0.3679\sigma_x^2 / e^{4\sigma_x^2} - 1$, which calculates to nearly zero for $T_{n_1,n_2} / \tau_c \geq 3$ and indicates the channel coefficients are completely independent.

The fading process for the two faded '1's as two correlated channels are $h_{n_1} = exp[2X_{n_1}]$ and $h_{n_2} = exp[2X_{n_2}]$ with a temporal joint PDF, as follows:

$$f_I(h_{n_1}, h_{n_2}) = \frac{1}{8\pi h_{n_1} h_{n_2} \sqrt{\det(\Sigma_{n_1,n_2})}} \exp\left(-\frac{1}{8} \begin{bmatrix} \ln(h_{n_1}) + 2\sigma_x^2 \\ \ln(h_{n_2}) + 2\sigma_x^2 \end{bmatrix}^T \Sigma_{n_1,n_2}^{-1} \begin{bmatrix} \ln(h_{n_1}) + 2\sigma_x^2 \\ \ln(h_{n_2}) + 2\sigma_x^2 \end{bmatrix} \right), \quad 3\text{-}21$$

where Σ_{n_1,n_2} is the covariance matrix defined by

$$\Sigma_{n_1,n_2} = \begin{bmatrix} \sigma_x^2 & C_{n_1,n_2} \\ C_{n_1,n_2} & \sigma_x^2 \end{bmatrix} \quad 3\text{-}22$$

Thus, $\det(\Sigma_{n_1,n_2}) = \sigma_x^4 - C_{n_1,n_2}^2$. It can be shown that the temporal correlation function of the product of any two fading coefficients at times n_1 and n_2 is defined by

$$R_h(\tau) = E[h_{n_1} h_{n_2}] = \exp\left[4\sigma_x^2 \exp\left[-\left(\frac{\tau}{\tau_c} \right)^{5/3} \right] \right] \quad 3\text{-}23$$

The expected value of product variable $\grave{h} = h_{n_1} h_{n_2}$ is always equal or greater than unity, i.e., $E[h_{n_1} h_{n_2}] \geq 1$; hence, increasing the dependency leads to an increase in the expected value—keeping in mind that h_{n_1} is fading channel coefficient at time n_1, while h_{n_2} is the same at time n_2. Thus, sequence H $= \{h_1, h_2, \dots, h_{n_1}, \dots, h_{n_2}, \dots, h_{N_h}\}$ can be defined as a random process. However, it is assumed that the mean and variance of fading coefficients are constant by time. From the aforementioned assumptions, the properties of process h can be summarized, as follows:

$$E[h] = \mu \quad \text{(a constant)}$$

$$E[(h_{n_1} - \mu_I)(h_{n_2} - \mu_I)] = f(\tau) \quad 3\text{-}24$$

for some function *f*. The properties for *h*, detailed above, represent a *wide sense stationary* (WSS) process, where the mean does not depend on time, but rather the covariance depends only on the time interval between the samples.

3.4.3 Estimation of Fading Strength σ_χ

The correlation of any two individually received signals for symbol '1' at the photo-detector is defined by

$$R_p(\tau) = E\left[i_{p,1}[n_1]i_{p,1}[n_2]\right] = E\left[(h_{n_1}+i_1)(h_{n_2}+i_2)\right]$$
$$= \exp\left[4\sigma_x^2 \exp\left[-\left(\frac{\tau}{\tau_c}\right)^{5/3}\right]\right] + I_0^2 + 2I_0 \qquad 3\text{-}25$$

The σ_x will be the solution of the above equation if the value of the average for the correlation function is known. The product average can be calculated by using the received signal for sequential '1's in the received pilot signal. If symbols '1' and '0' are periodically repeated in the pilot signal, then $T_{n_1,n_2} = 2T_b$. Since $\tau_c \gg 2T_b$ then $exp\left[-(2T_b/\tau_c)^{5/3}\right] \approx 1$, and the product average will be approximated by

$$R_p(\tau) \approx \exp\left[8\sigma_x^2 - 2\sigma_x^4\right] + I_0^2 + 2I_0 \ , \qquad 3\text{-}26$$

which is slightly simpler than (3-25). Also, information about the coherence time is not required. Consequently, σ_x can be found from the solution of above equation, where $\sigma_x^2 = 2 \pm \sqrt{4 - 0.5\ln[R_p(\tau) - I_0^2 - 2I_0]}$. The solution with plus leads to a value of σ_x in the range of $\sigma_x \geq \sqrt{2}$, while the solution with minus is between $0 \leq \sigma_x \leq \sqrt{2}$. The solution with plus is rejected, since $\sigma_x = 0$ (no channel fading) should be included as a possible solution. Thus, the correct answer will be

$$\sigma_x = \sqrt{2 - \sqrt{4 - 0.5\ln[R_p(\tau) - I_0^2 - 2I_0]}} \qquad 3\text{-}27$$

In practice, the expression for σ_x shown above can be implemented by the MSA estimator in Figure 3-1.

3.4.4 Estimation of CSI

The estimation of channel CSI can occur only when the fluctuation of fading is adequately slow when compared to a small transmission data rate, i.e., coherence time, τ_c. While this assumption is not the focus of this chapter, it will be included in upcoming chapters. Nonetheless, the MSA estimator in Figure 3-1 can be simply extended for the estimation of the instantaneous channel coefficient if it is assumed constant over the estimating slots. Using a TA, the estimator will be expressed by

$$\hat{h}_{n_1} = E[i_{p_{,1}}] - \hat{I}_0 = \frac{1}{MN}\sum_M \sum_N \left(i_{p_{,1}}[n,m]\right) - \hat{I}_0 \qquad 3\text{-}28$$

where m is the slot number, n is the time index and $\hat{I}_0$ is the estimated value of the noise mean provided by MSA in Figure 3-1, thus $i_{p_{,1}}[n,m]$ is the received signal for the pilot '1' at time n in slot m.

3.4.5 Testbed Design

An experimental prototype based on the S-by-S optimal detector has been, in part, designed in this dissertation. The FSO link is implemented under SISO configuration in a lab setup where the channel is assumed as an Additive Gaussian noise. A snapshot of the testbed is shown in Figure 3-2, and the related block diagram is shown in Figure 3-3.

The FSO signal is generated by an Optical/Electrical converter laser source from Terahertz Technologies, working at $\lambda = 850$nm via a multi-mode fiber optic cable that is

then collimated for transmission over a length of 80cm. The photodiode, which generates the photocurrent signal from the collected power, is PDA10CF by Thorlabs with a nominal bandwidth of 150MHz. Because the photodiode is not equipped with a built-in amplifier, an external amplifier has been deployed.

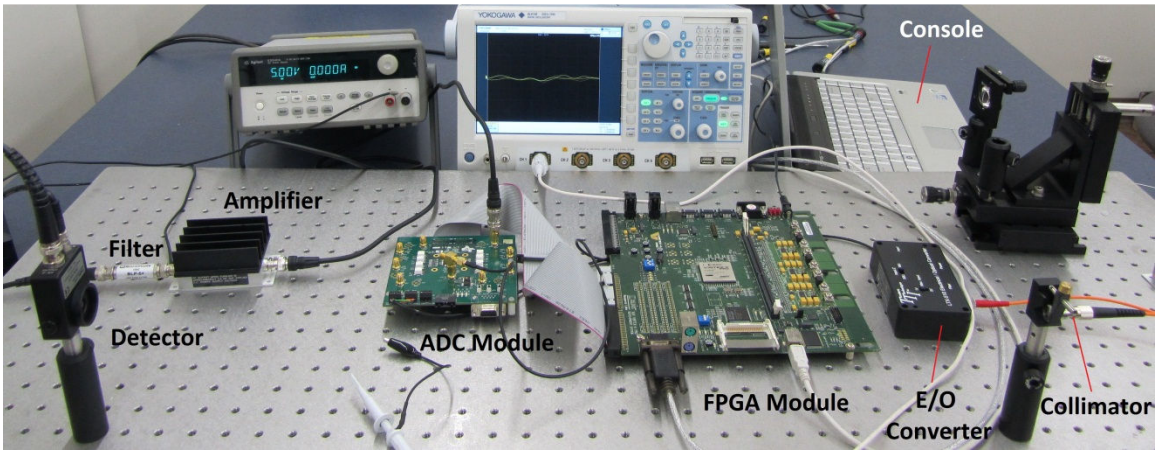

Figure 3-2: The FSO link implemented as a SISO testbed

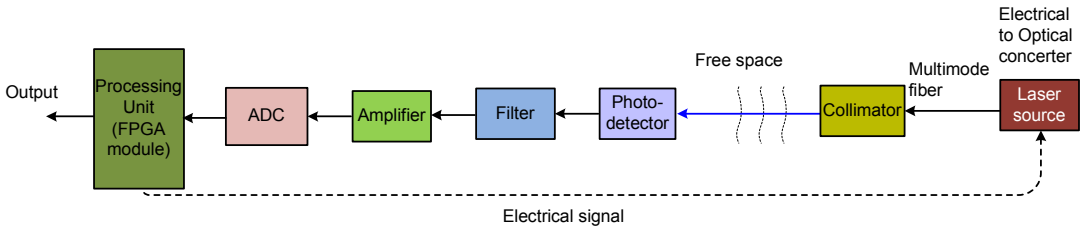

Figure 3-3: The testbed block diagram

The central unit of this testbed is a Xilinx® Embedded Development Kit—XUP Virtex II Pro FPGA board. Since the board accepts only digital IO ports, an analog to digital converter (ADC) is applied, making the signals compatible. The signal is then converted back to analog once entered into the FPGA board. The ADC module is the Texas Instruments' 12-bit ADS5272EVM module, which supports up to 8 input analog channels. The full-scale differential voltage is 2Vpp, and the data format is binary offset.

Hence, the most negative signal (-1V diff) will be 0x000, and the most positive signal (+1V diff) will be 0xFFF.

The XUP Development System employed in this research consists of a high performance Virtex-II Pro Platform FPGA surrounded by a comprehensive collection of peripheral components that can be used to create a more complex system [105]. Several programming tools have been utilized to generate the VHDL code of the hardware design.

System Generator for DSP™ [106] is part of the System Editions of ISE® Design Suite. When using System Generator for DSP, production quality FPGA implementations of DSP algorithms can be graphically designed and then created in a plug-in to MATLAB Simulink. Depending on the variety of peripherals, IO devices, and external memories, the VHDL code can be generated and uploaded to the board directly by the System Generator or a Platform Studio and the Embedded Development Kit (EDK) [107].

The FSO receiver utilizes an optimal detector under a Gaussian channel and is designed in the System Generator for DSP, as shown in Figure 3-4. The receiver is comprised of three major parts: the Digital to Analog Converter (DAC), which converts the received digital signal to the analog; the noise statistics estimator, which estimates the variance and mean of the noise; and the optimal detector, which detects the signal based on ML metrics in Eq. (2-24). The estimator uses the MSA estimation, given by Figure 3-1.

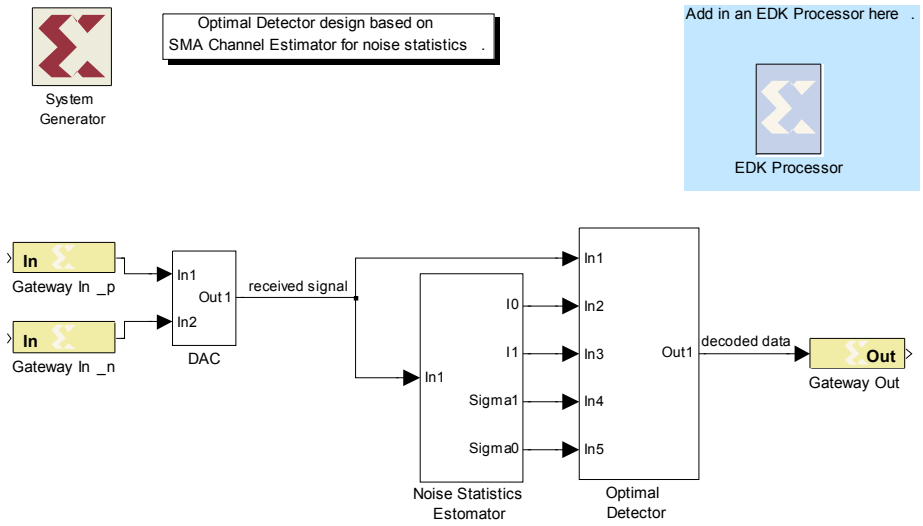

Figure 3-4: The implemented optimal receiver in the System Generator

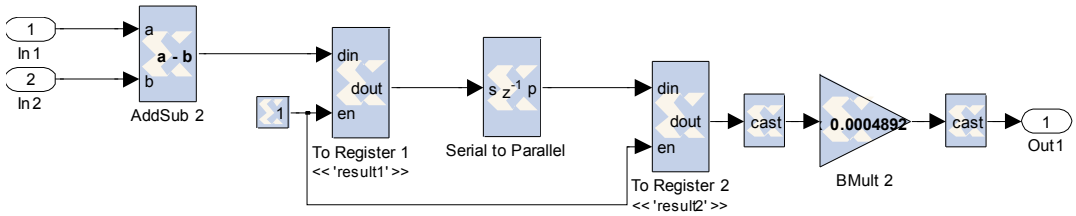

Figure 3-5: The DAC module in the System Generator

The DAC reads the digitized differential data on two IO pins of the FPGA, and then loads the converted analog signal to the estimator. The estimator block designed as part of Figure 3-4 has two major parts—the mean and variance estimators, as shown in Figure 3-6. The mean and variance estimators work with the assistance of pilot symbols and are shown in Figure 3-7 and Figure 3-8, respectively. A number of 16 pilot bits is considered for both ‘0’ and ‘1’ symbols. This design causes a delay of up to 32 bit periods, which is 1600ns at the system data rate of 20Mbps.

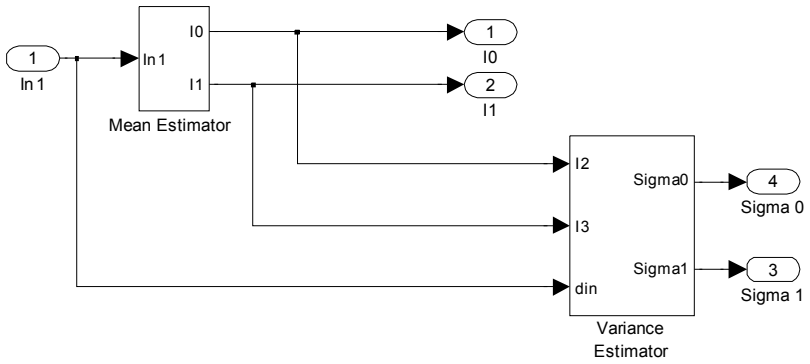

Figure 3-6: The Noise Statistics Estimator components

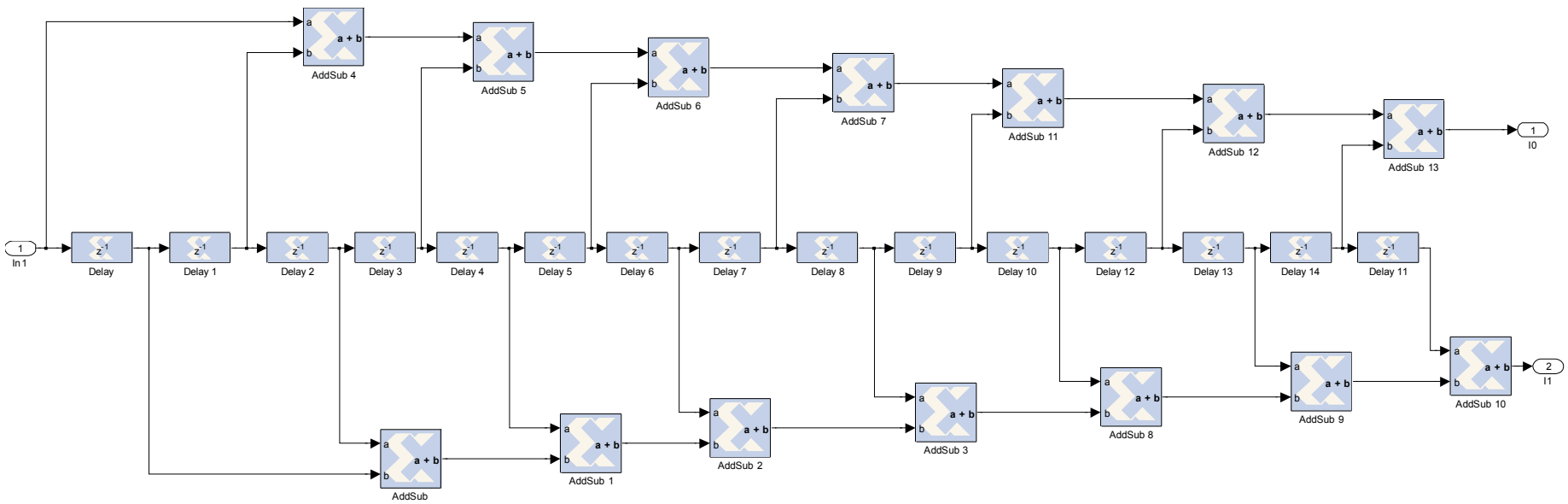

Figure 3-7: The circuit for mean estimator

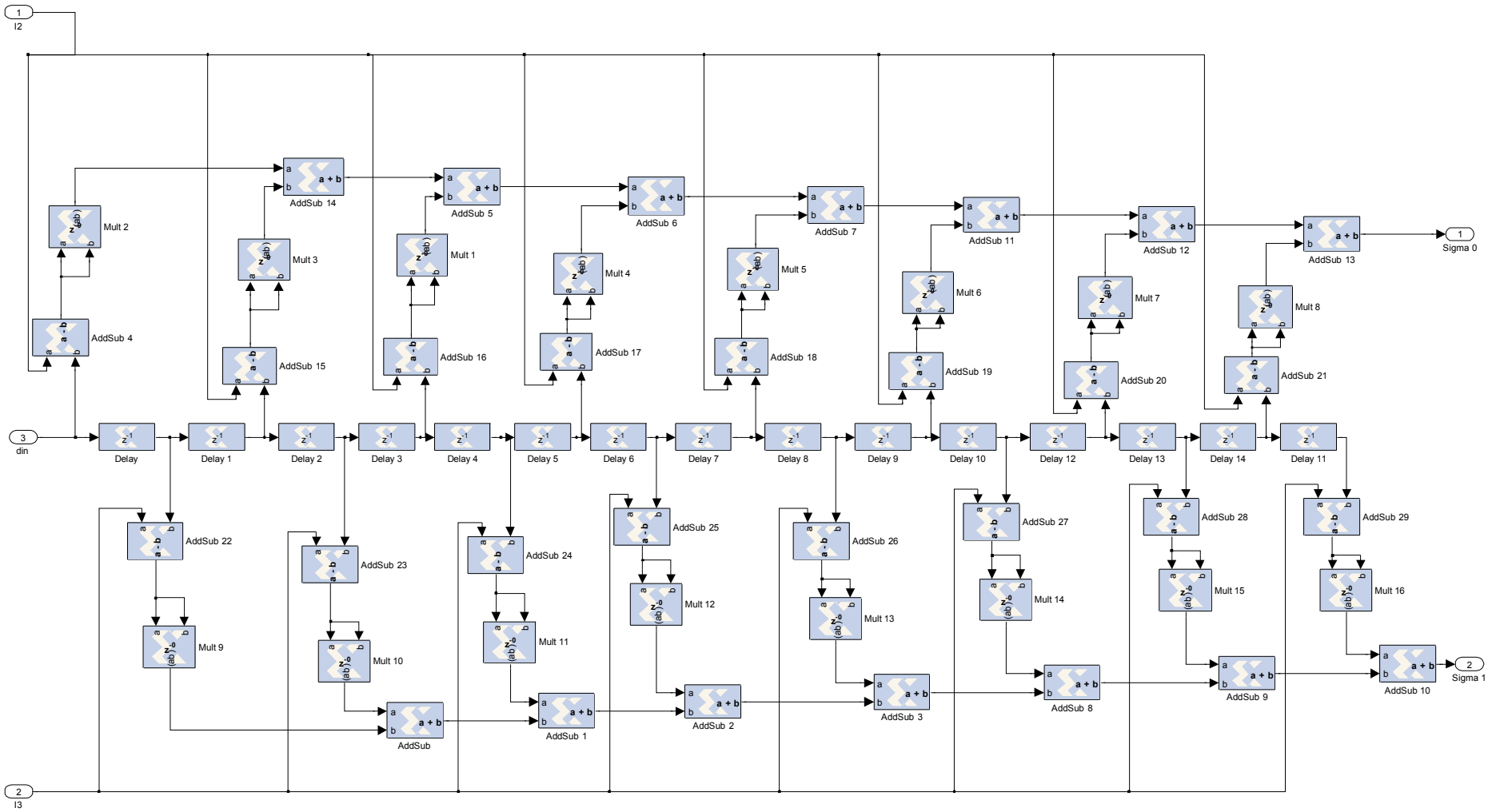

Figure 3-8: The circuit for variance estimator

The design implemented in this work offers a preliminary model of a SISO optimal receiver over a Gaussian additive noise channel. Even though it is simple, the design serves as a testbed foundation and can potentially be used for additional features and aspects in FSO communication, e.g., turbulence consideration and diversity. An estimator based on the analysis provided herein can be added to the design to approximate the statistics of the turbulence-induced fading. However, the channel under lab condition of this work is not affected by turbulence due to short transmission length. Such turbulence can be intentionally generated, and then included in the system by a heat generator, i.e., [108]. Lab conditions assure extremely slow fading for the turbulent channel. Thus, a CSI estimator using pilot signals can be developed. Furthermore, additional optimal detection approaches, as well as MIMO diversity schemes, can be implemented in this design.

3.5 Optimal Detection Analysis without CSI Availability

Thus far, this chapter has assumed that CSI is available at the receiver, resulting in a simple receiver design and providing the lower bound of BER. Hereafter in this chapter, it is assumed that the receiver has no information about the instantaneous CSI, but knows channel model, fading distribution, fading correlation, and noise statistics (by estimation). In this case, detection performance is highly dependent on the definition of the decision metric chosen for ML function. Under general conditional probabilities, ML decision criteria is determined as

$$\Lambda(i_d) = \frac{p(i_d|1)}{p(i_d|0)} \underset{0}{\overset{1}{\gtrless}} 1 \qquad 3\text{-}29$$

for any instantaneously received signal i_d . The following section reviews the conventional optimal detection method, and then establishes the proposed approach.

3.5.1 Conventional Symbol-by-Symbol Detection

Since fading does not affect symbol '0', $p(0)$ is Gaussian and $p(1)$ is not. The simplest expression for ML detection is provided by [79](Eq. 30) as symbol-by-symbol detection. This equation is rewritten based on channel parameters, where the conditional PDF probabilities are

$$p(i_d \mid 0) = \frac{1}{\sqrt{2\pi}\sigma_0} \exp\left[-\frac{(i_d - I_0)^2}{2\sigma_0^2} \right] \qquad 3\text{-}30$$

$$p(i_d \mid 1) = \frac{1}{\sqrt{2\pi}\sigma_1} \int_0^\infty f_I(h) \exp\left[-\frac{(i_d - I_o - 2RP_t h)^2}{2\sigma_1^2} \right] dh$$

Then, the likelihood function as the detection metric is calculated by

$$\Lambda(i_d) = \frac{\sigma_0}{\sigma_1} \int_0^\infty f_I(h) \exp\left[-\frac{(i_d - I_o - 2RP_t h)^2}{2\sigma_1^2} + \frac{(i_d - I_o)^2}{2\sigma_0^2} \right] dh \qquad 3\text{-}31$$

Bit error happens when $\Lambda(i_d) > 1$ if the transmitted symbol is '0' or $\Lambda(i_d) < 1$ if the transmitted symbol is '1', thus

$$BER_{S-by-S} = \frac{1}{2} \int_{\Lambda(i_d)>1} p(i_d|0)\ di_d + \frac{1}{2} \int_{\Lambda(i_d)<1} p(i_d|1)\ di_d \qquad 3\text{-}32$$

Consequently, the receiver requires the computation of Eq. (3-31) to determine the identity of bits for symbol-by-symbol ML detection.

3.5.2 Likelihood Thresholding Detection (LTD)

When CSI in not available, detection through symbol-by-symbol method requires the ML function to be computed individually for any received symbol, thus causing high processing load. Alternatively, a detection threshold can be defined in such a way that the

metric rule is considered as $i_d \underset{0}{\overset{1}{\gtrless}} I_D$. One simple way to define a detection threshold I_D is using the ML function. If the root of $\Lambda(i_d)=1$ is $i_d = I_D$, the probability of error for symbols '0' and '1' in a lognormal channel are respectively calculated by

$$p_e(1|0) = \frac{1}{2} erfc\left(\frac{I_D - I_0}{\sqrt{2}\sigma_0}\right)$$

$$p_e(0|1) = \frac{1}{\sqrt{32\pi}\sigma_x}\int_0^\infty \frac{1}{h}\exp\left(-\frac{[\ln(h)-2\mu_x]^2}{8\sigma_x^2}\right) erfc\left(\frac{I_0 - I_D + 2RP_t h}{\sqrt{2}\sigma_1}\right) dh \qquad 3\text{-}33$$

Then, assuming equal symbol probabilities, the averaged BER can be calculated using

$$BER_{LTD} = 0.5\, p_e(0|1) + 0.5\, p_e(1|0) \qquad 3\text{-}34$$

Figure 3-9 shows the way in which a threshold value is defined as the optimal detection threshold. Since $p(1)$ is affected by fading, a static threshold does not provide optimal detection of the OOK signal. Clearly, I_D providing optimal detection for $\sigma_x = 0.1$ is not applicable for other fading intensities $\sigma_x = 0.2$, 0.3 and $\sigma_x = 0.4$. Thus the value of I_D is highly dependent on the fading strength σ_x. For example, $I_D \approx 1.1$ when $\sigma_x = 0.1$, while $I_D \approx 0.9$ when $\sigma_x = 0.4$. In this section, an optimal detection is proposed based on finding a threshold value I_D in lognormal fading channels.

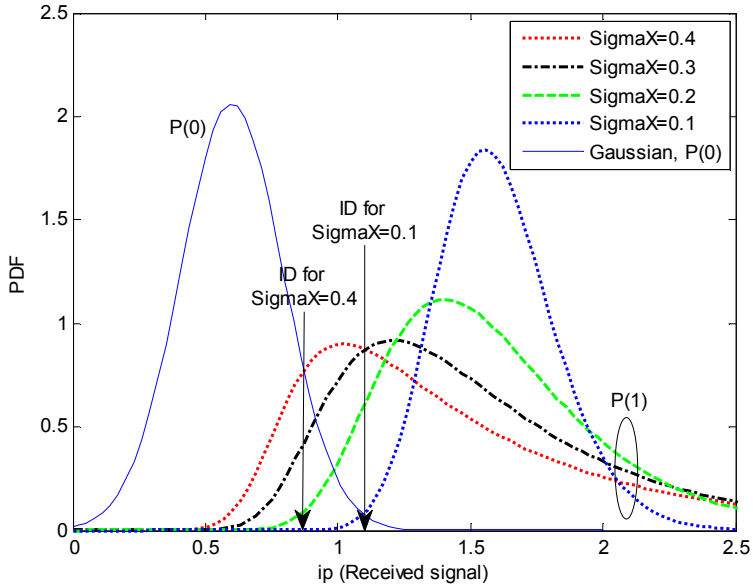

Figure 3-9: Typical threshold value I_D for optimal detection based on a given Gaussian noise with I_0=0.6, averaged SNR=6dB, and four different lognormal channels.

Based on maximizing likelihood function, i.e., $\Lambda(i_d)$, the threshold value for optimal detection is the solution to $\Lambda(I_D) = 1$, which leads to the representation

$$\Lambda(I_D) = \frac{p_e(0|1)}{p_e(1|0)} = 1 \qquad 3\text{-}35$$

The final equation then becomes

$$\int_{-\infty}^{\infty} \exp\left(-\frac{\left[X+\sigma_x^2\right]^2}{2\sigma_x^2}\right)\left(erfc\left(\frac{I_0 - I_D + 2RP_t e^{2X}}{\sqrt{2}\sigma_1}\right) - erfc\left(\frac{I_D - I_0}{\sqrt{2}\sigma_0}\right)\right)dX = 0 \qquad 3\text{-}36$$

The threshold value for optimal detection is the solution of above equation for I_D, which is only dependent on the fading intensity σ_x and noise statistics. Providing a closed-form expression for the I_D that satisfies the above equation is complicated. However, the solution for I_D can be numerically derived utilizing a simple root-finding method. This

dissertation suggests using a simple bisection method [109]. As numerically demonstrated in Section 2.7, increasing both the fading intensity, i.e., σ_x , and SNR provides a decrease of the threshold value, I_D. This result is also understood from the probability distribution functions in Figure 3-9.

The uncomplicated LTD method presented in this chapter proposes to calculate threshold value rather than a regularly computed likelihood ratio, e.g., symbol-by-symbol method, thus facilitating a less complex receiver design. If the noise and channel processes are assumed to be ergodic and stationary for the observation period the integral equation for threshold solution needs to be solved only once during that period. This corresponds to a significant improvement of receiver performance in terms of processing throughput, especially in high bit rates. Given that channel fading statistics have not changed, the current I_D works as the optimal threshold value for detection. However, an updating period can be considered if a time-variant channel model is assumed in practice.

The delivered BER by LTD yields

$$BER_{LTD} = \frac{1}{2} erfc\left(\frac{I_D - I_0}{\sqrt{2}\sigma_0} \right) \qquad 3\text{-}37$$

Explicitly, the BER performance of LTD is the same as the symbol-by-symbol performance provided by (3-32). It should be emphasized that the LTD method still requires information about the channel model, marginal fading distribution, fading correlation, and noise statistics; however, instantaneous CSI is not required. The concept of noise statistics and channel intensity estimation was investigated as a channel estimator in Section 2.4.

3.6 Correlation-based Detection

Generally speaking, if the CSI is known at time n_1, the state can be estimated at time n_2, due to the correlation of the CSI components. Such information is of benefit to the detection process, as it modifies the likelihood function and results in performance improvement [89]. This section mathematically investigates improvement of the likelihood function when channel coefficients are partially correlated. In this regard, PSAM modulation is employed to realize and evaluate the PCD scheme functionality. Alternatively, a second scheme will utilize a reduced complexity solution as PTD, addressing the computation of a detection threshold at the receiver.

3.6.1 PSAM-based Correlative Detection (PCD)

The correlativity between fading coefficients aids the detection process in terms of bit error performance under a time diversity approach. Without loss of generality, suppose that $i_d(n,m)$, where $N_p < n \leq N$ and $-\infty < m < \infty$ is the received signal for n-th information symbol in the m-th slot where $i_{p,1}(k,m)$ with $1 \leq k \leq N_p$ represents the received pilot signals for symbols '1'. N is the slot size, and N_p is the number of pilot symbols per slot. The structure of slots is shown in Figure 3-10. The fading coefficients are two symbols: h_d and h_p. Suppose that the receiver has knowledge of the temporal joint statistics of the fading. The conditional probability of $\mathbb{i}_{k,n,m}$ if symbol '0' is transmitted, $p(\mathbb{i}_{k,n,m}|0)$, will be given by

$$p\left(\mathbb{i}_{k,n,m}\middle|0\right) = \frac{1}{2\pi\sigma_0\sigma_1} exp\left[-\frac{(i_d(n,m)-I_0)^2}{2\sigma_0^2}\right]$$

$$\times \int_0^\infty f_I(h)\, exp\left[-\frac{\left(i_{p,1}(n,k)-I_0-2RP_t h\right)^2}{2\sigma_1^2}\right] dh\,, \qquad 3\text{-}38$$

and the conditional probability of $\mathbb{i}_{k,n,m}$ if symbol '1' is transmitted, $p(\mathbb{i}_{k,n,m}|1)$, will be given by

$$p(\mathbb{i}_{k,n,m}|1) = \frac{1}{2\pi\sigma_1^2}\int_0^\infty\int_0^\infty f_I(h_p,h_d)\, exp\left[-\frac{\left(i_{p,1}(k,m)-I_0-2RP_t h_p\right)^2}{2\sigma_1^2}\right.$$

$$\left.-\frac{(i_d(n,m)-I_0-2RP_t h_d)^2}{2\sigma_1^2}\right] dh_p\, dh_d \qquad 3\text{-}39$$

where the joint probability $f_I(h_p,h_d)$ is already defined. The joint likelihood function will be calculated as

$$\Lambda(\mathbb{i}_{k,n,m}) = \frac{p(\mathbb{i}_{k,n,m}|1)}{p(\mathbb{i}_{k,n,m}|0)} \qquad 3\text{-}40$$

This likelihood function is derived based on the method in [89]; however, the order of integrations is reduced by one order, resulting in a less complex receiver. The detection metric will be implemented based on the ML by the rule $\Lambda(\mathbb{i}_{k,n,m}) \underset{0}{\overset{1}{\gtrless}} 1$.

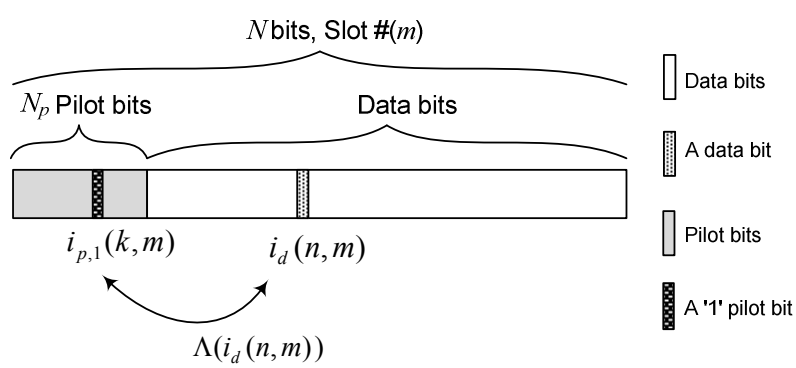

Figure 3-10: Slot structure used for pilot-based optimal detection

3.6.2 The Effect of Correlation

In analyzing the effect of channel correlation on the accuracy of the likelihood function, it is clear that $p(\mathbb{i}_{k,n,m}|0)$ is not affected by channel fading, whereas $p(\mathbb{i}_{k,n,m}|1)$ is expressed in terms of the correlation between channels. Since mutual correlation between two variables h_{n_1} and h_{n_2} is equal to the correlation between $h_{n_1} + i_{n_1}$ and $h_{n_2} + i_{n_2}$, where i_{n_1} and i_{n_2} are the samples of independent random noise, the effect of random noise can be readily excluded from analysis. A joint variable $Z \triangleq g(h_{n_1}, h_{n_2})$ is defined, where $g(h_{n_1}, h_{n_2}) \geq 0$ for any set of h_{n_1} and h_{n_2}. Random variable h_{n_1} is the channel coefficient at time n_1 , while h_{n_2} is the same but at time n_2. By definition the expected value of Z is expressed by

$$E[Z] = \int_0^\infty z\, f_Z(z)\, dz \ , \qquad 3\text{-}41$$

where $f_Z(z)$ is the PDF of Z. For jointly distributed discrete random variables, the determination of $f_Z(z)$ is avoided by employing instead the formula [104]

$$E[Z] = E[g(h_p, h_d)] = \int_0^\infty \int_0^\infty f_I(h_p, h_d)\, g(h_p, h_d)\ dh_p\, dh_d \ . \qquad 3\text{-}42$$

By choosing $g(h_p, h_d)$ as

$$g(h_p, h_d) \ \triangleq \frac{1}{2\pi\sigma_1^2}\left[exp\left[-\frac{(\hat{I}[n_p]-2RP_t h_p)^2}{2\sigma_1^2} - \frac{(\hat{I}[n_d]-2RP_t h_d)^2}{2\sigma_1^2}\right]\right] \qquad 3\text{-}43$$

the expected value of Z is equal to the conditional probability of symbol '1':

$$E[Z] = p(\mathbb{i}_{k,n,m}|1) \qquad 3\text{-}44$$

Hereafter, the notation $E[Z]$ will be used instead of $p(\mathbb{i}_{k,n,m}|1)$. A new discrete-time random process $\{\Psi[n]\}$ is now considered for sample times $1 \leq n \leq N$ defined by

$$\Psi[n] \triangleq \frac{1}{\sqrt{2\pi}\sigma_1} exp\left[-\frac{(\hat{I}[n]-2RP_t h[n])^2}{2\sigma_1^2}\right], \qquad 3\text{-}45$$

assuming $\hat{I}[n]$ is a known, deterministic parameter and one that is different at various times. Since the marginal distribution of random variable $h[n]$ is known, the mean value of $\Psi[n]$ is calculated by

$$E\big[\Psi[n]\big] = \frac{1}{\sqrt{2\pi}\sigma_1}\int_0^\infty f_I(h) exp\left[-\frac{(\hat{I}[n]-2RP_t h)^2}{2\sigma_1^2}\right] dh \qquad 3\text{-}46$$

which is always limited based on *Gauss Hermite quadrature* [110](Sec. 25.4.46):

$$E[\Psi[n]] \leq C \ , \qquad 3\text{-}47$$

for a given value of *C, C*>0. The *correlation function* of the process Ψ is expressed by

$$R_\Psi[n_1, n_2] = E\big[\Psi[n_1]\Psi[n_2]\big] =$$

$$\frac{1}{2\pi\sigma_1^2}\int_0^\infty\int_0^\infty f_I\big(h_{n_1}, h_{n_2}\big)\left[exp\left[-\frac{\big(\hat{I}[n_1]-2RP_t h_{n_1}\big)^2}{2\sigma_1^2} - \frac{\big(\hat{I}[n_2]-2RP_t h_{n_2}\big)^2}{2\sigma_1^2}\right]\right] dh_{n_1} dh_{n_2} \qquad 3\text{-}48$$

noting that $E[h] = 1$ while $f_I\big(h_{n_1}, h_{n_2}\big)$ and $E\big[h_{n_1}, h_{n_2}\big]$ are not dependent on time but rather on time interval $\tau = |n_1 - n_2|T_b$. It is concluded that $R_\Psi[n_1, n_2]$ is a strictly decreasing function dependent only on the time interval $|n_1 - n_2|$. The correlation function can simply be rewritten as a different notation

$$R_\Psi[n_1, n_2] = R_\Psi(\tau) \leq C \quad ; \tau \geq 0 \qquad 3\text{-}49$$

The above last two equations provide two important properties of the signal $\{\Psi[n]\}$, namely *quasi-stationary*. However, Section 2.4 demonstrated that $\{h[n]\}$ is a *sense stationary* process. Because the correlation function has the property that

$$R_\Psi(\tau) \leq R_\Psi(0) \ , \qquad 3\text{-}50$$

then (by using Cauchy-Schwarz inequality) $R_\Psi(0) = C = E[\Psi^2[n]]$. The correlation function of $\Psi\,[n]$ is maximized when the channel coefficients h_1 and h_2 are completely correlated. Now it is assumed that the deterministic parameters $\hat{I}[n_1]$ and $\hat{I}[n_2]$ are presupposed to be known and defined by $\hat{I}[n_1] \triangleq i_{p,1}(n_1, m) - I_0$ and $\hat{I}[n_2] \triangleq i_d(n_2, m) - I_0$. By using these definitions and replacing $n_1 = k$ and $n_2 = n$

$$R_\Psi(\tau) = E[Z] = p\left(\mathbb{i}_{k,n,m} \middle| 1\right) \ , \qquad \text{3-51}$$

which means the correlation function $R_\Psi(\tau)$ becomes equal to the nominator of the likelihood function $\Lambda(i_d(n,m)$. However, the denominator is still independent of the correlation. Thus, it is explicitly concluded that the closer the pilot symbol $i_{p,1}(k,m)$ is to the symbol $i_d(n,m)$, the more accurate the likelihood function. The worst-case scenario occurs when they are completely independent, because when $f_I\left(h_{n_1}, h_{n_2}\right) = f_I\left(h_{n_1}\right) f_I\left(h_{n_2}\right)$, the likelihood function diverges to the likelihood function to LTD detection. This analysis was accomplished for symbol '1', and, as shown, there is no correlation between a received data symbol '0' and the pilot symbols. In this way, the likelihood function for this symbol becomes equal to the symbol-by-symbol detection.

3.6.3 BER for PCD Method

The probability of error for a given symbol *n* in slot *m* using PCD detection method is given by

$$\tilde{P}_{PCD}(k,n,m) = 0.5 \iint_{\substack{i_{p,1}(k,m), i_d(n,m)\,, \\ \Lambda(i_d(n,m))<1}} p\left(\mathbb{i}_{k,n,m} \middle| 1\right)\ di_d(n,m) di_{p,1}(k,m)$$

$$+0.5 \iint_{\substack{i_{p,1}(k,m), i_d(n,m)\,, \\ \Lambda(i_d(n,m))>1}} p\left(\mathbb{i}_{k,n,m} \middle| 0\right)\ di_d(n,m) di_{p,1}(k,m) \qquad \text{3-52}$$

Since the conditional distribution functions, i.e., $p(\mathbb{i}_{k,n,m}|1)$ and $p(\mathbb{i}_{k,n,m}|0)$, are dependent on the position of symbol n in the slot m, the probabilities of error for different symbols in a slot are also different. The average BER, then, within an observation period of $N - N_p$ bits for a given pilot symbol k is calculated by

$$\overline{BER}_{PCD} = \frac{1}{(N-N_p)} \sum_{n=N_p+1}^{N} \tilde{P}_{PCD}(k,n,m)\,, \qquad 3\text{-}53$$

which is drawn from the fact that $\tilde{P}_{PCD}(k,n,m) = \tilde{P}_{PCD}(k,n,m+\delta)$ where $\delta \geq 1$. The above provides the bit error probability of an optimal detection based on the available noise and channel fading information when diversity is not applied. Although the order of integrations is decremented by one order, the likelihood function $\Lambda(\mathbb{i}_{k,n,m})$ is required to be computed for individual symbols. This, then, imposes an extra load on the receiver. In this instance, a thresholding-based detection will be able to reduce receiver complexity.

3.6.4 PSAM-based Thresholding Detection (PTD)

Using the LTD method in section 3.5.2, a threshold value for optimal detection was introduced at the point in which the channel coefficients are presumed to be uncorrelated. The solution is finding the root of equation $\Lambda(I_D) = 1$ for I_D, which is only dependent on fading strength σ_x and noise statistics. Such a technique significantly increases the receiver throughput in terms of processing overload. Likewise, it will be attempted to determine if a threshold value can be found for a PCD method.

In a PSAM-based detection, the probability of error for symbol '1' is dependent on the time distance between the received symbol and the pilot symbol; however, the distance does not affect the probability of error for a received '0'. For any given symbol n and pilot k in slot m, these probabilities are represented by

$$p_{k,n,m}(1|0) = \int_{-\infty}^{\infty}\int_{I_D}^{\infty} p\left(\mathbb{i}_{k,n,m}\middle|0\right)\ di_d(n,m)di_{p,1}(k\,,m)$$

$$p_{k,n,m}(0|1) = \int_{-\infty}^{\infty}\int_{-\infty}^{I_D} p\left(\mathbb{i}_{k,n,m}\middle|1\right)\ di_d(n,m)di_{p,1}(k\,,m) \qquad \text{3-54}$$

and by averaging all bits over a given slot

$$\bar{p}(1|0) = \frac{1}{N-N_p}\sum_{n=N_p+1}^{N} p_{k,n,m}(1|0)$$

$$\bar{p}(0|1) = \frac{1}{N-N_p}\sum_{n=N_p+1}^{N} p_{k,n,m}(0|1) \qquad \text{3-55}$$

Thus, the threshold value I_D for an optimal detection is theoretically the solution to the following equation:

$$\Lambda_{k,n,m}(I_D) = \frac{\bar{p}(0|1)}{\bar{p}(1|0)} = 1\ . \qquad \text{3-56}$$

The detection metric is defined based on the rule $i_d \underset{0}{\overset{1}{\gtrless}} I_D$ and can be applied for a given observation of detection. This scheme is referred to as PTD. Note that knowledge of the received signals i_d and $i_{p,1}$ are available. The detection merely requires noise statistics and marginal and joint fading distribution information, which was briefly discussed in Section 2.3.

3.7 Numerical Simulation

To aid in the analysis of the performance and effectiveness of the proposed LTD and PTD methods, this section details the numerical results obtained from computer simulations. BER is the key criterion of the performance evaluation demonstrated throughout the evaluation. The simulations assume a normalized lognormal fading as

$\mu_I = 1$, normalized transmitted power $2RP_t = 1$, and equal noise powers for symbols '0' and '1', $\sigma_0 = \sigma_1$. Noise power is varied to obtain different SNR values. The mean of the noise is constant throughout the simulation and set to I_0=0.2. Only one symbol '1' in the pilot field is assumed, thus $k = N_p = 1$ and $\tau/T_b = 500$. The proposed schemes do not make use of the CSI information of instantaneous channel coefficient; rather, the information of temporal joint and marginal PDFs is available at the receiver.

3.7.1 LTD Performance

The BER performance of the LTD method, BER_{LTD}, can be directly demonstrated by numerical computation of the expression. Any variation in noise power, signal power, or fading intensity fundamentally provides a change in BER. The underlying value of I_D is determined by numerically solving integral equation (3-36). As shown in Figure 3-11, a unique I_D for any given channel fading intensity and any given SNR value is shown in the figure. The results can be used as a lookup table to guarantee the receiver performance at high communication rates. Observations conclude that increasing SNR values results in a decrease of the threshold value, I_D. Assuming a fading strength of $\sigma_x = 0.4$, when the averaged SNR increases from 1dB to 17dB, I_D decreases from 0.52 to 0.34. Similar tendency is observed when the fading strength increases, e.g. I_D decreases from 0.61 to 0.41 when σ_x increases from 0.1 to 0.4 at SNR=10dB.

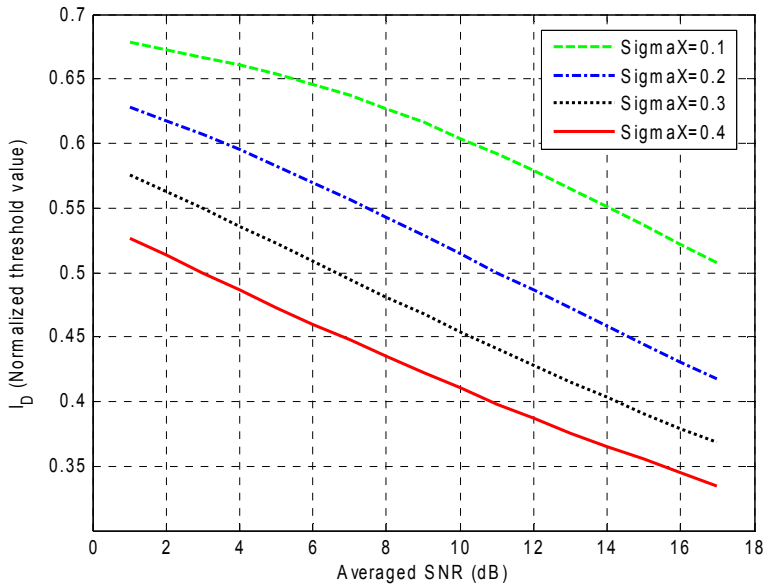

Figure 3-11: The threshold value of LTD method with SNR, while I_0=0.2 and for different values of σ_x

An example of BER performance for two different values of $\sigma_x = 0.1$ and 0.4 using the LTD method is shown in Figure 3-12. Although LTD provides similar performance when compared with the conventional S-by-S detection method, there is significant performance loss when compared to detection utilizing CSI.

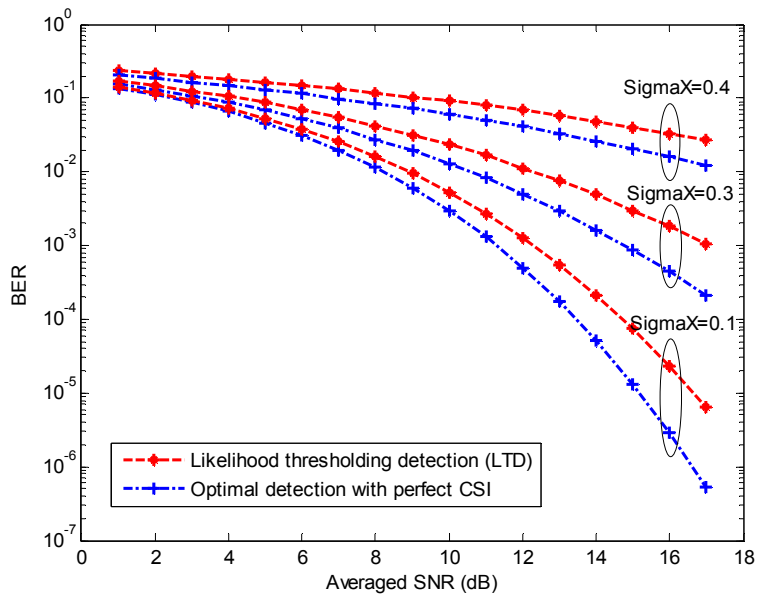

Figure 3-12: Probability of error using LTD detection method compared to that of detection with CSI for three different lognormal channels

3.7.2 Performance Comparison of PCD and PTD

Both PTD and PCD methods provide similar BER performance. This work used the slot structure in Figure 3-10 to send information symbols. The closest pilot symbol with respect to a received symbol is chosen for the PCD optimal detection of any received symbol. Thus, the detection of a received symbol $i_d(n,m)$ requires the first pilot symbol of the (m+1)-th slot if $n > (N - N_p)/2$. To perform a PCD method simulation, correlated random channel sequence $\mathrm{H} = \{h_n\}_{n=1}^{N_h}$ is needed for a very large number of N_h. However, finding sequence H is equivalent to knowing the Gaussian sequence $\mathrm{X} = \{X_1, X_2, \dots, X_{n_1}, \dots, X_{n_2}, \dots, X_{N_h}\}$. Applying a *Cholesky decomposition*[1] [111](Theorem 4.2.5) provides a correlated sequence X with a symmetric covariance matrix $\mathbb{C}_x$, similarly performed in [104](Sec. 12.11) when $N_h = 2$. Fortunately, Cholesky decomposition can

1- Also known as Cholesky factorization.

be calculated by a variety of mathematical software packages. The function is implemented in MATLAB as chol(.) or mvnrnd(.). Source codes are also available in other programming languages, including C++ [112]. A recently published work [113] has focused on the generation of correlated lognormal scintillation sequences. Such generating techniques can be exploited to generate fading samples, and then measure the error occurrences by applying the decision metric on the likelihood function. However, the BER analysis for correlated-based detection methods (e.g. PCD and PTD) is a time consuming procedure, especially for high SNRs where BER must be averaged over a large number of transmitted symbols. Additionally, using matrices in MATLAB instead of loops in C aids in the efficiency of numerical computation for three and four-dimensional integrations.

The BER performance comparison of the PTD method for a lognormal fading with $\sigma_x = 0.1$ is demonstrated in Figure 3-13. Two data slot sizes are considered in the simulation: N=200 and N=2000, while there is but one pilot symbol for each slot. Based on the above assumption, half of the symbols in a given slot use the pilot bit of the next slot. For example, to accomplish the detection of the first 999 symbols in case N=2000, the pilot symbol of the same slot is used, while the remaining 1000 symbols use the pilot bit of the next slot. From this figure, it becomes apparent that for a fading channel at an SNR of 17dB, the performance loss is as low as approximately 0.9dB and 1.3dB for N=200 and N=2000, respectively. The highest performance loss is numerically calculated to be approximately equal to 2dB when SNR is varied between 5 to 17 dB.

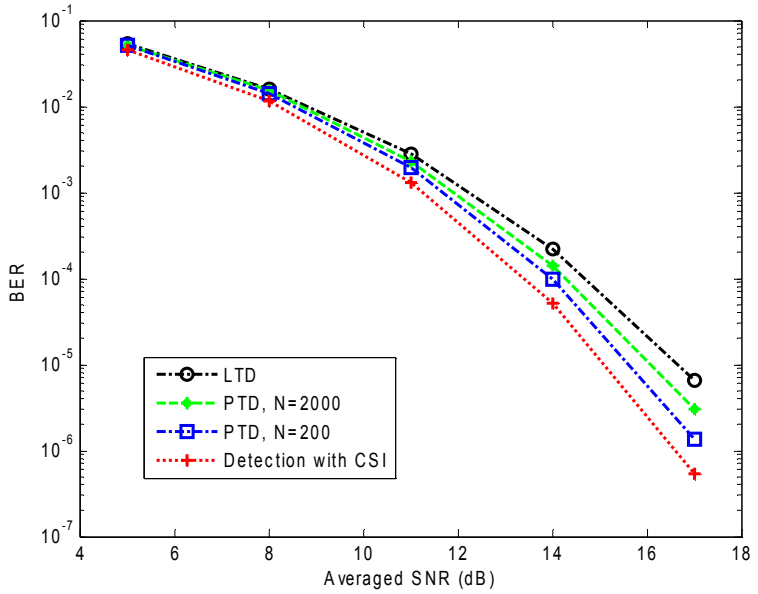

Figure 3-13: Comparing the probability of errors obtained for PTD detection, LTD detection, and detection with CSI methods, while $\sigma_\chi = 0.1$

Figure 3-14 presents the different detection schemes investigated in this chapter in terms of their BER performance and processing load. Table 3-1, on the other hand, provides numerical values of BER performance loss when compared to detection method using CSI information. The results are obtained while $\sigma_\chi = 0.1$, which represents a weak turbulence.

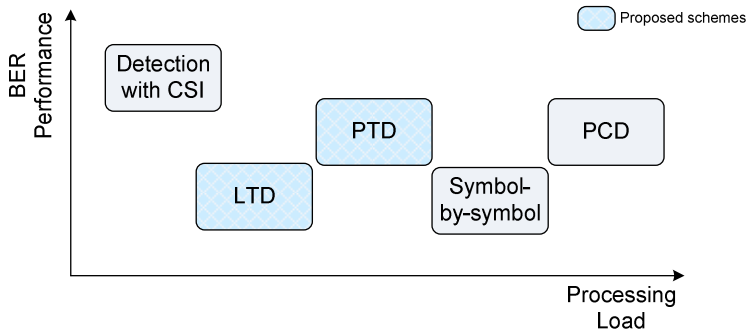

Figure 3-14: BER Performance comparison vs. processing load for different discussed detection schemes. LTD and PTD are suggested by this work

Table 3-1: Performance loss in dB at $\sigma_\chi = 0.1$ based on simulation analysis in Figure 3-13

Averaged SNR / Detection Method	$\bar{\gamma} = 8$	$\bar{\gamma} = 11$	$\bar{\gamma} = 14$	$\bar{\gamma} = 17$
LTD	1.3	1.7	1.8	2
PTD (*N*=2000)	0.9	1.1	1.2	1.3
PTD(*N*=200)	0.7	0.8	0.9	1

3.8 Concluding Results

With a goal to reduce the implementation complexity of an FSO receiver albeit keeping the system throughput, the feasibility of two threshold-based detection schemes without CSI was developed. These schemes reduce the computational load of the receiver at high data rates when assuming the fading and noise can be modeled as stationary random processes. In this case, the complex computations are done only once during the observation period. This reduced computation can be further reduced due to the dependency of detection threshold on only the fading strength and noise statistics (i.e., averaged received SNR).

Resultant from complex computations, which may or may not overload the receiver, the LTD method was shown to effectively reduce the computational load. However, this method comes with a slight loss of BER performance when compared to CSI detection schemes. The performance is, however, similar to symbol-by-symbol detection. Thus, the analysis found that the LTD method offers a trade-off between receiver complexity and BER performance improvement. To obtain superior BER performance for mutually correlated time-varying fading channels, the PTD method is also investigated and found

to operate on the basis of correlation between channel coefficients as temporal diversity. The resultant BER performance is remarkably better than LTD detection and can provide performance levels very close to CSI detection. The detection techniques proposed in this paper can be extended for FSO MIMO and cooperative systems to further enhance performance.

4. Switch-and-Stay and Switch-and-Examine Dual Diversity

Spatial diversity is widely adopted as a major approach toward performance improvement in wireless communications. This chapter proposes the application of two diversity schemes—switch-and-stay combining (SSC) and switch-and-examine (SEC) combining—in a dual-branch receiving optical wireless system. These schemes, when compared to the selection combining scheme, significantly lower the processing load associated with the monitoring of each branch's signal strength, thus reducing the complexity of the required hardware [114]. The reduction of processing load supports the typical high data rate that an optical wireless system is capable of offering.

4.1 Introduction

Existing spatial diversity and combining schemes have shown to significantly improve the performance of optical wireless communication systems [32], [33], [38], [94], [100], [115], [116], [117], [118]. The combining schemes studied and presented in previous works include SC, EGC, and MRC, i.e., OC. MRC implementation requires highly complex software and hardware; EGC and then SC complexity follow, respectively. SNR improvements achieved using EGC and MRC far exceed those achieved by a switching diversity scheme such as SC, SSC, or SEC. However, if dual

optical receiving apertures are placed further apart than the combined beam width with propagation-induced beam divergence and scintillation-caused spreading, it will possibly result in one aperture receiving a signal dominated by the actual transmitted data while another receives a signal dominated by noise. In this situation, using EGC for combining the signals from apertures causes server loss of signal quality. Furthermore, EGC and MRC require received aperture signals to be synchronized prior to combining when optical signals received on various apertures are exposed during Optical/Electrical conversion to a variety of delays. The aim of this chapter is to examine the processing load and BER performance of two switched diversity schemes—SSC, and SEC—compared to SC approach in a dual-branch optical system.

Utilization of spatial diversity for FSO applications was originally proposed in [94] and used EGC and SC schemes for signal combining in a lognormal channel. Tsiftsis, *et al*. in [32] have investigated BER of EGC, MRC, and SC over an independent and identically distributed (i.i.d.) K distribution turbulence model. Using Gamma-Gamma channel, Bayaki *et al.* in [38] have addressed diversity gain and BER in an uncorrelated channel model. Wang *et al.* in [115] applied SC for i.i.d. fading paths in a SIMO system configuration over Gamma-Gamma distribution model. Using MISO system setup, Garcia-Zambrana *et al.* in [116] have examined selection transmit diversity for an FSO system. A practical hardware design for a 7-channel MRC combiner is developed by Joyner *et al.* in [100] and is regarded as a low power, low noise, and cost-effective system-on-chip configuration. Khalighi *et al.* in [33] have evaluated the effect of aperture averaging and channel coding on EGC diversity to mitigate the effect of fading.

A wireless receiver applying SC scheme must constantly monitor signal strength of its multiple branches, and then select a branch with the highest SNR. Although seemingly simple, SC suffers from a high processing load due to persistent branch monitoring and repetitive switching, especially when the optical channel is highly faded due to atmospheric turbulence. These factors contribute to an increase in hardware complexity in optical wireless system implementation. Even so, SC is most practical for optical wireless implementation because optical links are subject to pointing and alignment errors. Alternatively, *Switched diversity* is viewed as a suboptimum implementation of SC [119], [120], as its BER performance is inferior to that of SC. Unlike SC diversity, switched diversity does not require persistent monitoring of all receiving signals.

This chapter investigates the application of two switched combining diversity schemes—SSC and SEC schemes—using a high speed FSO communication system. These schemes reduce implementation complexity resulting from a high processing load associated with the SC scheme. The processing load is defined as the average number of monitoring occurrences performed on each branch during an observation interval. A wireless receiver using SSC scheme monitors only the signal strength of the active branch. Once the instantaneous branch SNR drops below a threshold SNR γ_T, it switches to a new branch regardless of its SNR—even if the new branch is inferior to the original branch [119]. However, the developed SEC switches to a new branch only if its instantaneous SNR is higher than the threshold. If not, it selects the one with higher SNR. The SEC scheme has been developed to perform between SC and SSC schemes and will demonstrate that outage probabilities of SSC and SEC are equal to that of SC, [119](Sec. 9.9). Thus, SSC and SEC reduce software and hardware design complexity by

eliminating the persistent monitoring of all branches required by the SC scheme, significantly improving FSO system performance to support high data rate communication.

In this work, processing load and BER performance are investigated. IM/DD is assumed for the optical receiver. The FSO channel is lognormally distributed with spatially correlated irradiances due to atmospheric turbulence induced scintillation. The receiver is aware of instantaneous fading coefficients and CSI, of the time-varying channel. The last assumption indicates that the optical channel changes very slowly relative to the symbol rate, i.e., it is nearly constant over thousands of bits. In this case, a small number of pilot tones can give a significant amount of using the method discussed in section 3.4.4.

The remainder of this chapter is organized as follows: Section 2 offers a brief review of the system and channel model. Section 3 presents switched diversity based on an SSC concept, and Section 4 introduces switched diversity using an SEC combiner. Results of numerical simulation are presented in Section 5. Section 6 concludes the chapter.

4.2 System Model

The received optical signal in an FSO communication system is converted to an electrical signal by a photodetector. The resulting signal is a combination of faded modulated signal with additive noise [83], [121], as extensively discussed in the previous chapters. Without consideration of ISI, the receiver integrates received photocurrent for a bit interval. The instantaneous channel coefficient h, i.e., gain or irradiance, due to fading is commonly modeled as a lognormal distribution. It is given by $h = e^{2\chi}$, where log-amplitude χ is an identically distributed normal random variable with mean μ_χ and

standard deviation σ_χ, commonly referred to as Rytov parameter. For atmospheric channels with plane wave near ground and propagation distance near a few hundred meters, a $\sigma_\chi \geq 0.5$ represents strong turbulence, while $\sigma_\chi \leq 0.1$ denotes weak turbulence [121](Fig. 1). A longer propagation length and a lower wavelength cause stronger signal fading. Under small aperture size conditions, the instantaneous electrical SNR is defined by [122]

$$\gamma_i = \bar{\gamma} h_i^2 \quad ; \quad i = 1, 2 \tag{4-1}$$

where $\bar{\gamma}$ is defined as the branch average SNR, excluding the fading effect. Using an assumed modulation of NRZ OOK, $\bar{\gamma}$ is expressed by

$$\bar{\gamma} \triangleq \frac{R^2 P^2}{\sigma_v^2} \tag{4-2}$$

In above equation, $\sigma_v = \sqrt{N_0/2}$ is the standard deviation of noise with a spectral density N_0; this is assumed equal for both symbols '1' and '0' [34]. R is the receiver's responsivity, and P is the average optical power of OOK. Deterministic attenuation factors are neglected in the model. Note that $h_i \in \{h_1, h_2\}$ and $\gamma_i \in \{\gamma_1, \gamma_2\}$ are the instantaneous vectors of channel coefficients and SNRs for the dual optical branches, respectively. Using switching diversity, only one branch is selected at any given time. Symbol-by-symbol detection [122] based on the perfect availability of CSI knowledge is used for optical signal detection. It is further assumed the channel coefficients at different branches are identically distributed and correlated. Hence, an increase in the number of branches does not gain performance for SSC when N >2 [119], [120]. A dual-branch SIMO setup is shown in Figure 4-1.

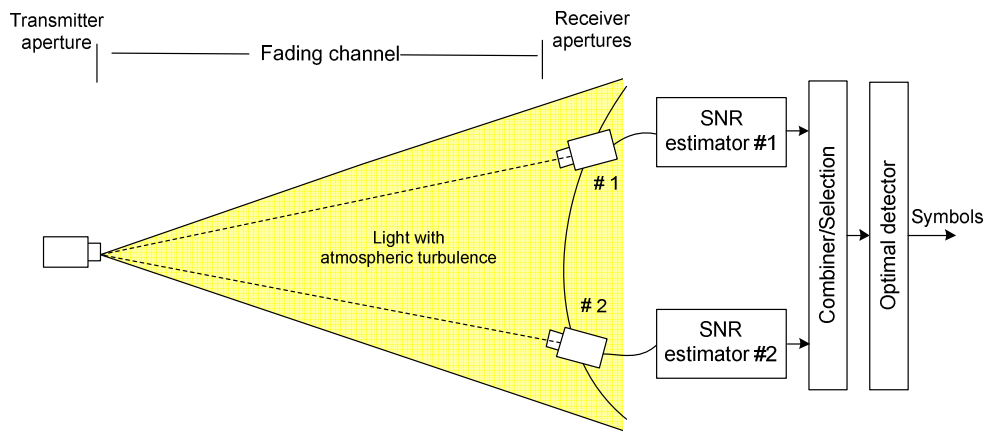

Figure 4-1: Design configuration of a dual-receiving FSO system model.

Since branches are balanced, $E[\gamma_1] = E[\gamma_2] = \bar{\gamma}$, implying branch average SNR normalization and resulting in $E[h_i^2] = 1$. Thus, using [83](Eq. 5), it can be shown that $\mu_\chi = -\sigma_\chi^2$. The marginal and joint PDF of SNR for the FSO channel are respectively expressed by the following equations

$$f_{\gamma_i}(\gamma_i) = \frac{1}{\sqrt{32\pi}\gamma_i\sigma_\chi}\exp\left[-\frac{\left(\ln(\gamma_i/\bar{\gamma})+4\sigma_\chi^2\right)^2}{32\sigma_\chi^2}\right] \quad 4\text{-}3$$

and

$$f_{\mathbf{\Gamma}}(\gamma_1,\gamma_2) = \frac{1}{32\pi\gamma_1\gamma_2\sigma_\chi^2\sqrt{1-\rho^2}}\exp\left\{-\frac{1}{32\sigma_\chi^2(1-\rho^2)}\left[\left(\ln(\gamma_1)-\ln(\bar{\gamma})+4\sigma_\chi^2\right)^2\right.\right.$$

$$\left.\left.+2\rho\left(\ln(\gamma_1)-\ln(\bar{\gamma})+4\sigma_\chi^2\right)\left(\ln(\gamma_2)-\ln(\bar{\gamma})+4\sigma_\chi^2\right)+\left(\ln(\gamma_2)-\ln(\bar{\gamma})+4\sigma_\chi^2\right)^2\right]\right\} \quad 4\text{-}4$$

where ρ is the spatial correlation coefficient between the paths, and the average SNR is given as $\mathbf{\Gamma} = \{\gamma_1, \gamma_2\}$. Tatarski [75], [90](Fig. 3.17) characterized and formulated the correlation coefficient as a function of the propagation length, separation distance between branches, and the optical signal wavelength. By means of experimental measurements, Anguita *et al.* [123] have demonstrated that such a correlation is a

function of receiver aperture size and, although not significant, turbulence strength, as well. A beam separation of at least 15cm is required to achieve a total signal decorrelation for a 200 m propagation length. Coherence length d_0 becomes the distance at which the channel correlation coefficient is equal to e^{-1}. By knowing the information on coherence length d_0, the correlation coefficient is expressed under conditions by $\rho = e^{-(d/d_0)^{5/3}}$ [90].

4.3 Switch-and-Stay Combining (SSC)

In the SIMO configuration, the received signals captured by the optical system apertures require combining—in this case selection before bit detection is performed, as shown in Figure 4-1. The combiner selects the appropriate branch based on its instantaneous SNR, while the detector optimally decodes the data bits. $\gamma[k]$ is defined as the instantaneous SNR at the output of the combiner at discrete time k. To statistically analyze the performance of the SSC scheme, the cumulative distribution function (CDF) or PDF of the resultant (combiner output) γ is needed. The CDF function is derived where $F_{SSC}(\gamma) = P(\gamma[k] \leq \gamma)$. Since the events of sequence $\{\gamma[k] = \gamma_i[k]\}_{i=1,2}$ are mutually exclusive, the CDF can be written as

$$F_{SSC}(\gamma) = P(\gamma[k] = \gamma_1[k] \text{ and } \gamma_1[k] \leq \gamma) + P(\gamma[k] = \gamma_2[k] \text{ and } \gamma_2[k] \leq \gamma)$$
$$= 2\,P(\gamma[k] = \gamma_n[k] \text{ and } \gamma_n[k] \leq \gamma) \qquad 4\text{-}5$$

where $n \in \{1, 2\}$ is the active branch, without loss of generality. The equality $\gamma[k] = \gamma_n[k]$ is valid in two possible cases:

$$\gamma[k] = \gamma_n[k] \text{ iff } \begin{cases} \gamma[k-1] = \gamma_m[k-1] \text{ and } \gamma_m[k] < \gamma_T \\ \gamma[k-1] = \gamma_n[k-1] \text{ and } \gamma_n[k] \geq \gamma_T \end{cases} \qquad 4\text{-}6$$

where $m \in \{1, 2\}$, $m \neq n$, is the inactive branch, and γ_T is the threshold SNR, i.e., *switching threshold*. It is assumed that the combining iteration period, defined as κ, is larger than the channel coherence time so that the correlated pair $\gamma_1[k]$ and $\gamma_2[k]$ are independent of their corresponding values at time $k-1$. The CDF representation in (4-5) is previously presented in [119](Eq. 9.269), and proof has been shown in [120]. It is expressed as

$$F_{SSC}(\gamma) = \begin{cases} P\{\gamma_1[k] < \gamma_T \text{ and } \gamma_2[k] \leq \gamma\} & \gamma < \gamma_T \\ P\{(\gamma_T \leq \gamma_1[k] \leq \gamma) \\ \quad \text{or } (\gamma_1[k] < \gamma_T \text{ and } \gamma_2[k] \leq \gamma)\} & \gamma \geq \gamma_T \end{cases} \tag{4-7}$$

Since the events $(\gamma_T \leq \gamma_1[k] \leq \gamma)$ and $(\gamma_1[k] < \gamma_T \text{ and } \gamma_2[k] \leq \gamma)$ are mutually exclusive, $F_{SSC}(\gamma)$ can be expressed as

$$F_{SSC}(\gamma) = \begin{cases} P\{\gamma_1[k] < \gamma_T \text{ and } \gamma_2[k] \leq \gamma\} & \gamma < \gamma_T \\ P(\gamma_T \leq \gamma_1[k] \leq \gamma) \\ \quad +P(\gamma_1[k] < \gamma_T \text{ and } \gamma_2[k] \leq \gamma) & \gamma \geq \gamma_T \end{cases} \tag{4-8}$$

Because all variables occur in time k, for the sake of simplicity, time instance is hereafter removed. Considering marginal PDF of $\gamma_n[k]$ in (3), the expression for $P(\gamma_T \leq \gamma_1 \leq \gamma)$ can be easily formulated in a closed-form as

$$P\{\gamma_T \leq \gamma_n \leq \gamma\} = \int_{\gamma_T}^{\gamma} f_\gamma(\gamma)\, d\gamma$$

$$= \begin{cases} 0 & \gamma < \gamma_T \\ Q\left(\frac{\ln(\gamma_T/\overline{\gamma}) + 4\sigma_\chi^2}{4\sigma_\chi}\right) - Q\left(\frac{\ln(\gamma/\overline{\gamma}) + 4\sigma_\chi^2}{4\sigma_\chi}\right) & \gamma \geq \gamma_T \end{cases} \tag{4-9}$$

The value for $P\{\gamma_1 < \gamma_T \text{ and } \gamma_2 \leq \gamma\}$ is achievable by recognizing that [124](App. B)

$P\{\gamma_1 \leq \gamma_T \text{ and } \gamma_2 \leq \gamma\} =$

$$1 - P\{\gamma_1 > \gamma_T\} - P\{\gamma_2 > \gamma\} + P\{\gamma_1 > \gamma_T \text{ and } \gamma_2 > \gamma\} \qquad 4\text{-}10$$

Therefore above equation can be rewritten in terms of the one- and two-dimensional Q-functions

$$P\{\gamma_1 \leq \gamma_T \text{ and } \gamma_2 \leq \gamma\} = 1 - Q\left(\frac{\ln(\gamma_T/\bar{\gamma}) + 4\sigma_\chi^2}{4\sigma_\chi}\right) - Q\left(\frac{\ln(\gamma/\bar{\gamma}) + 4\sigma_\chi^2}{4\sigma_\chi}\right)$$
$$+Q\left(\frac{\ln(\gamma_T/\bar{\gamma})+4\sigma_\chi^2}{4\sigma_\chi}, \frac{\ln(\gamma/\bar{\gamma})+4\sigma_\chi^2}{4\sigma_\chi}; \rho\right) \qquad 4\text{-}11$$

Finally, the CDF will be given by

$$F_{SSC}(\gamma) = \begin{cases} 1 - Q\left(\frac{\ln(\gamma_T/\bar{\gamma})+4\sigma_\chi^2}{4\sigma_\chi}\right) - Q\left(\frac{\ln(\gamma/\bar{\gamma})+4\sigma_\chi^2}{4\sigma_\chi}\right) \\ \quad + Q\left(\frac{\ln(\gamma_T/\bar{\gamma})+4\sigma_\chi^2}{4\sigma_\chi}, \frac{\ln(\gamma/\bar{\gamma})+4\sigma_\chi^2}{4\sigma_\chi}; \rho\right) & \gamma < \gamma_T \\ 1 - 2Q\left(\frac{\ln(\gamma/\bar{\gamma})+4\sigma_\chi^2}{4\sigma_\chi}\right) \\ \quad +Q\left(\frac{\ln(\gamma_T/\bar{\gamma})+4\sigma_\chi^2}{4\sigma_\chi}, \frac{\ln(\gamma/\bar{\gamma})+4\sigma_\chi^2}{4\sigma_\chi}; \rho\right) & \gamma \geq \gamma_T \end{cases} \qquad 4\text{-}12$$

The PDF of the resultant SNR γ can be mathematically determined by finding the derivative of the CDF with respect to γ. It is expressed by

$$f_{SSC}(\gamma) = \begin{cases} \frac{1}{\sqrt{32\pi}\gamma\sigma_\chi} \exp\left[-\frac{\left(\ln(\gamma/\bar{\gamma})+4\sigma_\chi^2\right)^2}{32\sigma_\chi^2}\right] \\ \quad \times \left(1 - Q\left[\frac{\ln(\gamma_T/\gamma^\rho \bar{\gamma}^{(1-\rho)})+4(1-\rho)\sigma_\chi^2}{4\sigma_\chi}\right]\right) & \gamma < \gamma_T \\ \frac{1}{\sqrt{32\pi}\gamma\sigma_\chi} \exp\left[-\frac{\left(\ln(\gamma/\bar{\gamma})+4\sigma_\chi^2\right)^2}{32\sigma_\chi^2}\right] \\ \quad \times \left(2 - Q\left[\frac{\ln(\gamma_T/\gamma^\rho \bar{\gamma}^{(1-\rho)})+4(1-\rho)\sigma_\chi^2}{4\sigma_\chi}\right]\right) & \gamma \geq \gamma_T \end{cases} \qquad 4\text{-}13$$

In the presence of perfect CSI information, the BER is found by averaging the error in optical channels over the fading probability density function. The BER expression of SSC is found by:

$$P_{SSC}^{e} = \int_{0}^{\infty} f_{SSC}(\gamma)\, Q(\sqrt{\gamma}) d\gamma \qquad \text{4-14}$$

An optimum value for γ_T, if any, minimizes the average BER of the signal after combining. The PDF of the resultant SNR can be alternatively expressed from the derivative of (8):

$$f_{SSC}(\gamma) = \begin{cases} g_{\gamma}(\gamma_T, \gamma) & \gamma < \gamma_T \\ f_{\gamma}(\gamma) + g_{\gamma}(\gamma_T, \gamma) & \gamma \geq \gamma_T \end{cases} \qquad \text{4-15}$$

where $g_{\gamma}(\gamma_T, \gamma)$ is defined by

$$g_{\gamma}(\gamma_T, \gamma) \triangleq \int_{0}^{\gamma_T} f_{\Gamma}(\gamma_1, \gamma)\, d\gamma_1 \qquad \text{4-16}$$

Thus, the average BER is expressed as

$$P_{SSC}^{e} = \frac{1}{\pi} \int_{0}^{\frac{\pi}{2}} \int_{0}^{\infty} g_{\gamma}(\gamma_T, \gamma) \exp\left(-\frac{\gamma}{2\sin^2\theta}\right) d\gamma\, d\theta$$

$$+ \frac{1}{\pi} \int_{0}^{\frac{\pi}{2}} \int_{\gamma_T}^{\infty} f_{\gamma}(\gamma) \exp\left(-\frac{\gamma}{2\sin^2\theta}\right) d\gamma\, d\theta \qquad \text{4-17}$$

Applying Fermat's theorem to find the optimum value for γ_T leads to finding the solution of the equation $\left.\frac{dP_{SSC}^{e}}{d\gamma_T}\right|_{\gamma_T^*} = 0$. Replacing P_{SSC}^{e} from above produces the following equation

$$\frac{1}{\pi} \int_{0}^{\frac{\pi}{2}} \int_{0}^{\infty} f_{\Gamma}(\gamma_T^*, \gamma) \exp\left(-\frac{\gamma}{2\sin^2\theta}\right) d\gamma\, d\theta - f_{\gamma}(\gamma_T^*) Q\left(\sqrt{\gamma_T^*}\right) = 0 \qquad \text{4-18}$$

Using the above equation to find γ_T^* is relatively complex; however, the solution may be achieved by numerical methods. If the special case where branches are assumed to be

spatially uncorrelated is considered, an exact closed-form expression for γ_T^* is produced by

$$\gamma_T^* = \left[Q^{-1}\left(\frac{1}{\pi}\int_0^{\frac{\pi}{2}} \mathcal{M}_\gamma\left(-\frac{1}{2\sin^2\theta}\right)\, d\theta\right)\right]^2 \quad \text{(uncorrelated branches)} \qquad 4\text{-}19$$

where Q^{-1} is the inverse Q-function and $\mathcal{M}_\gamma$ denotes MGF function of the SNR of a single branch, given by $\mathcal{M}_\gamma(s) = \int_0^\infty f_\gamma(\gamma)\, e^{s\gamma}\, d\gamma$, $-\infty < s < \infty$. The integral can be expressed in a closed form approximated by using Gauss–Laguerre quadrature [110]

$$\mathcal{M}_\gamma(s) \cong \frac{1}{\sqrt{\pi}}\sum_{i=1}^{N_p} w_i \exp\left[\bar{\gamma} e^{\sqrt{32}\sigma_\chi x_i - 2\sigma_\chi^2}\, s\right] \qquad 4\text{-}20$$

where $\{x_i\}_{i=1}^{N_p}$ are the roots of the N_p-th order Hermite polynomial $H_{N_p}(x)$, and $\{w_i\}_{i=1}^{N_p}$ are the associated weights. Abramowitz and Stegun [110](table 25.10) offer a table of abscissas and weights for values of $N_p < 20$. However, a N_p=5 provides an acceptable approximation for the above GMF function. The switching threshold level can be approximated as

$$\gamma_T^* \cong \left[Q^{-1}\left(\frac{1}{\sqrt{\pi}}\sum_{i=1}^{N_p} w_i\, Q\left(\sqrt{\bar{\gamma}} e^{\sqrt{8}\sigma_\chi x_i - \sigma_\chi^2}\right)\right)\right]^2 \quad \text{(uncorrelated branches)} \qquad 4\text{-}21$$

4.4 Switch-and-Examine Combining (SEC)

A receiver using the SEC diversity scheme will switch to the next branch when the current SNR value falls below the threshold SNR. The receiver maintains use of the new branch given that the SNR remains above the threshold. If not, then the branch with higher SNR is selected.

Similar to an SSC scheme, it is assumed that the combining iteration period κ is larger than the channel coherence time so that the correlated pair $\gamma_1[k]$ and $\gamma_2[k]$ are independent of their corresponding values at time $k-1$. m and n denote inactive and

active branches at time k, respectively. As in the SSC analysis section, $\gamma[k]$ is the combiner SNR output. Since events in the set $\{\gamma[k] = \gamma_i[k]\}_{i=1,2}$ are mutually exclusive, the CDF can be rewritten as

$$F_{SEC}(\gamma) = 2\,P(\gamma[k] = \gamma_n[k] \;\text{ and }\; \gamma_n[k] \leq \gamma) \qquad 4\text{-}22$$

The CDF may be expressed SEC as

$$F_{SEC}(\gamma) = 2\,P\{\gamma[k-1] = \gamma_m[k-1]\} \times P\left\{\begin{matrix} \gamma_m[k] \leq \gamma_T \\ \text{and } \gamma_m[k] \neq \max\{\gamma_1[k], \gamma_2[k]\} \\ \text{and } \max\{\gamma_1[k], \gamma_2[k]\} \leq \gamma \end{matrix}\right\}$$

$$+2P\{\gamma[k-1] = \gamma_n[k-1]\} \times P\{\gamma_T \leq \gamma_n[k] \leq \gamma\} \qquad 4\text{-}23$$

Substituting $\gamma = \infty$ in (4-22) results in $P\{\gamma[k] = \gamma_n[k]\} = 0.5$ and, similarly, $P\{\gamma[k-1] = \gamma_n[k-1]\} = P\{\gamma[k-1] = \gamma_m[k-1]\} = 0.5$. Thus the variables at time $k-1$ can be substituted by their values, and for the sake of simplicity, index k is removed hereafter. Also,

$$\gamma_{n_{\max}} \triangleq \max\{\gamma_1, \gamma_2\} \qquad 4\text{-}24$$

where $n_{\max}$ denotes the branch with greater SNR. Aperture $n_{\max}$ is equal to n at the time of switching. The CDF reduces to

$$F_{SEC}(\gamma) = P\{\gamma_m \leq \gamma_T \text{ and } n_{\max} = n \text{ and } \gamma_{n_{\max}} \leq \gamma\} + P\{\gamma_T \leq \gamma_n \leq \gamma\} \qquad 4\text{-}25$$

or equivalently,

$$F_{SEC}(\gamma) = P\{\gamma_m \leq \gamma_T \text{ and } \gamma_m < \gamma_n \text{ and } \gamma_n \leq \gamma\} + P\{\gamma_T \leq \gamma_n \leq \gamma\} \qquad 4\text{-}26$$

Based on the value of γ with respect to γ_T, two independent cases arise. If $\gamma < \gamma_T$, then

$$F_{SEC}(\gamma) = P\{\gamma_1 \leq \gamma \text{ and } \gamma_2 \leq \gamma\} = \int_0^{\gamma}\int_0^{\gamma} f_{\Gamma}(\gamma_1, \gamma_2)\, d\gamma_1\, d\gamma_2 \qquad 4\text{-}27$$

and if $\gamma \geq \gamma_T$, then

$$F_{SEC}(\gamma) = P\{\gamma_T \le \gamma_1 \le \gamma\} + P\{\gamma_1 \le \gamma_T \text{ and } \gamma_2 \le \gamma\}$$

$$= \int_{\gamma_T}^{\gamma} f_\gamma(\gamma)\, d\gamma + \int_0^{\gamma_T}\int_0^{\gamma} f_{\Gamma}(\gamma_1,\gamma_2)\, d\gamma_1\, d\gamma_2 \qquad 4\text{-}28$$

Following similar analyses provided in Section 3, above equation expresses the CDF of the resultant SNR:

$$F_{SEC}(\gamma) = \begin{cases} 1 - 2Q\left(\frac{\ln(\gamma/\overline{\gamma})+4\sigma_\chi^2}{4\sigma_\chi}\right) \\ \qquad + Q\left(\frac{\ln(\gamma/\overline{\gamma})+4\sigma_\chi^2}{4\sigma_\chi}, \frac{\ln(\gamma/\overline{\gamma})+4\sigma_\chi^2}{4\sigma_\chi}; \rho\right) & \gamma < \gamma_T \\ 1 - 2Q\left(\frac{\ln(\gamma/\overline{\gamma})+4\sigma_\chi^2}{4\sigma_\chi}\right) \\ \qquad + Q\left(\frac{\ln(\gamma_T/\overline{\gamma})+4\sigma_\chi^2}{4\sigma_\chi}, \frac{\ln(\gamma/\overline{\gamma})+4\sigma_\chi^2}{4\sigma_\chi}; \rho\right) & \gamma \ge \gamma_T \end{cases} \qquad 4\text{-}29$$

By comparing the CDF of SEC to that of SSC, it can be observed that the CDF expression for SEC is similar to that of SSC for $\gamma \ge \gamma_T$, while the PDF $f_{SEC}(\gamma)$ is derived to be

$$f_{SEC}(\gamma) = \begin{cases} \frac{1}{\sqrt{32\pi}\gamma\sigma_\chi} \exp\left[-\frac{\left(\ln(\gamma/\overline{\gamma})+4\sigma_\chi^2\right)^2}{32\sigma_\chi^2}\right] \\ \qquad \times \left(2 - 2Q\left[\frac{(1-\rho)\ln(\gamma/\overline{\gamma})+4(1-\rho)\sigma_\chi^2}{4\sigma_\chi}\right]\right) & \gamma < \gamma_T \\ \frac{1}{\sqrt{32\pi}\gamma\sigma_\chi} \exp\left[-\frac{\left(\ln(\gamma/\overline{\gamma})+4\sigma_\chi^2\right)^2}{32\sigma_\chi^2}\right] \\ \qquad \times \left(2 - Q\left[\frac{\ln(\gamma_T/\gamma^\rho\overline{\gamma}^{(1-\rho)})+4(1-\rho)\sigma_\chi^2}{4\sigma_\chi}\right]\right) & \gamma \ge \gamma_T \end{cases} \qquad 4\text{-}30$$

When using the SEC diversity scheme, BER is found by replacing $f_{SSC}(\gamma)$ by $f_{SEC}(\gamma)$: $P_{SEC}^e = \int_0^\infty f_{SEC}(\gamma)\, Q(\sqrt{\gamma}) d\gamma$.

The CDF of SEC is recalled as

$$F_{SEC}(\gamma) = \begin{cases} P\{\gamma_1[k] < \gamma \text{ and } \gamma_2[k] \le \gamma\} & \gamma < \gamma_T \\ P(\gamma_T \le \gamma_1[k] \le \gamma\ ) + \\ \quad P(\gamma_1[k] < \gamma_T \text{ and } \gamma_2[k] \le \gamma) & \gamma \ge \gamma_T \end{cases} \tag{4-31}$$

and the PDF of the resultant SNR can be determined by calculating the derivative of above equation

$$f_{SEC}(\gamma) = \begin{cases} f_{\Gamma}(\gamma, \gamma) & \gamma < \gamma_T \\ f_{\gamma}(\gamma) + g_{\gamma}(\gamma_T, \gamma) & \gamma \ge \gamma_T \end{cases} \tag{4-32}$$

The average BER is then rewritten as

$$\begin{aligned} P_{SEC}^{e} = \frac{1}{\pi}\int_0^{\frac{\pi}{2}}\int_0^{\gamma_T} f_{\Gamma}(\gamma,\gamma)\exp\left(-\frac{\gamma}{2\sin^2\theta}\right)d\gamma\, d\theta \\ + \frac{1}{\pi}\int_0^{\frac{\pi}{2}}\int_{\gamma_T}^{\infty} g_{\gamma}(\gamma_T,\gamma)\exp\left(-\frac{\gamma}{2\sin^2\theta}\right)d\gamma\, d\theta \\ + \frac{1}{\pi}\int_0^{\frac{\pi}{2}}\int_{\gamma_T}^{\infty} f_{\gamma}(\gamma)\exp\left(-\frac{\gamma}{2\sin^2\theta}\right)d\gamma\, d\theta \end{aligned} \tag{4-33}$$

When $\gamma_T = 0$, the SEC diversity scheme provides BER performance similar to a single branch receiving system. In contrast, when $\gamma_T = \infty$, as the second and third terms of above equation are eliminated, the average BER of the SEC converges to that of SC whose BER performance is optimal among the switched diversity schemes. The minima or maxima values are evaluated by finding the solution for the equation $\left.\frac{dP_e}{d\gamma_T}\right|_{\gamma_T^*} = 0$, leading to

$$f_{\gamma}(\gamma_T^*)\int_0^{\frac{\pi}{2}}\exp\left(-\frac{\gamma_T^*}{2\sin^2\theta}\right)d\theta = 0 \tag{4-34}$$

Solutions of this equation for γ_T^* are $\gamma_T^* = 0$ (minima) and $\gamma_T^* = \infty$ (maxima) that provide the minimum and maximum BER performance levels, respectively. The equation shows

that the higher the switching threshold level, the lower average BER. However, a high threshold level causes frequent branch monitoring and, consequently, repetitive switching among branches; a low value maintains the receiver connection to one branch. Thus, selection of the threshold level for SEC is a tradeoff between receiver complexity and BER performance.

4.5 Numerical Simulation

This section presents numerical results using computer simulations for investigating the performance of SSC and SEC switched diversity in a dual-branch FSO receiver. The average BER performance is obtained and compared to that of the SC combiner. The effect of optimum threshold will also be examined. Numerical calculation of the provided BER expression is used when evaluating BER of SSC. Similar analysis is repeated for SEC with no optimum threshold available for SEC. Uncorrelated branches are assumed when SC is examined. BER of SC is similarly found by $P_{SC}^{e} = \int_0^\infty f_{SC}(\gamma)\, Q(\sqrt{\gamma})d\gamma$, where $f_{SC}(\gamma)$ is the PDF of the resultant SNR under SC diversity. The CDF of two uncorrelated paths employing SC diversity is given by $F_{SC}(\gamma) = P\{\gamma_1 \leq \gamma\}P\{\gamma_2 \leq \gamma\} = \left(F_\gamma(\gamma)\right)^2$. The BER mathematically becomes

$$P_{SC}^{e} = 2\int_0^\infty f_\gamma(\gamma)\, F_\gamma(\gamma) Q\left(\sqrt{\gamma}\right)d\gamma \qquad \text{(uncorrelated branches)}$$

$$= \frac{1}{\sqrt{8\pi}\sigma_\chi}\int_0^\infty \frac{1}{\gamma}\exp\left[-\frac{\left(\ln(\gamma/\bar{\gamma})+4\sigma_\chi^2\right)^2}{32\sigma_\chi^2}\right] Q\left[-\frac{\ln(\gamma/\bar{\gamma})+4\sigma_\chi^2}{4\sigma_\chi}\right] Q(\sqrt{\gamma})d\gamma \qquad \text{4-35}$$

Although an approximate closed-form expression can be derived using Gauss-Hermite quadrature, numerical computation is used to plot the BER of SC with two uncorrelated

paths. Readers are referred to references [119], [124] and [125] for a more detailed derivation on the selection combining scheme analysis.

The performance of SSC is dependent on the value of the switching SNR threshold γ_T. The selection of an inappropriate value may possibly degrade its performance to that of a single branch system. The optimum SNR threshold for uncorrelated branches is previously given. The plots given in Figure 4-2 for a correlated branch with $\sigma_\chi = 0.2$ and $\bar{\gamma} = 20$ dB are numerically calculated using computer simulation. As expected, degradation in SSC performance emerges when the correlation between channels becomes stronger. Figure 4-3 highlights the relation between the BER, SNR threshold, and channel correlation coefficient. It demonstrates system BER performance as affected by correlation coefficient and switching threshold. The selection of γ_T has an important influence on the SSC performance. However, selecting either an extremely low or high threshold value provides approximately equivalent BER performance when the paths are fully correlated. Figure 4-4 demonstrates the BER performance of SSC with respect to the branch average SNR, $\bar{\gamma}$, under various spatial fading correlations while using the calculated optimum threshold value. Take for example, at a $\bar{\gamma}$ =20dB and $\sigma_\chi = 0.1$, BER is 3×10^{-11} for uncorrelated paths. The achieved performance is approximately 100 times superior to that of a single receiver—in other words, a gain of 1.8dB in SNR is achieved. There is, however, a loss of 1dB when compared to the SC scheme with dual branch system. Figure 4-4 shows the best performance SSC can achieve when using the optimum threshold; it demonstrates that SSC scheme is unlikely to provide a BER performance as good as SC. Note that Figure 4-4 includes the BER performance using only the SC scheme for the uncorrelated dual-branch system.

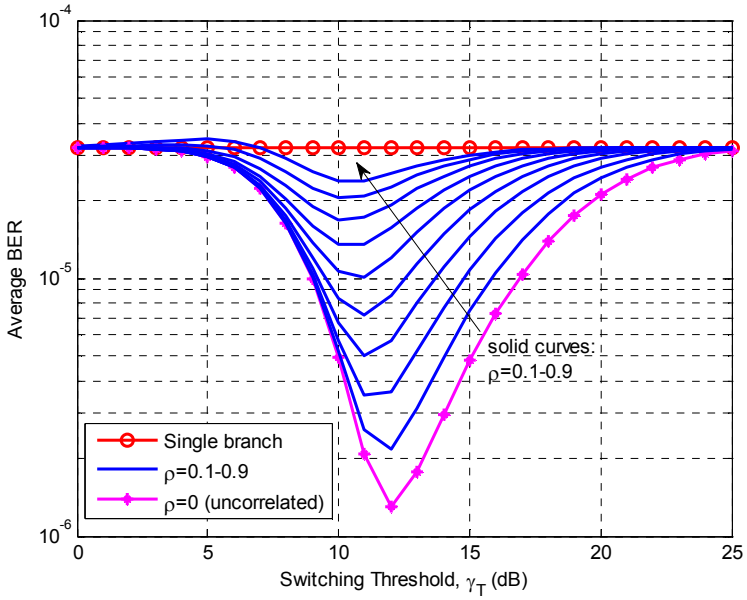

Figure 4-2: Bit error rate vs. switching threshold γ_T for several different values of correlation coefficients ρ using a dual-branch SSC combining. $\sigma_\chi = 0.2$ and $\bar{\gamma} = 20$dB

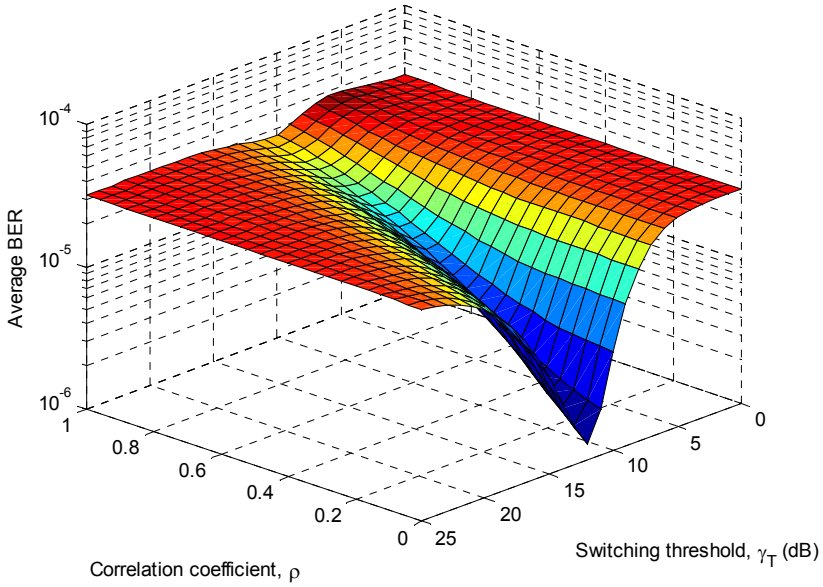

Figure 4-3: 3-D demonstration of bit error rate vs. switching threshold γ_T and correlation coefficient ρ in a dual-branch SSC. $\sigma_\chi = 0.2$ and $\bar{\gamma} = 20$dB

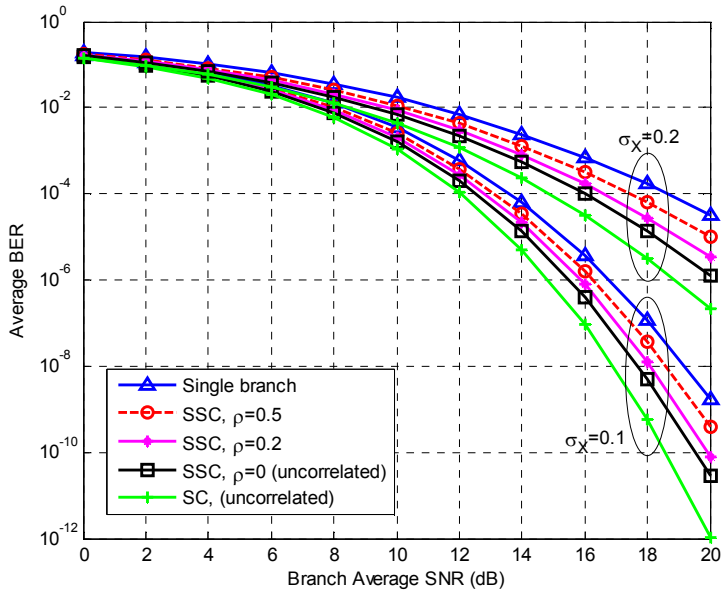

Figure 4-4: A comparison of bit error rate of dual-branch SSC scheme vs. average SNR $\bar{\gamma}$ when optimum threshold level is applied

As mentioned in Section 4.4, a dual-branch receiver using the SEC scheme has no optimum switching threshold for optimizing BER performance. Low values of γ_T degrade the BER performance to a single-branch receiver, i.e., no diversity; while high values of γ_T converge BER performance similar to that obtained by a dual-branch receiver using SC scheme. This requires persistent monitoring of the receiver branches, thus increasing the processing load. The average BER of SEC scheme for $\sigma_\chi = 0.2$ and $\rho = 0.1$ is shown in Figure 4-5. The figure presents the effect of the correlation coefficient along with the switching threshold value on BER. It confirms that the changes of ρ cause negligible BER variation when γ_T value is low, resulting in a BER of SEC that converges with one obtained using a single branch system. In contrast, when γ_T values are relatively high, the mutual correlation between branches degrades BER performance considerably. Like SSC, the selected switching threshold γ_T in SEC has a direct impact

on BER performance. Specifically, for $\sigma_\chi = 0.2$ (fading strength) and $\bar{\gamma} = 20$ dB (average branch SNR), BER is 1.83×10^{-7} for $\rho = 0$ (uncorrelated branches) $\gamma_T > 15$dB; and is 1.71×10^{-5} for $\rho = 1$ (fully correlated branches) and $0\,\text{dB} < \gamma_T < 25\,\text{dB}$. The former BER is similar to that obtained using SC diversity; the latter denotes no diversity.

Finding a suitable value for the switching threshold of SEC scheme is influenced by the tradeoff between branch monitoring occurrences and BER performance. The higher the switching threshold level, the lower the average BER. As shown in Figure 4-6, at one value of $\bar{\gamma}$, BER asymptotically becomes extremely small as γ_T increases. However, increasing γ_T directly impacts the processing load, causing it to become higher. If $\gamma_T = \bar{\gamma}$ (average branch SNR) is chosen, BER performance of SEC closely resembles that of SC, as shown in Figure 4-7.

Processing load as a result of switching diversity scheme implementation is defined as the average number of branch monitoring occurrences within a given observation period. Using this definition, the *additional processing load* (APL) due to monitoring the inactive branches in our dual branch system is always 1 for SC and $\epsilon\kappa/\tau$ for SSC and SEC, where ϵ is the number of monitoring occurrences of inactive branches within an observation period of τ, while κ is a single combining iteration period. APL shown in Figure 4-8 is measured using computer simulation. Threshold crossing triggers SNR evaluation of the inactive branch for switching purposes. Processing load is related and determined by counting the number of downward threshold crossings that occur when the active branch instantaneous SNR falls below the threshold. Figure 4-8 shows that the SSC scheme reduces APL by approximately 91% over SC at a branch average SNR of $\bar{\gamma} = 17$ dB when using optimum threshold. An SEC scheme reduces APL by

approximately 35% over SC at a branch average SNR of $\bar{\gamma} = 17\text{dB}$ using threshold $\gamma_T = \bar{\gamma}$. APL is constant for SEC and decreases for SSC as average branch SNR increases. Additionally, simulation observation demonstrated that APL is nearly unchanged as the correlation becomes stronger.

Finding the optimal threshold could be considered a drawback of implementing switched diversity in practice. Since the threshold is dependent upon average branch SNR and Rytov parameter and not on CSI, a look up table can be simply developed to allow practical implementation of a switched diversity FSO system. This paper applies switched diversity SEC for a dual receiving diversity SIMO system. The same approach could be extended to examine systems with a higher number of apertures in a MIMO setup. This work also uses OOK modulation in the analyses; however, other common modulation formats for FSO, e.g., the multicarrier technique in [126], can be similarly applied.

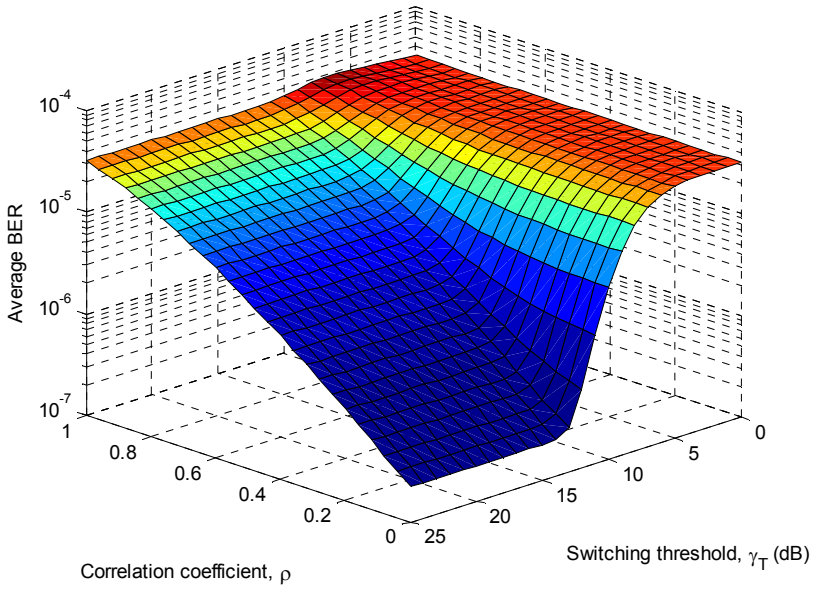

Figure 4-5: Bit error rate vs. switching threshold γ_T and correlation coefficient ρ using a dual-branch SEC combining at $\sigma_\chi = 0.2$ and $\bar{\gamma} = 20\text{dB}$

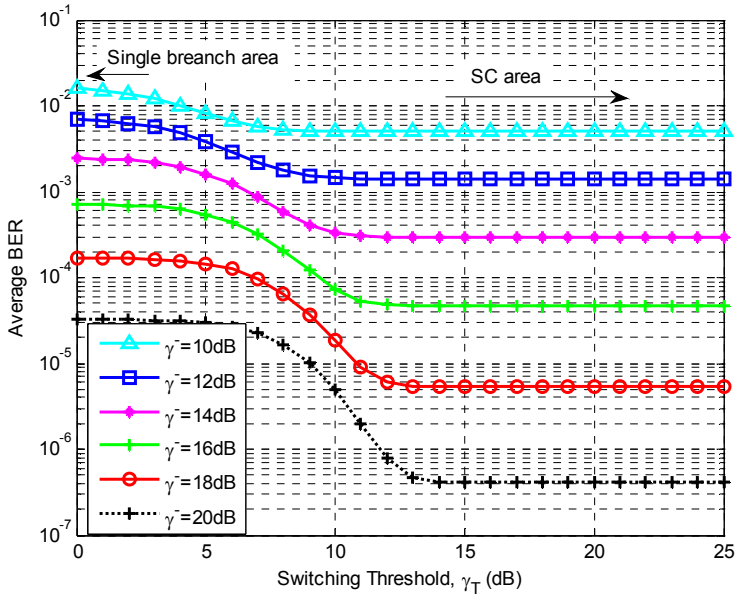

Figure 4-6: Bit error rate vs. switching threshold γ_T for several different values of $\bar{\gamma}$ using a dual-branch SEC combiner. $\sigma_\chi = 0.2$ and $\rho = 0.1$

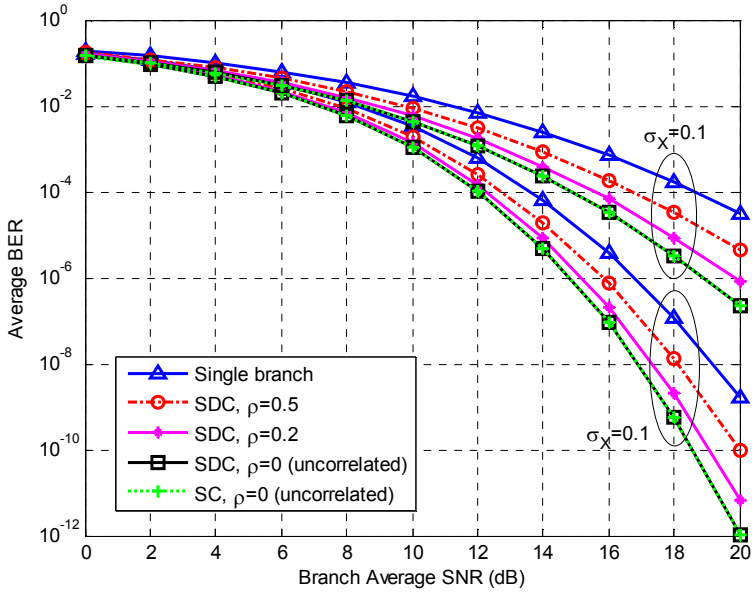

Figure 4-7: A comparison of bit error rate of dual-branch SEC scheme vs. average SNR $\bar{\gamma}$ when switching threshold is chosen as $\gamma_T = \bar{\gamma}$

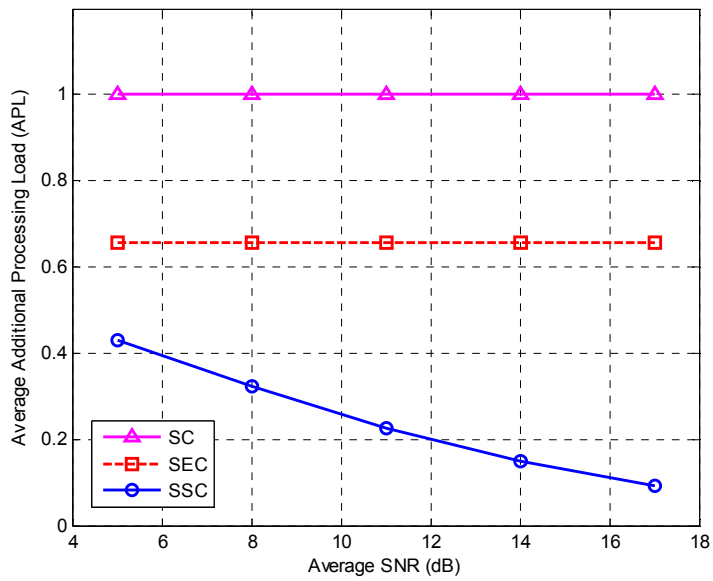

Figure 4-8: Additional processing load (APL) due to diversity combining. $\sigma_\chi = 0.2$ and $\rho = 0$

4.6 Concluding Results

This chapter presented two promising switched diversity schemes for a dual-branch optical receiving system, namely SSC and SEC. Both maintain an acceptable BER performance and achieve a significant reduction in processing load. Switching scenarios are analytically and numerically evaluated under lognormally correlated fading channels. Unlike SC, SSC and SEC schemes examine SNR values of a new branch only when switching is deemed necessary. These are suitable for multi-receiving high speed FSO systems undergoing misalignment issues.

The BER performance achieved by a dual branch SSC combiner ranges from that of a single branch to an optimal value. Although SSC cannot provide a BER performance comparable to that of SC, it contributes in reducing processing load—a significant outcome, especially in that FSO systems offer high data rate communication. Unlike SSC, SEC can achieve an approximate BER performance that is close to that of SC by choosing an ample switching threshold value. The higher the threshold value, the higher

the processing load due to diversity. Threshold level selection for SEC is, therefore, a tradeoff between BER performance and receiver complexity. With a threshold value of $\gamma_T = \bar{\gamma}$, numerical simulations exhibit a comparably close BER performance with SC (Figure 4-7).

5. Switch-to-Dominant Combining Diversity

As discussed in the previous chapter, among all the diversity combining schemes, switched diversity has low complexity and is simple to implement. In this chapter, an innovative spatial diversity scheme based on switched diversity is proposed. The scheme, namely switch-to-dominant combining (SDC), contributes to a superior BER performance when compared to conventional switched diversity schemes [127], including switch-and-stay and switch-and-examine diversity. The optical multi-receiver wireless system operates in a spatially correlated and lognormally distributed fading channel.

5.1 Introduction

Optimal detection of FSO signals with a data rate measuring in Gigabits is cause for an enormous processing load at the receiver's detector. The load is intensified even more if a diversity solution is exploited. Although conventional SC diversity systems are considered the most practical diversity technique for wireless optical systems, in particular those with angular diversity, they suffer from high processing load, persistent branch monitoring, and repetitive switching, increasing implementation complexities even more. Likewise, MRC introduces a severe processing load and is very sensitive to channel estimation error, especially for signals with low SNR [119]. EGC is particularly

inefficient for systems that have branches with acutely low SNR conditions. Misalignment in FSO-based systems makes EGC not practical for diversity purposes.

This chapter focuses on switched diversity combining approach which can potentially reduce such implementation complexities in optical receiver diversity systems. Several schemes employ variations based on defined switching strategies. Two schemes are discussed in chapter 4. SSC [119], [120], [125], [128] scheme switches to an alternate branch once the existing received SNR drops below a threshold γ_T, regardless of the new branch's SNR—even if it is inferior to the original branch. SEC diversity [128], [129] is similar to SSC with one minor modification. If SNR drops below the threshold, switching continues to alternate between branches until an acceptable SNR is observed. Although SSC and SEC systems have relatively low hardware complexities [114], their BER performance is inferior compared to SC diversity, which is a major disadvantage for current switched diversity techniques. Additionally, SSC does not improve the BER performance for N >2 as long as the branches are identically distributed [128].

This chapter proposes a modified switching scheme in which all branches are examined subsequent to the detection of low SNR quality for the current branch. The scheme ensures the branch with the highest SNR value is selected. When employed in optical wireless systems, the new scheme, referred to throughout this dissertation as SDC diversity, offers BER performance superior to SSC and SEC diversity schemes [127]. BER performance, processing load, and outage probability parameters are investigated over a lognormal atmosphere turbulence model. This research is the first of its kind to propose a modified switched diversity for multi-receiving wireless optical links.

Chapter 4 has previously provided the study of SSC and SEC performance in a dual branch receiving setup of FSO system [114].

The balance of this chapter is organized as follows: Section 5.2 offers a brief review of system and channel models. Section 5.3 introduces switching diversity using an SDC combiner. Numerical simulation results are presented in Section 5.4. Finally, concluding results are enumerated in Section 5.5.

5.2 System Model

The typical structure of an N-receiving SIMO system is illustrated in Figure 5-1 and shows balanced configuration when a receiver's apertures are aligned with the optical transmitter.

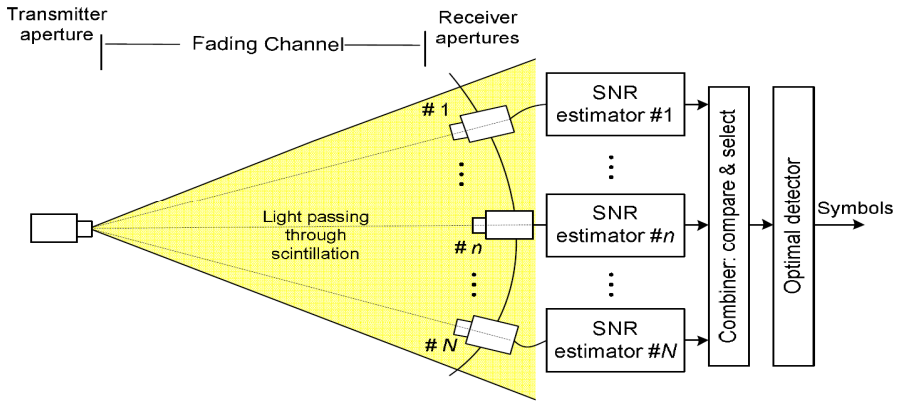

Figure 5-1: Setup configuration of a multi-receiving FSO system model.

The modulation format is the popular OOK intensity modulation with direct detection using a small detector. In this case, the received electrical current $r_i[k]$ for any corresponding channel coefficient $h_i[k]$ at receiver i at discrete-time k can be obtained by Eq. (2-1). Assuming a discrete-time sampling, the time index k is neglected in the analysis. The instantaneous electrical SNR for each branch will be defined by Eq. (4-1). The branches are assumed balanced, thus, the non-fading part of the average SNR is

identical for all apertures $i = 1, \dots, N$, and is given by (4-2). It is assumed that CSI is readily available at the receiver, indicating that the variation of fading intensities is relatively slow thus enabling the receiver to effectively estimate the coefficients. Fading coefficient has a lognormal distribution. The paths are assumed identically faded.

PDF and CDF of instantaneous branch SNR for the given branch i, known as marginal distributions, then, yield

$$f_{\gamma_i}(\gamma_i) = \frac{1}{\sqrt{32\pi}\gamma_i\sigma_\chi} \exp\left[-\frac{\left(\ln(\gamma_i/\bar{\gamma})+4\sigma_\chi^2\right)^2}{32\sigma_\chi^2}\right] \qquad 5\text{-}1$$

and

$$F_{\gamma_i}(\gamma_i) = 1 - Q\left[\frac{\ln(\gamma_i/\bar{\gamma})+4\sigma_\chi^2}{4\sigma_\chi}\right] \qquad 5\text{-}2$$

respectively, denoting that γ is also lognormally distributed. Since the channel coefficients $\mathbf{H} \triangleq \{h_i\}_{i=1}^N$ are correlated, the vector of SNR described by $\mathbf{\Gamma} \triangleq \{\gamma_i\}_{i=1}^N = \{h_i^2\bar{\gamma}_i\}_{i=1}^N$, has correlated elements as well. In this case, PDF of the correlated fading coefficients is jointly lognormal, given by

$$f_{\mathbf{\Gamma}}(\gamma_1, \gamma_2, \dots, \gamma_N) = \frac{\exp\left(-\frac{1}{32}(\ln[\mathbf{\Gamma}]-\ln[\bar{\mathbf{\Gamma}}]-4\bar{\mathbf{\Psi}})\Sigma_\chi^{-1}(\ln[\mathbf{\Gamma}]-\ln[\bar{\mathbf{\Gamma}}]-4\bar{\mathbf{\Psi}})^T\right)}{4^N(2\pi)^{\frac{N}{2}}\left(\det\left[\Sigma_\chi\right]\right)^{\frac{1}{2}}\mathrm{P}[\mathbf{\Gamma}]} \qquad 5\text{-}3$$

where $\mathrm{P}[\mathbf{\Gamma}] \triangleq \prod_{i=1}^N \gamma_i$ is the product function of γ_i's, and $\bar{\mathbf{\Gamma}} \triangleq [\bar{\gamma}\ \ \bar{\gamma}\ \ \dots\ \bar{\gamma}]_{1\times N}$ is the mean vector of SNR. Also, $\bar{\mathbf{\Psi}}$ is expressed by $\bar{\mathbf{\Psi}} = [-\sigma_x^2\ \ -\sigma_x^2\ \ \dots -\sigma_x^2]_{1\times N}$, when the paths are identically faded, i.e., correlated and identically distributed (c.i.d.). Here, Σ_χ is the covariance matrix in Eq. (3-18). The correlation coefficient $\rho_{i,j}$, $0 \le \rho_{i,j} \le 1$, is dependent by coherence length. Coherence length d_0 is approximated by the Fresnel length $d_0 \approx \sqrt{\lambda L}$. The simultaneous reception from multiple receive apertures does not require relatively large receiver/transmitter separation distance; uncorrelated FSO links

can be achieved by placing the receive apertures just a few centimeters apart [37], [123], [130], [131].

5.3 Performance of Switch-to-Dominant Combining (SDC)

This section analytically evaluates the performance of the proposed SDC combining. The functionality of older switched diversity schemes, i.e., SSC and SEC, are studied in chapter 4.

5.3.1 SDC Switching Scenario

This work follows an SEC similar, but more generalized, approach to the development of SDC scheme. An SDC combiner examines the quality of all branches immediately following the observation of a below threshold drop in the SNR level. The branch with the highest quality SNR is then chosen. SDC is in fact a hybrid SEC/SC scheme. The scheme has higher processing load than SSC and SEC; but its BER performance is improved over that of SSC and SEC. Furthermore, increasing the number of branches results in even further BER improvements.

In order to statistically analyze the performance of SDC scheme, the CDF or PDF statistics of γ are needed. Let's include the discrete time index k in the following analytical discussion. It is assumed that the receiver stays connected with the new branch for a significant duration of time within the range of channel coherence time. Then CSI is periodically re-estimated. Thus if a switching is needed, it occurs at time

$$t_{\text{comb}} = k\tau \qquad \text{5-4}$$

where τ, $\tau \geq \tau_c$, is the combining iteration period (τ_c is the channel coherence time). Without loss of generality, suppose that a downward crossing of the switching threshold

has occurred at time $k-1$ and the N-branch receiver is currently (time k) connected to branch n. To avoid confusion of notation, several definitions are recalled:

$\gamma_n[k]$: received SNR at branch n at time k

$\gamma[k]$: combined (output) SNR at time k

γ: combined (output) SNR variable, i.e., instantaneous SNR of the combiner's output

$\bar{\gamma}$: average branch SNR with no fading effect

γ_T: switching threshold level of SNR

γ_{out}: outage threshold

m: active branch at time $k-1$ but inactive at time k

n: active branch at time k

Therefore, γ_T is a physical layer parameter set based on switching scheme optimization, while γ_{out} is preset by higher layers. It will be shown that a minimal outage leads to $\gamma_T = \gamma_{out}$.

By definition, the CDF function of SDC is expressed by $F_{SDC}(\gamma) = P(\gamma[k] \leq \gamma)$. Due to the fact that the events of sequence $\{\gamma[k] = \gamma_i[k]\}_{i=1}^{N}$ are mutually exclusive, the CDF can be expressed as:

$$F_{SDC}(\gamma) = N\, P(\gamma[k] = \gamma_n[k] \text{ and } \gamma_n[k] \leq \gamma) \qquad 5\text{-}5$$

Using an SDC switching strategy, event $\gamma[k] = \gamma_n[k]$ only occur in cases, where

$$\gamma[k]=\gamma_n[k] \quad \text{iff} \quad \begin{cases} \gamma[k-1]=\gamma_1[k-1] \ \cap \ \gamma_1[k]<\gamma_T \\ \quad \cap \ \gamma_n[k]=\max\{\gamma_1,\gamma_2,\dots,\gamma_N\} \\ \text{or} \\ \gamma[k-1]=\gamma_2[k-1] \ \cap \ \gamma_2[k]<\gamma_T \\ \quad \cap \ \gamma_n[k]=\max\{\gamma_1,\gamma_2,\dots,\gamma_N\} \\ \text{or} \\ \vdots \\ \gamma[k-1]=\gamma_n[k-1] \ \cap \ \gamma_n[k]<\gamma_T \\ \quad \cap \ \gamma_n[k]=\max\{\gamma_1,\gamma_2,\dots,\gamma_N\} \\ \text{or} \\ \gamma[k-1]=\gamma_n[k-1] \ \cap \ \gamma_n[k]\geq\gamma_T \\ \text{or} \\ \vdots \\ \gamma[k-1]=\gamma_N[k-1] \ \cap \ \gamma_N[k]<\gamma_T \\ \quad \cap \ \gamma_n[k]=\max\{\gamma_1,\gamma_2,\dots,\gamma_N\} \end{cases} \qquad 5\text{-}6$$

Noting that the events of sequence $\gamma[k-1]=\gamma_i[k-1]\,, i=1,2,\dots,N$ are mutually exclusive and that the occurrence probability of each case is $1/N$, the CDF becomes

$$F_{SDC}(\gamma)=\sum_{i=1}^{N} P\left\{\begin{matrix} \gamma[k-1]=\gamma_i[k-1] \text{ and } \gamma_i[k]<\gamma_T \text{ and} \\ \gamma_n[k]=\max\{\gamma_1[k],\gamma_2[k],\dots,\gamma_N[k]\} \\ \text{and } \gamma_n[k]\leq\gamma \end{matrix}\right\}$$

$$+NP\{\gamma[k-1]=\gamma_n[k-1] \text{ and } \gamma_n[k]\geq\gamma_T \text{ and } \gamma_n[k]\leq\gamma\} \qquad 5\text{-}7$$

Assuming identically distributed channel paths, condition

$$P\{\gamma[k-1]=\gamma_1[k-1] \ \text{ and } \ \gamma_1[k]\leq\gamma\}=$$

$$=P\{\gamma[k-1]=\gamma_2[k-1] \ \text{ and } \ \gamma_2[k]\leq\gamma\}=\cdots$$

$$=P\{\gamma[k-1]=\gamma_N[k-1] \ \text{ and } \ \gamma_N[k]\leq\gamma\} \qquad 5\text{-}8$$

is satisfied. Thus, the CDF is rewritten to

$$F_{SDC}(\gamma)=N\,P\left\{\begin{matrix} \gamma[k-1]=\gamma_m[k-1] \text{ and } \gamma_m[k]<\gamma_T \\ \text{and } \gamma_n[k]=\max\{\gamma_1[k],\gamma_2[k],\dots,\gamma_N[k]\} \\ \text{and } \gamma_n[k]\leq\gamma \end{matrix}\right\}$$

$$+N\,P\{\gamma[k-1]=\gamma_n[k-1] \text{ and } \gamma_T\leq\gamma_n[k]\leq\gamma\} \qquad 5\text{-}9$$

If a closed-form expression can be provided for CDF, the PDF of γ, $f_{SDC}(\gamma)$, is given by differentiation of this equation.

5.3.2 BER and Outage Probability

The instantaneous bit error probability of an FSO channel with additive noise and OOK modulation, is computed by $P_e = Q(\sqrt{\gamma})$. Clearly, in the presence of perfect CSI of atmospheric turbulence, the BER for a receiver with diversity is obtained by averaging P_e over all fading variables

$$P_{SDC}^{e} = \int_0^{\infty} f_{SDC}(\gamma)\, Q(\sqrt{\gamma}) d\gamma \qquad 5\text{-}10$$

where $f_{SDC}(\gamma)$ is PDF of the combiner's output.

Now the combining iteration period τ is assumed to be large enough compared to channel coherence time so that the correlated pair of $\gamma_n[k]$ and $\gamma_m[k]$ are independent of their corresponding values at time $k-1$. Accordingly, the CDF is evaluated in the form

$$F_{SDC}(\gamma) = N\, P\{\gamma[k-1] = \gamma_m[k-1]\}\; P\left\{\begin{matrix} \gamma_m[k] < \gamma_T \\ \text{and } \gamma_n[k] = \max\{\gamma_1[k], \gamma_2[k], \dots, \gamma_N[k]\} \\ \text{and } \gamma_n[k] \le \gamma \end{matrix}\right\}$$

$$+NP\{\gamma[k-1] = \gamma_n[k-1]\}P\{\gamma_T \le \gamma_n[k] \le \gamma\} \qquad 5\text{-}11$$

Substituting $\gamma = \infty$ in (11) gives $P\{\gamma[k] = \gamma_n[k]\} = 1/N$ and similarly, $P\{\gamma[k-1] = \gamma_n[k-1]\} = P\{\gamma[k-1] = \gamma_m[k-1]\} = 1/N$. Since all variables are now at time k, the time index will be neglected for the sake of simplicity. The CDF can be simplified to

$$F_{SDC}(\gamma) = P\left\{\bigcap_{i=1, i\neq n}^{N} \gamma_i < \gamma_n \text{ and } \gamma_m < \gamma_T \text{ and } \gamma_n \le \gamma\right\} + P\{\gamma_T \le \gamma_n \le \gamma\} \qquad 5\text{-}12$$

Based on the value of γ compared to γ_T, two independent cases appear. If $\gamma < \gamma_T$, the value of $P\{\gamma_T \le \gamma_n \le \gamma\} = 0$ and the first term in (5-12) is derived from

$$F_{SDC}^{\gamma<\gamma_T}(\gamma) = \underbrace{\int_0^{\gamma}\int_0^{\gamma}\int_0^{\gamma_n} \dots \int_0^{\gamma_n}}_{N-\text{fold}} f_{\Gamma}(\gamma_1, \dots, \gamma_N)\; \underbrace{d\gamma_N \dots d\gamma_j \dots d\gamma_1}_{(N-2)-\text{fold}; j\neq m,n}\, d\gamma_m d\gamma_n \qquad 5\text{-}13$$

which is equivalent to

$$F_{SDC}^{\gamma<\gamma_T}(\gamma) = \underbrace{\int_0^{\gamma}\int_0^{\gamma}\dots\int_0^{\gamma}}_{N-\text{fold}} f_{\boldsymbol{\Gamma}}(\gamma_1,\dots,\gamma_N)\, d\gamma_N \dots d\gamma_1 \qquad 5\text{-}14$$

where $f_{\boldsymbol{\Gamma}}(\gamma_1,\gamma_2,\dots,\gamma_N)$ is the joint PDF. Since it is assumed that paths area c.i.d., PDF of SDC will be given by

$$f_{SDC}^{\gamma<\gamma_T}(\gamma) = N \underbrace{\int_0^{\gamma}\int_0^{\gamma}\dots\int_0^{\gamma}}_{(N-1)-\text{fold}} f_{\boldsymbol{\Gamma}}(\gamma,\gamma_2,\dots,\gamma_N)\, \underbrace{d\gamma_N \dots d\gamma_2}_{(N-1)-\text{fold}} \quad ; \quad \gamma < \gamma_T \qquad 5\text{-}15$$

If $\gamma \geq \gamma_T$, the probability similarly becomes

$$F_{SDC}^{\gamma\geq\gamma_T}(\gamma) = \underbrace{\int_0^{\gamma}\int_0^{\gamma_T}\int_0^{\gamma}\dots\int_0^{\gamma}}_{N-\text{fold}} f_{\boldsymbol{\Gamma}}(\gamma_1,\dots,\gamma_N)\, \underbrace{d\gamma_N \dots d\gamma_j \dots d\gamma_1}_{(N-2)-\text{fold};\, j\neq m,n} d\gamma_m d\gamma_n$$

$$+ \int_{\gamma_T}^{\gamma} f_{\gamma}(\gamma')\, d\gamma' \qquad 5\text{-}16$$

where $f_{\gamma}(.)$ is the PDF of a single branch. Since branches are identically distributed, m and n can be any two of the branches. Thus the CDF reduces to

$$F_{SDC}^{\gamma\geq\gamma_T}(\gamma) = \underbrace{\int_0^{\gamma}\int_0^{\gamma_T}\int_0^{\gamma}\dots\int_0^{\gamma}}_{N-\text{fold}} f_{\boldsymbol{\Gamma}}(\gamma_1,\dots,\gamma_N)\, d\gamma_N \dots d\gamma_1 + \int_{\gamma_T}^{\gamma} f_{\gamma}(\gamma')\, d\gamma' \qquad 5\text{-}17$$

$f_{SDC}(\gamma)$ in this case will be expressed by

$$f_{SDC}^{\gamma\geq\gamma_T}(\gamma) = (N-1) \underbrace{\int_0^{\gamma}\int_0^{\gamma}\dots\int_0^{\gamma}}_{(N-1)-\text{fold}} f_{\boldsymbol{\Gamma}}(\gamma,\gamma_2,\dots,\gamma_N)\, \underbrace{d\gamma_N \dots d\gamma_2}_{(N-1)-\text{fold}} + f_{\gamma}(\gamma) \quad ; \quad \gamma \geq \gamma_T \qquad 5\text{-}18$$

BER is then calculated by

$$P_{SDC}^{e} = \int_0^{\gamma_T} f_{SDC}^{\gamma<\gamma_T}(\gamma)\, Q(\sqrt{\gamma})\, d\gamma + \int_{\gamma_T}^{\infty} f_{SDC}^{\gamma\geq\gamma_T}\, Q(\sqrt{\gamma})\, d\gamma \qquad 5\text{-}19$$

However, providing closed-form expressions for BER and outage probabilities for $N > 2$ based on the aforementioned analysis is quite difficult.

By definition, outage probability denotes the probability that the resultant output SNR drops below a predetermined threshold γ_{out}, i.e., $P(\gamma \leq \gamma_{out})$. Consequently, this is obtained by replacing γ with γ_{out} in the CDF expression. For switched diversity, the probability is expected to be a function of switching threshold γ_T.

The optimum value for γ_T, when the minimization of outage probability is taken into consideration, can be achieved even notwithstanding the math analysis. When $\gamma_T < \gamma_{out}$ is considered, a range of $\gamma_T < \gamma < \gamma_{out}$ exists in which the received SNR may drop below the minimum required quality, although it remains above the switching threshold level. Hence, the system does not switch to a new branch and an outage happens. In the case $\gamma_T > \gamma_{out}$, any given value for γ_T in this range does not affect the outage probability. Rather, it affects the number of switching occurrences. When the value of switching threshold γ_T becomes bigger, the number of switching occurrences increases thus resulting in a more practical complexity. Therefore, the optimum value for the switching threshold, subject to the minimization of the outage probability, is given by $\gamma_T = \gamma_{out}$. Mathematically, by choosing $\gamma = \gamma_T$, the second part of (5-16) will be zero and the expression for outage probability reduces to

$$P_{SDC}^{out} = P\{\cap_{i=1}^{N} \gamma_i[k] \leq \gamma_T\} \qquad 5\text{-}20$$

which is explicitly equal to the outage probability of SC. As a result, this argument implies that all combining diversity schemes SC, SSC and SDC provide identical outage probabilities. Of note is that the above discussion regarding outage probability should not be confused with BER performance. Although any given SNR value in the range of $\gamma_T > \gamma_{out}$ has no impact on outage probability, it affects the resultant SNR and

ultimately the BER performance. In this case, there may be a gap of $\gamma_T < \gamma < \gamma_{n_{\max}}$ in which the receiver reaches a lower SNR than SC, where $\gamma_{n_{\max}} = \max\{\{\gamma_i\}_{i=1}^{N}\}$.

5.3.3 Optimum Threshold

At the end of the last subsection, it was demonstrated that the minimization of outage probability for SDC is achievable by choosing $\gamma_T = \gamma_{out}$, which is identical to that of SC combiner. Of interest is whether or not any optimal points for BER of SDC exist. In this regard, the PDF function can be alternatively evaluated rather than BER. When choosing $\gamma_T = \infty$, the PDF of the resultant SNR represents the PDF of SC:

$$f_{SDC}(\gamma) \to f_{SC}(\gamma) \quad \text{if} \quad \gamma_T \to \infty \tag{5-21}$$

In other words, BER performance improves to a level offered by a SC diversity system. By contrast, when choosing $\gamma_T = 0$, as the first part of (5-19) becomes zero, SDC provides a PDF similar to a system with a single branch:

$$f_{SDC}(\gamma) \to f_{\gamma}(\gamma) \quad \text{if} \quad \gamma_T \to 0 \tag{5-22}$$

Note that SC is viewed as the optimal implementation of any switched diversity and in contrast, a single branch represents the worst case scenario (no diversity). Therefore, the above investigated values for γ_T provide the minimum and maximum BER performance levels. In fact, the higher the switching threshold level, the lower average BER. Consequently, no local optimization is available for SDC (contrary to SSC). On the other hand, a high threshold level causes repetitive branch monitoring and switching, while a low value locks the receiver connected to one branch. Thus, selection of the threshold level for SDC is a tradeoff between the BER performance and receiver complexity.

5.4 Numerical Simulation

This section presents numerical results using computer simulations to investigate the performance of SDC switched diversity for an FSO receiver equipped with N branches. Bit error rate, outage probability and processing load are performance criteria used in the analysis. Computer simulations assume a normalized lognormal fading of $E[h_i] = 1$ for $i = 1, \ldots, N$. Noise power is varied to obtain various average branch SNR values. Both combiner and detector make use of CSI, i.e., instantaneous branch SNR. They are mutually correlated.

The average BER of SDC scheme is shown in Figure 5-2 and is plotted under case $\sigma_\chi = 0.2$ and $\rho = 0.1$. Theoretically, there is no local minimum or optimum switching threshold for optimizing BER performance. Figure 5-3 presents the effect of switching threshold levels and correlation coefficient values on BER. Based on the value of γ_T, BER performance of SDC varies from that of a single receiver, i.e., no diversity, to that of SC. The figure shows that the fluctuations of ρ causes negligible BER variation when γ_T is low, as the combiner is locked to one branch. By contrast, the mutual correlation between branches considerably degrades the performance for relatively high values of γ_T. Specifically, if a large enough value for γ_T is chosen, the variation in BER for a value of fading strength of $\sigma_\chi = 0.2$ and average branch SNR of $\bar{\gamma} = 20$dB is between 2.25×10^{-7} for uncorrelated ($\rho = 0$) to 2.45×10^{-5} for highly correlated ($\rho = 0.9$) branches.

Although a higher threshold level provides superior BER performance; it introduces more repetitive branch monitoring and switching occurrences. Hence, finding a proper value for switching threshold of SDC is influenced by a tradeoff between switching repetitions and BER performance. Regardless, an option must be determined. It is chosen to consider the case $\gamma_T = \bar{\gamma}$, where $\bar{\gamma}$ is the average branch SNR. This produces an

interesting result since for the observation range of numerical simulation in Figure 5-2, the delivered performance by SDC is close proximity to that by SC.

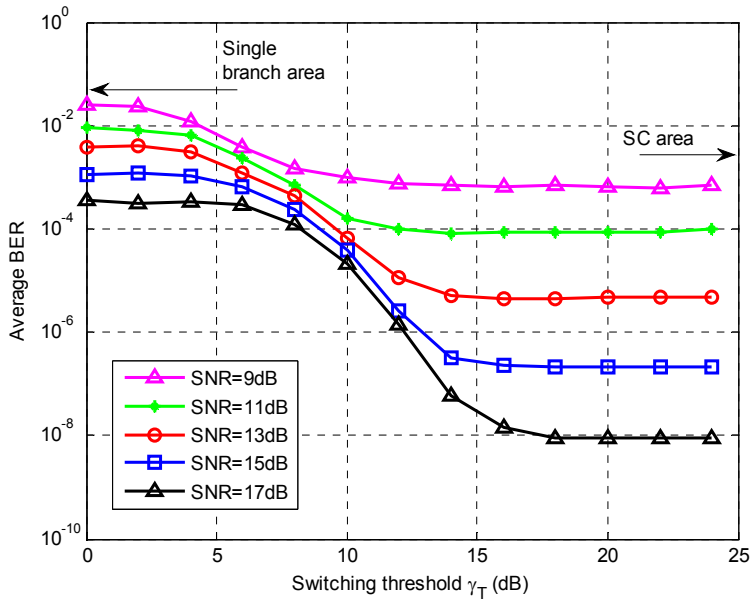

Figure 5-2: Bit error rate vs. switching threshold γ_T for several different values of $\bar{\gamma}$ using a N=*6* SDC combiner. $\sigma_\chi = 0.2$, $\rho = 0$

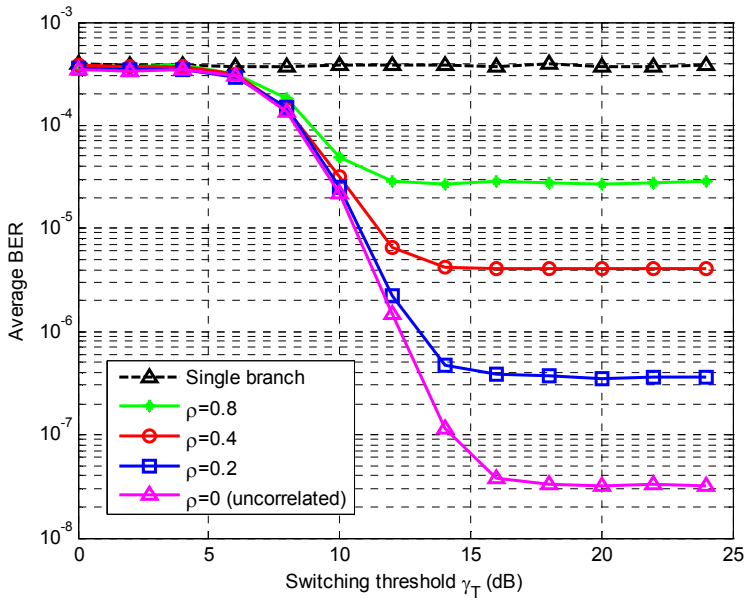

Figure 5-3: Bit error rate vs. switching threshold γ_T for several different values of correlation coefficients ρ for an N=6 SDC. $\sigma_\chi = 0.2$, $\bar{\gamma} = 17$

Figure 5-4 shows a comparison in BER performance for SDC scheme relative to the performance of SSC and SC schemes in multi-branch SIMO system. The corresponding BER of SSC is provided in [114]. Note that CDF of SC is equal to $P\{\bigcap_{i=1}^{N}\gamma_i \leq \gamma\}$. Hence, BER of SC is expressed as follwos when integration by part is utilized:

$$P_{SC}^{e} = \int_0^{\infty} \frac{d}{d\gamma} P\left\{\bigcap_{i=1}^{N} \gamma_i \leq \gamma\right\} P_b(\gamma) d\gamma$$

$$= \frac{1}{\sqrt{8\pi}} \int_0^{\infty} \frac{1}{\sqrt{\gamma}} P\{\bigcap_{i=1}^{N}\gamma_i \leq \gamma\} \exp\left(-\frac{\gamma}{2}\right) d\gamma \qquad 5\text{-}23$$

Although an approximate closed-form expression may be derived using Gauss-Laguerre quadrature for small N's, numerical computation has been used to plot the BER in Figure 5-4.

Performance gain has been shown to be insignificant when SSC is employed [6]. For example, the best performance gain at $\bar{\gamma}$ =17dB for dual SSC with uncorrelated paths at $\sigma_\chi = 0.2$ is about 2.6dB relative to a single receiver; while it is approximately 4dB when an SC strategy is applied. The gain looks same for SDC when the threshold option $\gamma_T = \bar{\gamma}$ is chosen. As shown in the figure, SSC cannot provide a BER performance as good as SC. It does not even achieve additional gain for $N > 2$. But increasing the number of receiving branches to $N = 4$ and 6, SDC results are in close proximity to BER performance of SC. For $N = 2$, SDC turns to the proposed SEC in [6]. Figure 5-4 also shows that path correlation causes significant performance degradation. Specifically, by comparing to uncorrelated paths at $N = 4$, a correlation of $\rho = 0.2$ for $N = 6$ wastes more than two of the branches. In other word, the loss in SNR for $N = 6$ is 2.2dB and 4dB for $\rho = 0.2$ and $\rho = 0.4$, respectively.

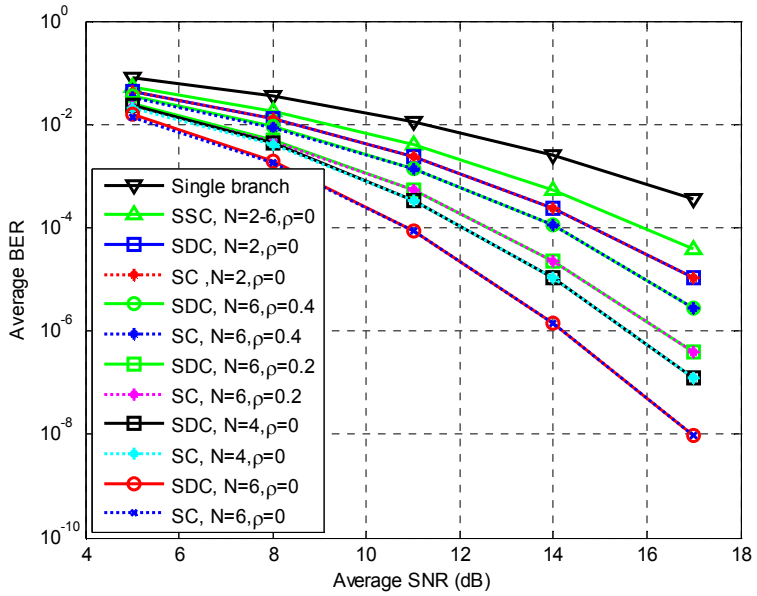

Figure 5-4: Comparison of bit error rate vs. average SNR $\bar{\gamma}$ when optimum switching threshold is applied for SSC and $\gamma_T = \bar{\gamma}$ is applied for SDC. $\sigma_\chi = 0.2$

The outage probability performance is also numerically evaluated in this section. To analytically employ outage probability of SDC, it is necessary to only consider the computation of CDF, and then replace $\gamma = \gamma_{out}$. The outage probability is a function of γ_T. SC offers optimum outage probability performance. It was shown earlier, in Section 5.3.2, that the outage probabilities for all diversity schemes SC, SSC and SDC are identical if γ_T is chosen equal to the outage threshold, i.e. $\gamma_T = \gamma_{out}$. In this case outage probability of SDC is minimized. Figure 5-5 shows that for $\sigma_\chi = 0.1$, there is significant outage performance loss when an improper switching threshold is selected. This is especially true for low fading conditions. Similar concept is verified for SSC and SEC [6], thus identical outage probability can be achieved when using the combining techniques—SC, SSC, SEC, and SDC. Note that selection of such a threshold for γ_T does not guarantee the minimization of BER performance of SDC.

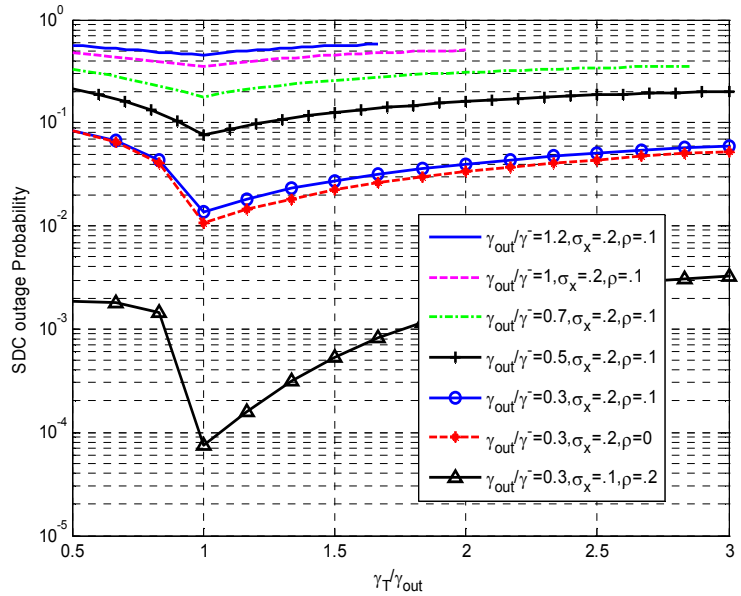

Figure 5-5: The outage probability vs. normalized switching threshold γ_T and outage threshold γ_{out} dual-branch SSC and SDC schemes (N=2)

The final simulation component focuses on the processing load, which is previously applied for SEC and SSC in section 4.5. The definition for processing load resulting from diversity is defined as the average number of branch monitoring occurrences per combining cycle. Using this definition, the APL parameter is characterized as the monitoring occurrences load of the inactive branches. The associated APL with SDC is numerically derived and shown in Figure 5-6, where it is compared to SSC and SC. It is apparent that relative to SC at an average branch SNR of $\bar{\gamma} = 17\,\text{dB}$, SDC saves approximately 35% of the processing load with threshold $\gamma_T = \bar{\gamma}$; however it is approximately 91% for SSC with optimal threshold. It was observed that SDC processing load remained nearly unchanged as the correlation becomes stronger or the number of increases.

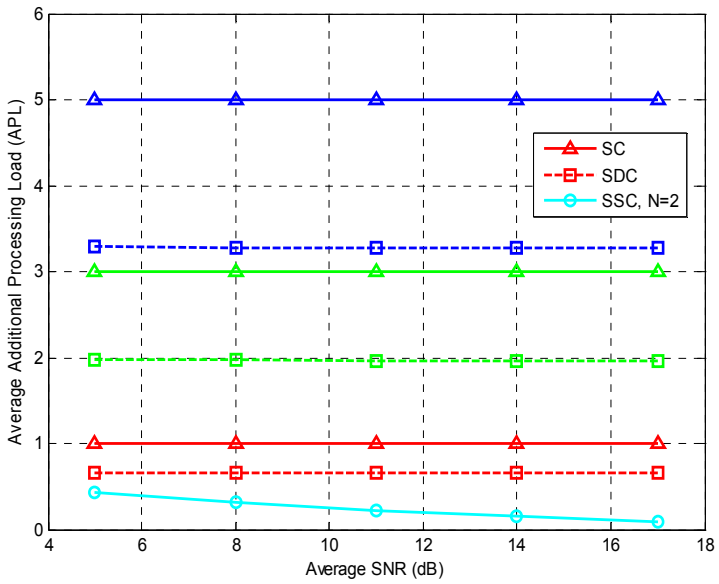

Figure 5-6: Additional processing load (APL) due to diversity combining. $\sigma_\chi = 0.2$, $\rho = 0$. blue: N=6, green: N=4, red: N=2.

5.5 Concluding Results

Switched diversity schemes eliminate unnecessary monitoring and repetitive switching, resulting in a low processing load at the combiner. This outcome proves significant, especially given that FSO applications are subject to a high processing load as a consequence of high data rate communication. This chapter proposed a novel switched diversity scheme, namely SDC. The utilization of SDC is happened in a multi-receiving optical wireless communication receiver, and then compared results with those obtained using a SC scheme. SDC was found to offer identical outage probability and achieve comparable BER performance while, at the same time, reducing the combiner-processing load. Likewise, SDC significantly improved BER performance when measured against SSC diversity scheme. Unlike SSC, SDC receiver performance improves as the number of branches increases. SDC scheme, however, requires a higher processing load than SSC scheme.

No optimal value for γ_T that minimizes the BER of SDC was found in the results obtained in this study. Thus, the selection of the SDC switching threshold remains a tradeoff between BER performance and branch monitoring occurrences. These, in turn, influence receiver complexity. If $\gamma_T = \bar{\gamma}$ is chosen, SDC branch monitoring processing load decreases at nearly 35% (Figure 5-6) while SDC BER is maintained (Figure 5-4). If $\gamma_T = \gamma_{out}$ is chosen, SDC outage probability is minimized; however, a moderate loss of BER performance is observed.

6. Mobile FSO

Mobility-capable FSO nodes have been characterized as a way to resolve the incompatibility of optical wireless nodes with movement and misalignment. Providing a multi-branch angular diversity introduces mobility to the FSO node, resulting in reliability enhancement of the optical wireless connection over movement, which exempts the employment of a complicated PAT solution. In this chapter, all receiving branches are assumed to be circularly placed on a plane, the same plane as the transmitting branches are, while on different platforms [132]. Under such MIMO structure, an angular diversity scheme will be utilized to provide the signal combining at the receiver.

6.1 Introduction

Despite exceptional benefits of wireless optical links, conventional links offer a very low degree of reliability and robustness regarding the optical connection. In fact, high directionality of narrow optical beams is the major issue facing practical development of the links.

Categorized in SIMO and MIMO fashions, a mobile FSO node translates into a limited mobility provided to the optical wireless network. Asymmetrically unbalanced

transceiver apertures with intentional misalignment are installed in such a way as to establish node mobility while maintaining the connection. A mobile FSO based on SIMO is characterized in [133] but this chapter considers a more general case which is the MIMO topology.

FSO-based mobile nodes potentially can be used in a vehicular or mobile ad hoc network (VANET/MANET) in areas where infrastructure is unavailable [63] or in a optical-based wireless sensor network, namely WOSN [134]. Previous works on mobile FSO mainly focused on alignment and tracking issues [61], [62], [70] and design of multi-element structures [68], [66] characterized to ensure uninterrupted data flow by auto-aligning transmitter and receiver modules. An unbalanced, multi-receiving structure of optical power distribution in a nonrandom model is characterized in [135]. The works cited concentrate on design and/or experimental views of a deterministic angular diversity. But the contribution of this work includes statistical analysis of mobile FSO nodes over random atmospheric turbulence and limited mobility. However, similar to the previous works, the receiving branches are not identically aligned to transmitter. Hence, the objective is not developing a channel model or a diversity scheme, but how to employ an efficient diversity combining toward practical development of a mobile FSO. However, this work is a continuation of a prior work, i.e., [72], where the mobile FSO is typically suggested to work for providing an immediate communication link under disastrous events.

A circular configuration of transceiver apertures is assumed, which depicted in Figure 6-1. FSO branches design is based on LD or LED for transmitter and photodiodes for receiver. The design is suitable for short-range networking applications. The circular

configuration is an example of mobile FSO while the analysis can be applied to other FSO-based angular diversity designs. It can also accommodate the development of fiber-bundled transceiver, which is analytically introduced and experimentally evaluated in [72], [136].

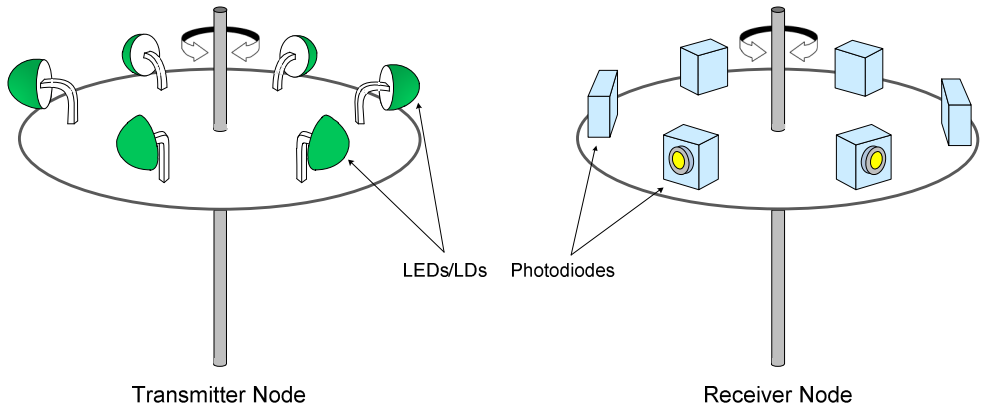

Figure 6-1: Two typical 6-branch nodes of the proposed structure for mobile FSO

The system under the consideration of this work is built on MIMO configuration with transmit selection diversity. Under the multi-receiving structure, the system also requires a receive diversity combining scenario. This chapter discusses the deployment feasibility of an efficient combining approach, namely threshold generalized selection combining (T-GSC). Designed for threshold-based selection strategies, a T-GSC combiner selects all the branches that have SNR values strong compared to a preset threshold. The scheme contributes to high combining performance when implemented in mobile FSO.

It is effectively considered that transmitter/receiver apertures are placed in a regime where they are in close proximity, thus channel coefficients are spatially correlated. Such channels are characterized by turbulence-induced fading models and expressed by a PDF, e.g., lognormal function. Both combiner and detector are aware of exact instantaneous fading coefficients imposed by the time-varying channel. Such assumption indicates that

the optical channel changes very slowly relative to the symbol rate due to both mobile movement and channel fading, i.e., change is nearly constant over millions of bits. In this case, a few pilot tones offer much information about the channel state, as discussed in section 3.4.4. Selection of the modulation format is, however, not the focus of this work, as the concept of diversity scheme is independent of the employed IM/DD method.

This chapter is organized as follows. In Section 6.2, basic definitions and system model assumptions and statistical analysis on the mobile node structure are presented. Section 6.3 covers available approaches for diversity combining. Simulation results are presented in Section 6.4, and Section 6.5 concludes the chapter.

6.2 System Model

Under an atmospheric-induced turbulence channel, the instantaneous electrical SNR of the n-th misaligned receiver is given by [122]

$$\gamma_n = h_n^2 \alpha_n^2 \bar{\gamma} \qquad 6\text{-}1$$

where h_n is the fading channel coefficient, i.e., gain, due to atmospheric turbulence that models the intensity gain of the channel associated with the n-th receiver from the transmit aperture; $\bar{\gamma}$ is defined as the average branch SNR excluding misalignment and the fading effect; and α_n, $0 \leq \alpha_n \leq 1$, is the attenuation coefficient random variable (RV) due to misalignment.

Under a lognormal distribution, the channel coefficient will have PDF of the form of Eq. (2-19). Channel coefficients are correlated in time and space domains due to the movement of atmospheric eddies. Although Taylor's hypothesis indicates that spatial and temporal correlations are not apart, the impact of temporal dependency is skipped when the combining iteration period is large relative to coherence time. Temporal

correlativeness may be taken into account when a SISO system is investigated such as what is provided in chapter 3, or the works in [83], [89]. Alternatively, spatial correlativeness should be considered when a spatial-based diversity system is used to improve detection performance. Thus, the multi-receiving system considered in this work has spatially correlated links, where detector size and bit interval are much smaller than coherence length and coherence time, respectively.

Without loss of generality, the probability distribution of N distributed and correlated fading coefficients is jointly an N-dimensional PDF. Throughout this chapter, $\mathbf{\Gamma}$ is defined as an N-elements vector representing the SNR: $\mathbf{\Gamma} = \{\gamma_n\}_{n=1}^{N} = \{\alpha_n^2 h_n^2 \bar{\gamma}_n\}_{n=1}^{N}$, where $\bar{\gamma}_n$ is the average branch signal belonging to branch number n with no fading or misalignment effects. Note that $\bar{\gamma}_1 = \bar{\gamma}_2 \ldots = \bar{\gamma}_N = \bar{\gamma}$, as P_t and noise power are identical for all transmitters, regardless the number of branches. It is assumed that h_n and α_n, and consequently γ_n, are ergodic and stationary random processes in the time domain. Also it is assumed that $E[h_n] = 1$ for any $n = 1,2, \ldots, N$ and $\bar{\mathbf{\Psi}}$ is defined as the average vector by $\bar{\mathbf{\Psi}} \triangleq \{E[\chi_n]\}_{n=1}^{N} = [-\sigma_x^2 \ -\sigma_x^2 \ \ldots \ -\sigma_x^2]_{1\times N}$, as the paths are identically faded. Matrix Σ_χ is defined as the covariance matrix $\Sigma_\chi = \{C_{i,j}\}$, $i, j = 1, \ldots, N$, where $C_{i,j}$ is the mutual covariance function.

Mobile FSO is adopted as an unbalanced, multi-aperture transceiver. The top view of the transmitter-receiver set is shown in Figure 6-2. The receiving mobile node is wirelessly connected to a mobile transmitter node by a full-duplex optical link. It is assumed that the propagation length is considered much longer than the diameter of the node's platform: $L \gg D$. This ensures that the transmitter provides a persistent loading coverage on the receiving node so that at any given time the receiving node sees the beam

of only one transmitter. The transmitting node structure must be designed to ensure the practical possibility of such an assumption. Thus, the system of the proposed mobile FSO represents a MIMO configuration on a transmit selection diversity. The objective of this section is to characterize the dynamics of such a configuration and mathematically address joint SNR distribution of the branches, which is required for performance analysis. Any two adjacent receiver apertures on the framework are installed by separation angles $\{\theta_n\}_{n=1}^{N}$. Also, angles $\{\varphi_n\}_{n=1}^{N}$ are introduced as misalignment angles of receivers in counterclockwise direction relative to the transmitter baseline.

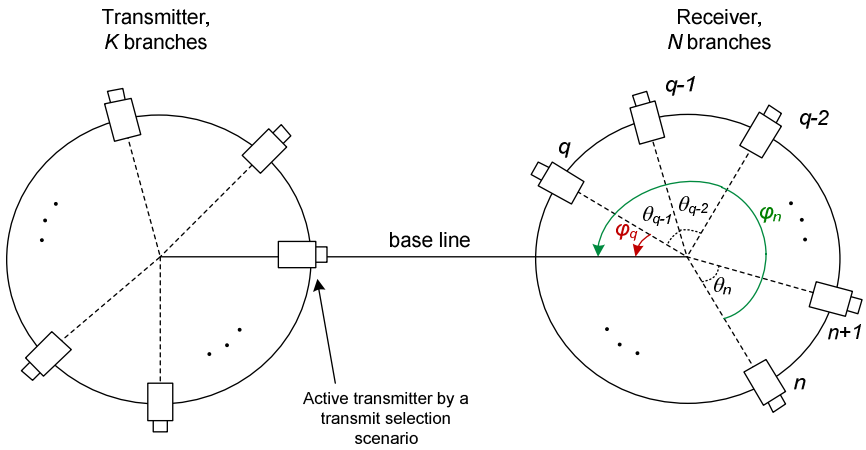

Figure 6-2: Illustration of the MIMO configuration under the circular mobile FSO design

By including the misalignment coefficient, the electrical signal of the n-th receiver in discrete time samples will be expressed by the following system model:

$$r_n = 2RP_t h_n \alpha_n s + v_n \; ; \quad n = 1, 2, \dots, N \qquad 6\text{-}2$$

The instantaneous branch SNR is characterized by $\gamma_n = \frac{R^2 P_t^2 h_n^2 \alpha_n^2}{\sigma_v^2}$. CSI is defined as $\{\gamma_n\}_{n=1}^{N}$, where possessing knowledge of this equivalently leads to the knowledge of $\{\alpha_n h_n\}_{n=1}^{N}$. Note that the notation of discrete-time sampling is simply neglected in the

model. Recall that α_n, $0 \leq \alpha_n \leq 1$, is the random orientation of the n-th receiver resulting from misalignment or angular reception. Specifically, α_n directly relates to the misalignment angle of branch n in the transmission plane and can be considered by [69](Eq. 2)

$$\alpha_n = \begin{cases} \exp(-\varphi_n^2), & -\frac{\pi}{2} < \varphi_n < \frac{\pi}{2} \\ 0, & \frac{\pi}{2} \leq \varphi_n \leq \frac{3\pi}{2} \end{cases} ; \quad n = 1, 2, \dots, N \qquad \text{6-3}$$

which varies according to aperture. Although misalignment angles are random variables, they are dependent on each other based on the separation angles $\{\theta_n\}_{n=1}^{N}$. For any given receiver n, all the angles can be expressed by:

$$\varphi_n = \varphi_q + \sum_{i=n}^{q-1} \theta_i \ ; \quad n = 1, 2, \dots, N \qquad \text{6-4}$$

where q is a given aperture with angle φ_q. Note that $\{\theta_n\}_{n=1}^{N}$ are deterministic and fixed; therefore, (6-4) indicates that all random variables $\{\varphi_n\}_{n=1}^{N}$ can be expressed in only one given angle. Some symmetry can be included in the mobile node structure to simply characterize the received signal power within the receivers. Assuming the nodes are uniformly placed on the framework, i.e., $\theta_1 = \theta_2 = \cdots = \theta_N = \theta$, the separation angle becomes $\theta = 2\pi/N$. For any receiver n, a random angle φ_n can be written in terms of the given receiver q and simply by assuming $q = 1$,

$$\varphi_n = \varphi_1 + \frac{2(n-1)\pi}{N} \ ; \quad n = 1, 2, \dots, N \qquad \text{6-5}$$

This equation indicates that if one of the given RVs, defined as φ_1; $-\frac{\pi}{2} < \varphi_1 < \frac{3\pi}{2}$, has a PDF expressed by $f_{\varphi_1}(.)$, then the PDF of all other RVs are expressed by

$$f_{\varphi_n}(\varphi_n) = f_{\varphi_1}\left(\varphi_1 - \frac{2(n-1)\pi}{N}\right); \quad n = 1, 2, \dots, N \qquad \text{6-6}$$

Aided by [137](Eq. 13), the PDF of α_n is achievable from (5)

$$f_{\alpha_n}(\alpha_n) = \begin{cases} \delta(\alpha_n)\left(1 - \int_{-\frac{\pi}{2}}^{\frac{\pi}{2}} \frac{\exp(\phi^2)}{2|\phi|}\left(f_{\varphi_n}(\phi) + f_{\varphi_n}(-\phi)\right) d\phi\right) & \alpha_n = 0 \\ \frac{1}{2\varphi_n' \alpha_n}\left(f_{\varphi_n}(\varphi_n') + f_{\varphi_n}(-\varphi_n')\right) & 0 < \alpha_n \leq 1 \\ 0, & \alpha_n < 0 \; or \; \alpha_n > 1 \end{cases} \quad \text{6-7}$$

where $\varphi_n' = \sqrt{\ln(1/\alpha_n)}$, which is always real and non-negative for $0 < \alpha_n \leq 1$. In this way $\int_{-\infty}^{\infty} f_{\alpha_n}(\alpha_n)\, d\alpha_n = 1$ can be easily verified. Recall that misalignment angle φ_n is a RV influenced by the receiving node mobility and expressed by the distribution of $f_{\varphi_n}(\varphi_n)$; Gaussian and uniform distributions offer two possible cases, e.g., $f_{\varphi_n}(\varphi_n) = f_{\varphi_n}(-\varphi_n) = 1/2\pi$, thus, the PDF of α_n in the above equation can be simplified. It can be also assumed that due to node symmetry $f_{\varphi_n}(\varphi_n) = f_{\varphi_n}(-\varphi_n)$ due to symmetry of the node.

To statistically derive the marginal PDF of γ_n, the PDF of both h_n^2 and α_n^2 are needed, where $h_n^2 = e^{4\chi_n}$. The expression for the PDF of h_n^2, can be easily deduced from the PDF of h_n:

$$f_{h_n^2}(h) = \frac{1}{\sqrt{32\pi} h^2 \sigma_\chi} \exp\left[-\frac{\left(\ln(h) + 2\sigma_\chi^2\right)^2}{8\sigma_\chi^2}\right] \quad \text{6-8}$$

Let's consider $f_{\alpha_n^2}(\alpha_n)$ as the PDF of α_n^2, which is represented in terms of $f_{\alpha_n}(\alpha_n)$ by $f_{\alpha_n^2}(\alpha_n) = \frac{1}{2\alpha_n} f_{\alpha_n}(\alpha_n)$:

$$f_{\alpha_n^2}(\alpha_n) = \begin{cases} \delta(\alpha_n)\left(1 - \int_0^{\frac{\pi}{2}} \frac{1}{\phi} f_{\varphi_n}(\phi) \exp(2\phi^2)\, d\phi\right) & \alpha_n = 0 \\ \frac{1}{2\sqrt{\ln(1/\alpha_n)}\alpha_n^2} f_{\varphi_n}\left(\sqrt{\ln(1/\alpha_n)}\right) & 0 < \alpha_n \leq 1 \\ 0, & \alpha_n < 0 \; or \; \alpha_n > 1 \end{cases} \quad \text{6-9}$$

Since h_n and α_n can be confidently assumed as uncorrelated, given the state of α_n for the conditional probability in $f_{\gamma_n}(\gamma_n) = \int_{-\infty}^{\infty} f_{\gamma_n}(\gamma_n|\alpha_n) f_{\alpha_n^2}(\alpha_n)\, d\alpha$, the marginal PDF of the resultant SNR becomes

$$f_{\gamma_n}(\gamma_n) = \frac{1}{\bar{\gamma}} \int_{-\infty}^{\infty} \frac{1}{\alpha} f_{h_n^2}\left(\frac{\gamma_n}{\bar{\gamma}\alpha}\right) f_{\alpha_n^2}(\alpha)\, d\alpha \qquad 6\text{-}10$$

The PDF then becomes

$$f_{\gamma_n}(\gamma_n) = \begin{cases} \delta(\gamma_n)\left(1 - \int_0^{\frac{\pi}{2}} \frac{1}{\phi} f_{\varphi_n}(\phi) \exp(2\phi^2)\, d\phi\right) & \gamma_n = 0 \\ \frac{1}{2\bar{\gamma}} \int_0^1 \frac{1}{\sqrt{\ln(1/\alpha)}\alpha^3} f_{h_n^2}\left(\frac{\gamma_n}{\bar{\gamma}\alpha}\right) f_{\varphi_n}\left(\sqrt{\ln(1/\alpha)}\right) d\alpha & 0 < \gamma_n < \infty \end{cases} \qquad 6\text{-}11$$

where $f_{h_n^2}(.)$ is the marginal PDF of h_n^2 for the n-th receiver. The marginal CDF accordingly becomes

$$F_{\gamma_n}(\gamma_n) = 1 - \int_0^{\frac{\pi}{2}} \frac{1}{\phi} f_{\varphi_n}(\phi) \exp(2\phi^2)\, d\phi$$

$$+ \frac{1}{2\bar{\gamma}} \int_0^{\gamma_n} \int_0^1 \frac{1}{\sqrt{\ln(1/\alpha)}\alpha^3} f_{h_n^2}\left(\frac{\gamma}{\bar{\gamma}\alpha}\right) f_{\varphi_n}\left(\sqrt{\ln(1/\alpha)}\right) d\alpha\, d\gamma \qquad 6\text{-}12$$

The joint representation of the PDF is now required. For turbulence, joint distribution is available by

$$f_{h^2}(h_1, h_2, \dots, h_M) = \frac{\exp\left[-\frac{1}{8}(\ln[\boldsymbol{H}] - 2\bar{\boldsymbol{\Psi}})\Sigma_\chi^{-1}(\ln[\boldsymbol{H}] - 2\bar{\boldsymbol{\Psi}})^T\right]}{4^M (2\pi)^{\frac{M}{2}} (\det[\Sigma_\chi])^{\frac{1}{2}} (\mathrm{P}[\boldsymbol{H}])^2} \qquad 6\text{-}13$$

where T is the transpose operator, $\mathrm{P}[\boldsymbol{H}] \triangleq \prod_{m=1}^{M} h_m$, and M is the number of correlated paths. These paths are associated with the illuminated receivers. The SNR of non-illuminated branches, from $M + 1$ to N, are not correlated to these paths, as they have a zero SNR. Assuming an even value for the number of branches of the circular

configuration provided, it can be concluded that $M = N/2$. In fact, the number of effective receivers is cut in half; thus, joint representation of node SNR is extended to

$$f_{\mathbf{\Gamma}_{\mathrm{ON}}}\left(\gamma_1, \gamma_2, \dots, \gamma_{\frac{N}{2}}\right) = \frac{1}{(2\bar{\gamma})^{\frac{N}{2}}} \times \int_0^1 \frac{1}{\left(\alpha_1^2 \alpha_2^2 \dots \alpha_{N/2}^2\right)\left(\sqrt{\ln(1/\alpha_1)\ln(1/\alpha_2)\dots\ln\left(1/\alpha_{N/2}\right)}\right)} \times f_{h^2}\left(\frac{\gamma_1}{\bar{\gamma}\alpha_1}, \frac{\gamma_2}{\bar{\gamma}\alpha_2}, \dots, \frac{\gamma_{N/2}}{\bar{\gamma}\alpha_{N/2}}\right) f_{\varphi_1}\left(\sqrt{\ln(1/\alpha_1)}\right) d\alpha_1 \qquad 6\text{-}14$$

where $\mathbf{\Gamma}_{\mathrm{ON}} \triangleq \{\gamma_n\}_{n=1}^{N/2}$. Note that the illuminated receivers are numbered from 1 to $N/2$. α_m, $\alpha_m \neq 0$ and $m = 1, \dots, N/2$, can be deduced in terms of α_1 by

$$\alpha_m = \exp\left[-\left(-\sqrt{\ln(1/\alpha_1)} + \frac{2(m-1)\pi}{N}\right)^2\right] \quad ; \quad m = 1, \dots, N/2 \qquad 6\text{-}15$$

The joint CDF of $\mathbf{\Gamma}_{\mathrm{ON}}$ is then calculated by

$$F_{\mathbf{\Gamma}_{\mathrm{ON}}}(\gamma_1, \gamma_2, \dots, \gamma_{N/2}) = \underbrace{\int_0^{\gamma_1}\int_0^{\gamma_2}\dots\int_0^{\gamma_{N/2}}}_{N/2-\mathrm{fold}} f_{\mathbf{\Gamma}_{\mathrm{ON}}}(\gamma_1', \gamma_2', \dots, \gamma_{N/2}')\, d\gamma_{N/2}' \dots d\gamma_2' d\gamma_1' \qquad 6\text{-}16$$

Although only half of the receivers are active for combining purposes, the N-dimensional joint PDF for all branches is provided by

$$f_{\mathbf{\Gamma}}(\gamma_1, \gamma_2, \dots, \gamma_N) = \frac{1}{(2\bar{\gamma})^{\frac{N}{2}}}\left(1 - \int_0^{\frac{\pi}{2}} \frac{1}{\phi} f_{\varphi_n}(\phi) \exp(2\phi^2)\, d\phi\right)^{\frac{N}{2}} \delta\left(\gamma_{\frac{N}{2}+1}\right)\delta\left(\gamma_{\frac{N}{2}+2}\right)\dots\delta(\gamma_N) \times \int_0^1 \frac{1}{\left(\alpha_1^2\alpha_2^2\dots\alpha_{\frac{N}{2}}^2\right)\left(\sqrt{\ln(1/\alpha_1)\ln(1/\alpha_2)\dots\ln\left(1/\alpha_{\frac{N}{2}}\right)}\right)}$$

$$\times f_{h^2}\left(\frac{\gamma_1}{\bar{\gamma}\alpha_1}, \frac{\gamma_2}{\bar{\gamma}\alpha_2}, \ldots, \frac{\gamma_{N/2}}{\bar{\gamma}\alpha_{N/2}}\right) f_{\varphi_1}\left(\sqrt{\ln(1/\alpha_1)}\right) \; d\alpha_1 \qquad 6\text{-}17$$

6.3 Receiver Combining Approaches

Spatial diversity analysis for turbulence-induced FSO channels with balanced apertures when CSI is known at the receiver side has been extensively investigated in literature, e.g., [31], [32], [114], and [127]. This section statistically evaluates the performance of efficiently applicable combining techniques for mobile FSO.

6.3.1 Available Approaches

When compared to all diversity techniques, MRC provides superior combining performance. This method works for perfect CSI availability. Implementation complexities are inherent, and the system is extremely sensitive to channel estimation error, especially for signals suffering low SNR conditions.

EGC also is inefficient for systems characterized with branches that have acutely low SNR. An explicit deficiency exists with EGC in mobile FSO when the probability of a non-illuminated receiver is extremely high. Depending on the value of N, the number of non-illuminated receivers on the framework for the proposed design is either $(N-1)/2$ or $(N+1)/2$ if N is odd, and $N/2$ or $N/2-1$ if N is even. These apertures import only noise to the combiner, thus degrading combining performance.

Conventionally, SC follows a selection strategy based on best quality in which the combiner monitors signal strength received through all branches and selects the one with the highest SNR value. Although this process may seem efficient for mobile FSO, SC diversity does not fully exploit diversity offered by the branches. Thus, SC is characterized by low BER performance relative to high processing load due to repetitive branch monitoring. However, the processing load can be mitigated by the exploitation of

a switched diversity, e.g., switch-and-examine combining [129], [114], at the expense of additional BER loss.

Generalized selection combining (GSC) technique is introduced to bridge the performance gap between SC and other conventional techniques, e.g., MRC and EGC, [119]. Based on a GSC combiner, a number of the strongest branches in terms of SNR are selected for a posterior MRC or EGC combining. The advantage of GSC is that it excludes low quality branches that could potentially cause estimation error and affect output signal. Selection of strongest branches is scenario-defined. As a result, GSC combining scheme can be classified as a hybrid SC/MRC approach, which contributes to an improved practical combining efficiency within a mobile FSO system. This work statistically depicts a thresholding-based GSC, namely T-GSC, for mobile FSO. The performance relative to a conventional scheme is provided for comparison. Performance characterization for SC, EGC, and MRC are also reviewed.

6.3.2 Quantification of SC, EGC, and MRC

SC diversity has been previously proposed for balanced receivers to improve the performance of multi-transceiving wireless optical systems, [32], [37], [94], [122]. Using an SC diversity technique, the signal at the receiver with the highest instantaneous SNR is selected for detection. Equivalently, $n_{\max}$ is the branch with maximum corresponding SNR, $\gamma_{n_{\max}} = \max\{\gamma_1, \gamma_2, \dots, \gamma_N\}$. Since the instantaneous SNR relates directly to channel coefficient h, analysis may be alternatively performed on this variable. The CDF of the combiner's output SNR, γ, is previously expressed. The PDF of γ can be mathematically derived by $f_{SC}(\gamma) = \frac{\partial}{\partial \gamma} F_{SC}(\gamma)$. Note that all N branches are not identically distributed, as over half have zero SNRs. Hence, PDF is reduced to

$$f_{SC}(\gamma) = f_{\gamma_{n_{\max}}}(\gamma) = \frac{N}{2}\underbrace{\int_0^{\gamma}\int_0^{\gamma}\cdots\int_0^{\gamma}}_{(N/2-1)-\text{fold}} f_{\Gamma_{\text{ON}}}(\gamma, \gamma_2, \ldots, \gamma_{N/2})\, d\gamma_{N/2} \ldots d\gamma_2 \qquad 6\text{-}18$$

Note that $f_{\Gamma_{\text{ON}}}(.)$ is the joint PDF of branch SNRs. By employing optimal detection, the average BER for a large number of symbols is written by

$$P_{SC}^{e} = \int_0^{\infty} f_{SC}(\gamma)\, P_b(\gamma) d\gamma \qquad 6\text{-}19$$

where $P_b(\gamma)$ is the instantaneous probability of bit error for any individually received symbol. For most modulation cases, e.g., OOK and binary pulse position modulation (BPPM), BER is given by $P_b(\gamma) = Q(\sqrt{\gamma})$, where $Q(.)$ is Q-function.

In practice, optimal detection of the selected branch signal occurs with a CSI-based S-by-S metric given OOK modulation by using [31](Eq. 20) for a SISO link and then replacing r_n by $r_n - I_0$, as

$$r_{n_{\max}} \underset{0}{\overset{1}{\gtrless}} \sqrt{\frac{\gamma_{n_{\max}}}{4\bar{\gamma}}} + I_0 \qquad \text{(SC)} \qquad 6\text{-}20$$

where $r_{n_{\max}}$ is the received electrical signal associated with the selected branch. Note that a normalized power leads to assuming $2RP_t$ is equal to 1, otherwise the above metric converts to $r_{n_{\max}} \underset{0}{\overset{1}{\gtrless}} \sigma_v \sqrt{\gamma_{n_{\max}}} + I_0$.

For a receive diversity employing an EGC combiner with intensity modulated OOK signals, BER expression is expressed by [31](Eq. 29)

$$P_{EGC}^{e} = \underbrace{\int_0^{\infty}\int_0^{\infty}\cdots\int_0^{\infty}}_{N-\text{fold}} f_{\Gamma}(\gamma, \gamma_2, \ldots, \gamma_N) Q\left(\frac{1}{N}\sqrt{\sum_{n=1}^{N}\gamma_n}\right) d\gamma_N \ldots d\gamma_2\, d\gamma_1 \qquad 6\text{-}21$$

where $f_{\Gamma}(\gamma, \gamma_2, \ldots, \gamma_N)$ is N-dimensional PDF of SNR. Also, optimal decision rule is achieved by similarly applying manipulation into [31](Eq. 20), as

$$\sum_{n=1}^{N}\sqrt{\gamma_n}r_n \underset{0}{\overset{1}{\gtrless}} \sigma_v \sum_{n=1}^{N}\gamma_n + I_0 \sum_{n=1}^{N}\sqrt{\gamma_n} \qquad \text{(EGC)} \qquad 6\text{-}22$$

The optimal detection rule of the receive diversity employing an MRC combiner is given by replacing r_n with r_n/h_n, as

$$\sum_{n=1}^{N} r_n \underset{0}{\overset{1}{\gtrless}} \frac{\sigma_v}{\sqrt{\bar{\gamma}}}\sum_{n=1}^{N}\gamma_n + \frac{NI_0}{\sqrt{\bar{\gamma}}} \qquad \text{(MRC)} \qquad 6\text{-}23$$

where the corresponding BER can be similarly expressed by (6-21).

6.3.3 Threshold Generalized Selection Combining (T-GSC)

Originally introduced by Kong and Milstein in [106] and extensively described in [105] for Rayleigh and in [107] for Nakagami fading, conventional GSC selects a fixed number of strong branches. Alternatively, threshold GSC (T-GSC) [1], contributes in a more efficient selection strategy by including the branches with a larger SNR than the predetermined threshold, γ_T. Such a threshold can be determined dynamically, as well. For example, in a normalized threshold GSC (NT-GSC) [119], $\gamma_T = \gamma_{n_{\max}}\eta_T$, where η_T is a fixed fraction within $0 \leq \eta_T \leq 1$. In a minimum selection GSC (MS-GSC) [108], a minimum number of branches are selected provided that the combined SNR is larger than the threshold. Inspired by MS-GSC, output threshold GSC (OT-GSC) [133] focuses on the resultant output SNR by taking into account the minimum usage of the combiner's resources. Further analyses on the characterization and optimization of GSC are provided in [132], [95].

It seems that multi-branch mobile FSO is an appropriate application for GSC combining, as branches are potentially susceptible to low SNR reception. By this work, a T-GSC scheme is employed for the sake of simple design relative to other GSC

approaches. Branch SNRs are tested against a preset threshold γ_T. All satisfying $\gamma_n \geq \gamma_T$ are attended into the combining process, while the remainders are switched off pending the subsequent branch monitoring period. If none of the channels satisfies the condition, a simple SC is applied. Using a posterior MRC combiner, performance efficiency is maximized and that influence of channel estimation error is minimized under such combining strategy.

Like SC, the utilized combining techniques focus on the availability of instantaneous branch SNR, i.e., CSIs, which are correlated and non-identically distributed (c.n.d.), while at the same time assumed to be perfectly known during combining. Channel estimation, branches combining, and, when necessary, branch switching are periodically performed at times $t_{\text{comb}} = k\tau$, where τ is the combining iteration period and k is the time index. As previously mentioned, if it is assumed that $\tau \gg \tau_c$, then inactive receiver branches can be switched off for additional power saving. A savings for transmitter node can also be realized when unaligned transmitting branches are switched off.

To pursue thresholding at input, a set of variables

$$\gamma_n' = \begin{cases} 0 & 0 \leq \gamma_n < \gamma_T \\ \gamma_n & \gamma_n \geq \gamma_T \end{cases} \qquad \text{6-24}$$

can be defined. The distribution of γ_n' is given in the form of PDF and CDF of γ_n, by [119](Eq. 9.522)

$$f_{\gamma_n'}(\gamma_n') = \begin{cases} F_{\gamma_n}(\gamma_T)\,\delta(\gamma_n') & \gamma_n' = 0 \\ 0 & 0 < \gamma_n' < \gamma_T \\ f_{\gamma_n}(\gamma_n') & \gamma_n' \geq \gamma_T \end{cases} \qquad \text{6-25}$$

where $\delta(\gamma_n^{'})$ is the Dirac delta function; $f_{\gamma_n}(\gamma_n^{'})$ is deduced from (6-10) by $f_{\gamma_n}(\gamma_n^{'}) = \frac{1}{2\bar{\gamma}}\int_0^1 \frac{1}{\sqrt{\ln(1/\alpha)}\alpha^3} f_{h_n^2}\left(\frac{\gamma_n^{'}}{\bar{\gamma}\alpha}\right) f_{\varphi_n}\left(\sqrt{\ln(1/\alpha)}\right) d\alpha$; and $F_{\gamma_n}(\gamma_T)$ is CDF of γ_n at γ_T. The $N/2$-dimensional joint variable is adapted for $\mathbf{\Gamma}'$defined by $\mathbf{\Gamma}' \triangleq \{\gamma_n^{'}\}_{n=1}^{N/2}$, as

$$f_{\mathbf{\Gamma}'}\left(\gamma_1^{'}, \gamma_2^{'}, \dots, \gamma_{\frac{N}{2}}^{'}\right) =$$

$$\begin{cases} F_{\mathbf{\Gamma}_{\mathrm{ON}}}(\underbrace{\gamma_T, \gamma_T, \dots, \gamma_T}_{N/2-\mathrm{fold}})\, \delta(\gamma_1')\, \delta(\gamma_2') \dots \delta(\gamma_{N/2}') & \gamma_1' \text{ or } \gamma_2' \text{ or }, \dots, \gamma_N' = 0 \\ 0 & 0 < \gamma_1' \text{ or } \gamma_2' \text{ or }, \dots, \gamma_N' < \gamma_T \\ f_{\mathbf{\Gamma}_{\mathrm{ON}}}(\gamma_1', \gamma_2', \dots, \gamma_{N/2}') & \gamma_1', \gamma_2', \dots, \gamma_N' \geq \gamma_T \end{cases} \quad 6\text{-}26$$

Assuming uncorrelated noise samples at different receiving apertures, the output SNR of the MRC combiner is equivalent to the sum of the SNR at each aperture:

$$\gamma = \sum_{n=1}^{N} \gamma_n' \quad 6\text{-}27$$

MGF function of the output SNR can now be achieved. Note that the elements of $\{\gamma_n^{'}\}_{n=1}^{N/2}$ are correlated with a PDF given by (6-26). In this case, MGF is

$$M_\gamma(s) = \underbrace{\int_0^\infty \int_0^\infty \dots \int_0^\infty}_{\frac{N}{2}-\mathrm{fold}} f_{\mathbf{\Gamma}'}\left(\gamma_1', \gamma_2', \dots, \gamma_{\frac{N}{2}}'\right) \exp\left[s\left(\gamma_1' + \gamma_2' + \dots + \gamma_{\frac{N}{2}}'\right)\right] d\gamma_{\frac{N}{2}}' \dots d\gamma_1' \quad 6\text{-}28$$

Having MGF of the instantaneous output SNR leads to the evaluation of average BER:

$$P_{T-GSC}^{e} = \frac{1}{\pi}\int_0^{\pi/2} \mathcal{M}_\gamma\left(-\frac{1}{2\sin^2\varphi}\right) d\varphi \quad 6\text{-}29$$

Note that PDF of γ can be presented by calculating the inverse Laplace transform of MGF:

$$f_\gamma(\gamma) = \mathcal{L}^{-1}\{\mathcal{M}_\gamma(s)\} \quad 6\text{-}30$$

CDF is now mathematically achievable by $F_\gamma(\gamma) = \int_0^\gamma f_\gamma(\gamma')\ d\gamma'$. Outage probability with an outage threshold of γ_{out} is given by $F_\gamma(\gamma_{out})$. Providing closed-form expressions for PDF, BER and CDF of γ based on the aforementioned analysis are quite difficult, if not impossible, to achieve. Therefore, numerical analyses in Section 6.4 are carried out to demonstrate performance evaluation.

The optimal detection rule of the receive diversity employing an MRC combiner following T-GSC is given by replacing N by N_T in (6-23):

$$\sum_{n=1}^{N_T} r_n \underset{0}{\overset{1}{\gtrless}} \frac{\sigma_v}{\sqrt{\bar{\gamma}}} \sum_{n=1}^{N_T} \gamma_n + \frac{N_T I_0}{\sqrt{\bar{\gamma}}} \qquad (\mathrm{T-GSC}) \qquad 6\text{-}31$$

where N_T is the number of branches attending the MRC combining.

6.4 Numerical Simulation Analysis

Analytical simulation is possible by computing the integral expressions through BER probability. Deriving exact closed-form expressions for error probabilities of mobile FSO when $N > 2$, is extremely complex, especially when channels are mutually correlated. Alternatively, numerical analysis of BER will be provided.

The popular S-by-S detection method with be utilized along with the availability of perfect CSI. OOK modulation is employed in the simulations by assuming equal noise powers for symbols '0' and '1'. Lognormal distribution is applied for channel fading distribution while the values of correlation coefficient are assumed as $\{\rho_{i,j}\}_{i,j=1,i\neq j}^{N} = \rho$ where $\rho_{i,j} = 1$ for $i = j$. By default, a weak turbulence of $\sigma_\chi = 0.1$ is assumed. Misalignment coefficients $\{\alpha_n\}_{n=1}^{N}$ have a value between 0 and 1. In order to proceed, a uniform distribution for misalignment angle φ_1 is chosen by $f_{\varphi_1}(\varphi_1) = 1/2\pi$ changing

from $-\pi/2$ and $3\pi/2$. It was mentioned earlier that all variables $\{\varphi_n\}_{n=2}^{N}$ can be determined on the basis of φ_1.

Throughout the simulation, a setup of N receiving branches at the receiver side is considered. The transmitter with K branches is assumed perfectly aligned with a receiving mobile FSO node such that only one transmitting branch is connected to the receiver node at any given time. K is an implementation-dependent parameter. In order to develop a power-saving approach, a simple closed-loop power control process is explicitly required to turn off unnecessary transmitters. This same concept is suggested by [116] and [138] as a feedback transmitter selection scenario. An even value for N, ranging from $N = 4$ to 14, will be included. The involved combining diversity schemes were chosen within SC, EGC, MRC and T-GSC methods. Performance evaluation was carried out in terms of BER and outage probability.

To compare the BER performance of available combining schemes, Figure 6-3 is presented for $N = 10$. MRC performance is superior. EGC exhibits the poorest efficiency. SC performance is moderate. Given an average branch SNR equal to $\bar{\gamma} =$ 20dB, EGC loss approximately is 8dB, while SC loss is approximately 1dB. Low SNR values result in T-GSC scheme performance approximate to SC when $\gamma_T = 5$dB. Under such SNR values, the probability of having more than one branch with an instantaneous SNR greater than γ_T is very low. Thus, T-GSC diverges to SC as the combiner selects the branch with the best quality. By contrast, T-GSC converges to MRC for high SNR values, as the number of branches attending the combining process increases. This results in an improvement in the amount of diversity offered by branches. At $\bar{\gamma} = 20$dB, T-GSC shows a loss as small as 0.3dB.

The impact of the number of branches, N, and correlation coefficient, ρ, on T-GSC performance been evaluated in Figure 6-4 and Figure 6-5, respectively. By increasing the number of branches from 4 to 14 at $\bar{\gamma} = 23$dB, a performance gain of approximately 14dB is achieved. Path correlation has a slight influence on BER when the correlation changes from $\rho = 0$ to $\rho = 0.4$, as shown in Figure 6-5. At $N = 12$ and $\bar{\gamma} = 20$dB, the performance loss with a correlation of $\rho = 0.4$ is approximately 1.2dB with respect to uncorrelated branches.

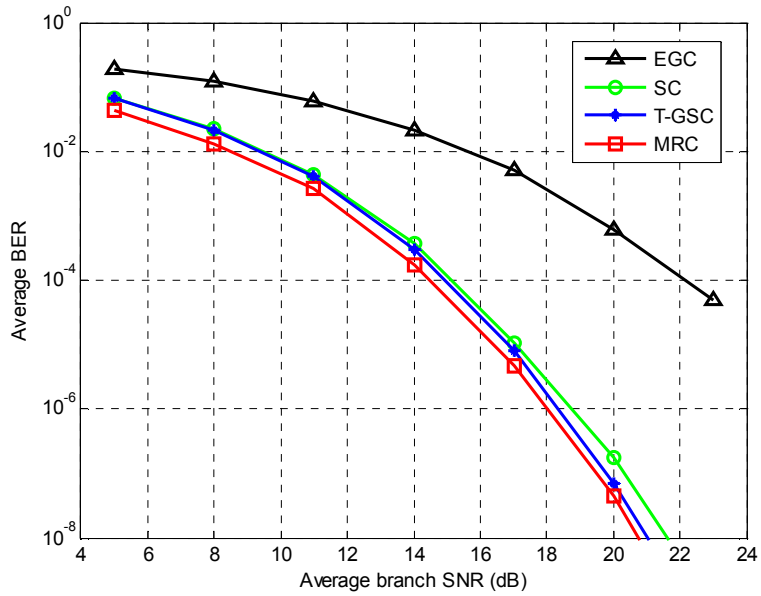

Figure 6-3: Bit error rate performance of the T-GSC compared to EGC, SC and MRC. $N = 10$, $\rho = 0$, $\sigma_\chi = 0.1$ and $\gamma_T = 5$dB

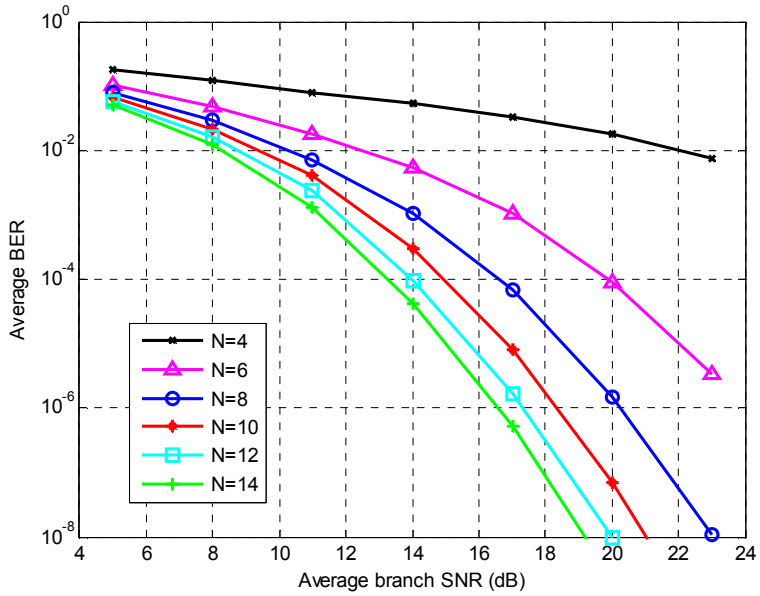

Figure 6-4: The effect of the number of branches on the BER performance of T-GSC. $\rho = 0$, $\sigma_\chi = 0.1$, $\gamma_T = 5$dB

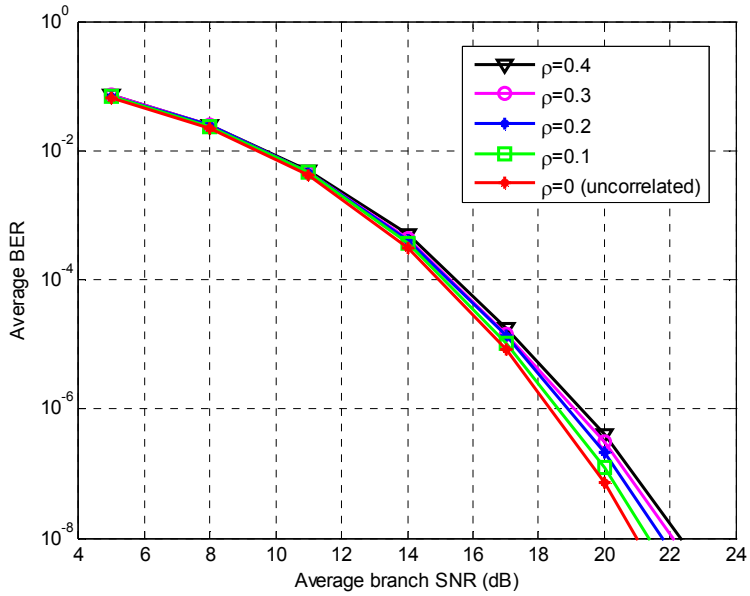

Figure 6-5: The effect of correlation coefficient on the BER performance of T-GSC. $N = 10$, $\sigma_\chi = 0.1$, $\gamma_T = 5$dB

Outage probability is evaluated as a performance criterion in Figure 6-6 and Figure 6-7 for $\rho = 0$ and an outage threshold of $\gamma_{out} = 5$ dB. T-GSC effectively

improves the outage probability relative to EGC; however, a very small loss is shown when T-GSC or SC is used rather than MRC. Specifically, under $N = 10$ independent branches at an SNR of $\bar{\gamma} = 17$dB show a loss of EGC=8dB, while the loss is 1.2dB for SC and 0.7dB for T-GSC.

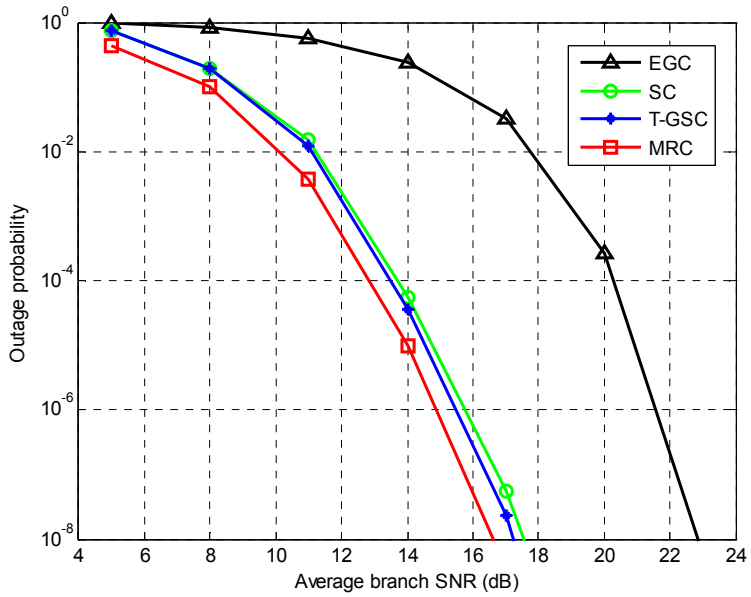

Figure 6-6: Outage probability of the T-GSC compared to EGC, SC and MRC. $N = 10$, $\rho = 0$, $\sigma_\chi = 0.1$, $\gamma_T = 5$dB, and $\gamma_{out} = 5$dB

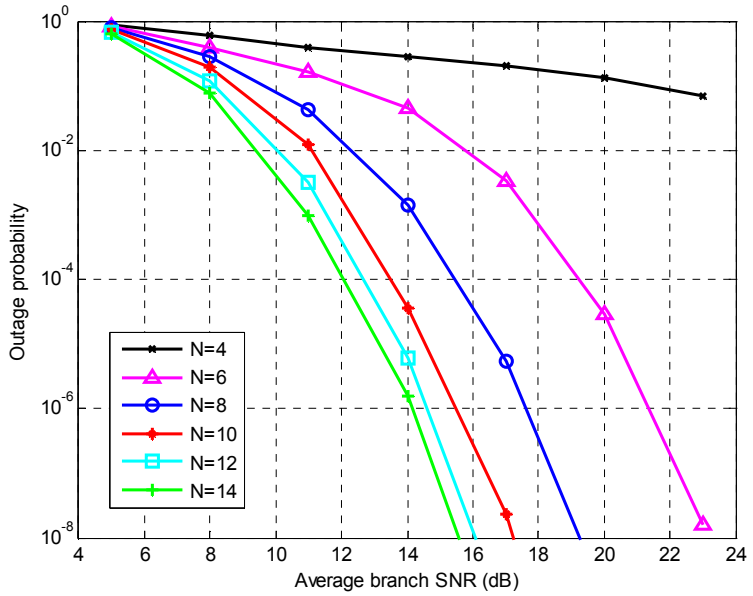

Figure 6-7: The effect of the number of branches on the outage probability of T-GSC. $\rho = 0$, $\sigma_\chi = 0.1$, $\gamma_T = 5$dB and $\gamma_{out} = 5$dB

6.5 Concluding Results

Introducing mobility to FSO nodes that have traditionally been subject to misalignment can increase marketability and encourage the development optical wireless communication applications. Under a multi-branch node design, mobile FSO is comprised of merely a few transmitter/receiver apertures intentionally misaligned to provide an optical coverage under angular diversity. The proposed mobile FSO is built on MIMO with transmit selection diversity based on feedback, and exempts the employment of a traditional mechanical PAT system. An appropriate receive diversity combining scheme was exploited to maintain performance efficiency. Branches were shown to be unbalanced, with half not illuminated. In addition, turbulent channels were considered spatially correlated. Accordingly, T-GSC diversity technique is suggested for combining at the receiver side. T-GSC provides superior BER and outage performance when

compared to EGC and SC. T-GSC is not subject to estimation errors associated with MRC when branches are under low SNR conditions.

7. Conclusions

This dissertation explores the design of diversity solutions for FSO communications with an aim to enhance connectivity robustness. The research includes turbulence-induced fading characteristics, namely scintillation, caused by random fluctuation of transmission media refractivity. Although the study undertaken explicitly focuses on reliability performance improvement of optical wireless communication, its purpose was twofold. First, efficient design of appropriate diversity combining schemes for high data rate optical links was investigated. Second, the feasibility of using a mobile node, namely mobile FSO, was examined under an angular diversity. The latter was found less sensitive to misalignment and movement.

Like RF wireless links, an optical wireless link is comprised of several blocks, including modulation, channel, and detection, among others. The implementation of an optimal detector depends on the availability of CSI, which affects design complexities. If CSI is not available, extensive computation is required to calculate optimal detection of the ML function for any individual bit. This dissertation proposes a thresholding approach, where a threshold value can be computed and then applied as the detection metric. This process omits consistent computational load to the receiver. Furthermore, if

channel coefficients are temporally correlated, a new ML function can be defined by including the correlation between the given and pilot bit. This can be categorized as a time diversity approach, where outcome incorporates superior BER detection performance.

CSI availability can exploit special diversity when random fluctuation of the channel coefficient is slow relative to bit rate. Spatial diversity introduces reliability to the optical link. If a link is obscured or even faded by atmospheric turbulence, alternative links can maintain connectivity. Several techniques for RF domain are currently available. Some are applicable to the optical domain, as well. However, receiving branches in optical links usually remain unbalanced due to significant sensitivity to misalignment and obscuration. This may, in fact, degrade the efficiency of some of the most popular combining schemes, e.g., EGC and MRC, for FSO applications. Additionally, high data rate communication in Gigabits offered by the optical links places some limitation on processing resources at a conventional combiner, e.g., SC.

A *switched diversity* combining approach potentially reduces these types of implementation complexities in a multi-receiving optical wireless receiver. During execution the receiver remains on a selected branch for as long as the SNR remains above a predetermined threshold—even if satisfactory signals are available on alternate branches. The receiver performs branch monitoring, and most likely switching, when the existing signal strength falls below the threshold. Switched diversity is often considered suboptimum to SC diversity implementation, as its performance is generally inferior,. Receiver design can be simplified by avoiding unnecessary switching among the receiver's apertures, i.e., branches. Unlike SC diversity, switched diversity does not

require persistent monitoring of all receiving signals, thus, reducing processing load. Several schemes employ variations based on defined switching strategies. Although systems employing SSC and SEC schemes face relatively low hardware complexities, their BER performance is inferior when compared with SC diversity. This proves a major disadvantage for current switched diversity techniques. Additionally, SSC does not improve BER performance for N >2 when branches are identically distributed. This dissertation proposes an optimized switched diversity scheme (SDC) to achieve comparable BER performance while at the same time reducing combining processing load. It should be noted that the SDC scheme requires a higher processing load than the SSC scheme. An SDC combiner examines the quality of all branches immediately following the observation of a threshold that drops below the SNR level. Consequently, the branch with the highest quality SNR is chosen. SDC is in fact a hybrid SEC/SC scheme. The design and analysis developed in this dissertation entails the foundation of efficient diversity schemes for SIMO or MIMO configuration and formulates the performance evaluation of schemes applicable for various optical wireless link applications, e.g., VLC in IEEE 802.15.7 standard.

Directional reception of narrow FSO beams is a major deterrent to the practical development of FSO links. Mobile FSO offers mobility to an optical network. Asymmetrically unbalanced receiver apertures with intentional misalignment can be installed to establish node mobility while maintaining optical connection. This work considers a circular node structure comprised of apertures intentionally unbalanced in alignment. Under such unbalanced branch configuration, 360-degree coverage is provided with the deployment of angular diversity combining in instances when the need

for a conventional complicated PAT system is exempt. The transmitter follows a transmit selection diversity rule based on a feedback. For the receiver side, SC, EGC, MRC, and T-GSC techniques were candidates for combining purposes. EGC provided unacceptable values, i.e., poorest BER performance and outage probability, and MRC was found to be the most efficient numerically. T-GSC provided superior performance over EGC and SC. MRC faced implementation complexities. When compared with MRC, T-GSC is influenced less by estimation error. Overall performance superiority for mobile FSO was obtained when T-GSC was used over SC and EGC. A circular structure was designed for this dissertation to allow mathematical analysis evaluation. Other structures, e.g., 3d-spherical, that deploy an angular diversity combining scheme can be designed and evaluated following a similar analysis.

The work presented herein focuses on the design of diversity solutions for FSO communication. The proposed technique has both unique advantages and technical challenges that should be addressed in future work. In addition to the development of other features/challenges associated with FSO, useful extensions could focus on the experimental aspects. These include:

- *New diversity solutions*. Future research should extend the proposed designs to include additional diversity solutions. Wavelength diversity, i.e., several optical beams employed at different light wavelengths that provide redundancy to the optical connection, is a possible candidate.
- *Multiuser MIMO*. Design challenges for a data link-layer of a complex system multiuser MIMO is beyond the scope of pure physical-layer design implementation.

In future work, design study of a MIMO link under a multiuser architecture is proposed. An efficient design of MAC layer must first be targeted.

- *Experiments*. This dissertation considers practical design challenges to the efficiency of multi-receiving FSO links over various implementation aspects. The diversity techniques provided can be implemented under a lab or field test-bed using non-realtime (offline) and realtime (online) test routines. Under the offline mode shown in Figure 7-1, test measurement data are recorded for appropriate post-processing, which will be carried out offline to provide corresponding test results. While under online test routines demonstrated in Figure 7-2, test measurement data are processed while the test scenario is running. This category of test routines is applicable when a QoS criterion concept related to the proposed protocol/technique is under investigation. The QoS criteria can be among realtime processing performance, memory usage, or resource allocation performance.

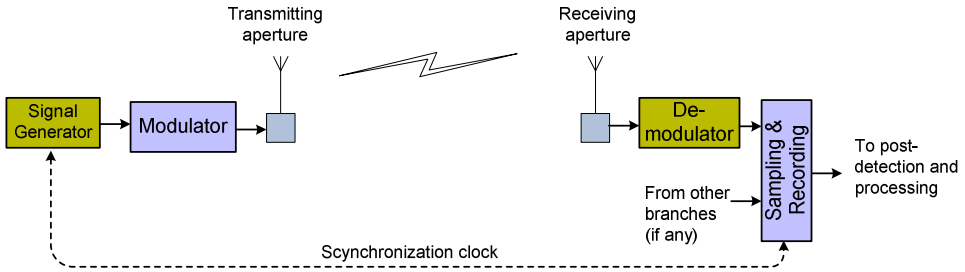

Figure 7-1: Non-realtime testbed

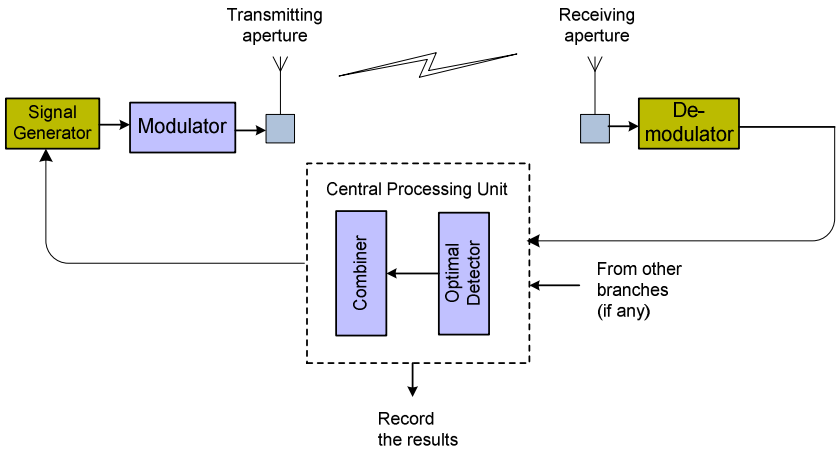

Figure 7-2: Realtime testbed

- *IEEE 802.15.7*. Commercial application of FSO systems will be realized via the development of VLC technology, which is standardized by IEEE. This standard identifies the physical layer and data link layer of a VLC-based WPAN network. As a user-dependent feature, the diversity technologies presented can adhere to the standard for enhancing connection performance. Additionally, MIMO technology can be added to the standard to support both superior performance and higher data rates.

References

1. IEEE802.15.7, *Short-Range Wireless Optical Communication Using Visible Light*. 6 September 2011, IEEE-SA. p. 1-309.

2. Gfeller, F.R. and U. Bapst, *Wireless In-House Data Communication via Diffused Infrared Radiation.* Proceedings of the IEEE, 1979. **76**(11): p. 1474-1486.

3. Mahdy, A. and J.S. Deogun, *Wireless Optical Communications: A Survey*, in *WCNC'04*. 2004. p. 2399-2404.

4. Kashyap, A., A. Rawat, and M. Shayman, *Routing and traffic engineering in hybrid RF/FSO networks*, in *IEEE ICC'05*. 2006. p. 3427-3433.

5. Vangala, S. and H. Pishro-Nik, *A Highly Reliable FSO/RF Communication System Using Efficient Codes*, in *IEEE GLOBECOM'07*. 2007. p. 2232-2236.

6. Kashyap, A., A. Rawat, and M. Shayman, *Integrated Backup Topology Control and Routing of Obscured Traffic in Hybrid RF/FSO Networks*, in *IEEE GLOBECOM '06*. 2006. p. 1-6.

7. Falahpour, M., Moradi, H., Refai, H. H., LoPresti, P. G., Atiquzzaman, M., *Performance Comparison of Classic and Fuzzy Logic Controllers for Communication Airships*, in *28th DASC*. 2009: Orlando, FL.

8. Jahir, Y., M.R. Atiquzzaman, H., and P.G. LoPresti, *Multipath hybrid Ad hoc networks for avionics applications in disaster area*, in *28th IEEE/AIAA DASC'09*. 2009.

9. Yun, G. and M. Kavehrad, *Spot-Diffusing and fly-safe receivers for indoor infrared wireless communications*, in *IEEE ICSTWC'92*. 1992: BC, Canada. p. 262-265.

10. Minh, H.L., Ghassemlooy, Z., O'Brien, D., Faulkner, G., *Indoor Gigabit Optical Wireless Communications: Challenges and Possibilities*, in *ICTON'10*. 2010. p. 1-6.

11. Kavehrad, M. and J. Fadlullah. *Wideband Optical Propagation Measurement System for Characterization of Indoor Optical Wireless Channels*. in *SPIE Photonic West'10*. 2010. San Francisco.

12. Kim, I.I. and E. Korevaar, *Availability of Free Space Optics (FSO) and Hybrid FSO/RF Systems*, in *SPIE*. 2001. p. 84-95.

13. Moradi, H., Falahpour, M., Refai, H. H., LoPresti, P. G., and Atiquzzaman, M., *Availability Modeling of FSO Mesh Networks through Turbulence-induced Fading Channels*, in *IEEE INFOCOM'10*. 2010. p. 1-5.

14. Clark, P. and A. Sengers, *Wireless Optical Networking: Challenges and Solutions*, in *IEEE MILCOM'04*. 2004. p. 416-422.

15. Gurumani, S., *Implementation of Dynamic Path Reconfiguration among Hybrid FSO/RF links*. 2007, University of Oklahoma.

16. Gurumani, S., Moradi, H., Refai, H. H., LoPresti, P. G., Atiquzzaman, M., *Dynamic Path Reconfiguration among Hybrid FSO/RF Nodes*, in *IEEE GLOBECOM'08*. 2088. p. 1-5.

17. Moradi, H., Falahpour, M., Refai, H. H., LoPresti, P. G., and Atiquzzaman, M., *Toward an Optimal Combined FSO/RF System via an Adaptive Bit Rate Control*, in *SPIE Photonics West*. 2010: San Francisco, CA, USA. p. 1-10.

18. Frigyes, I. and L. Csurgai-Horvath, *Free-Space Optics and E-Band Radio: Complementary Techniques for Gbit/Sec Wireless*, in *WCNC'10 Workshops*. 2010: Sydney, Australia. p. 1-5.

19. Vangala, S. and H. Pishro-Nik, *Optimal Hybrid RF-Wireless Optical Communication for Maximum Efficiency and Reliability*, in *Proceedings of the 41st CISS'07*. 2007. p. 684-689.

20. Luna, R., Borah, D. K., Jonnalagadda, R., Voelz, D. G., *Experimental Demonstration of a Hybrid Link for Mitigating Atmospheric Turbulence Effects in Free-Space Optical Communication.* IEEE Photonics Technology Letters, 2009. **21**(17): p. 1196-1198.

21. Ho, T., Trisno, S., Smolyaninov, I., Milner, S., Davis, C. C., *Studies of Pointing, Acquisition, and Tracking of Agile Optical Wireless Transceivers for Free Space Optical Communication Networks*, in *SPIE Conference, Remote Sensing*. 2003: Barcelona, Spain. p. 147-158.

22. Llorca, J., Desai, A., Baskaran, E., Milner, S., Davis, C. C., *Optimizing Performance of Hybrid FSO/RF Networks in Realistic Dynamic Scenarios*, in *Proc. SPIE*. 2005. p. 1-9.

23. Ho, T.H., Trisno, S., Desai, A., Llorca, J., Milner, S., and Davis, C. C., *Performance and analysis of reconfigurable hybrid FSO/RF wireless networks*, in *Proc. SPIE*. 2005.

24. Jahir, Y., Atiquzzaman, M., Refai, H., LoPresti, P.G., *AODVH: Ad Hoc On-Demand Distance Vector Routing for Hybrid Nodes*, in *IEEE ICC'10*. May 2010. p. 1-5.

25. Tapse, H., Borah, D. K., *Performance of Regular Low Density Parity Check Codes over Hybrid Optical/RF Channels*, in *IEEE Globecom'08*. 2008. p. 1-5.

26. Moradi, H., Falahpour, M., Refai, H. H., LoPresti, P. G., Atiquzzaman, M., *On the Capacity of Hybrid FSO/RF Links*, in *IEEE Globecom'10*. Dec. 2010: Miami, FL. p. 1-5.

27. Goldsmith, A., and Varaiya, P., *Capacity of fading channels with channel side information.* IEEE Transactions on Information Theory, November 1997: p. 1986-1992.

28. Gagliardi, R.M., and Karp, S., *Optical Communications*. 2nd ed. 1995: John Wiley & Sons, Inc.

29. Riediger, M.L.B., Schober, R., and Lampe, L., *Fast multiple-symbol detection for free-space optical communications.* IEEE Trans. Commun., April 2009. **57**(4): p. 1119-1128.

30. Riediger, M.L.B., Schober, R., and Lampe, L., *Multiple-Symbol Detection for Photon-Counting MIMO Free-Space Optical Communications.* IEEE Trans. Wireless Commun., Dec. 2008. **7**(12): p. 5369-5379.

31. Navidpour, S.M., Uysal, M., and Kavehrad, M., *BER Performance of Free-Space Optical Transmission with Spatial Diversity.* IEEE Trans. Wireless Commun., Aug. 2007. **6**(8): p. 2813-2819.

32. Tsiftsis, T.A., Sandalidis, H.G., Karagiannidis, G.K., and Uysal, M., *Optical wireless links with spatial diversity over strong atmospheric turbulence channels.* IEEE Trans. Wireless Commun., Feb. 2009. **8**(2): p. 951-957.

33. Khalighi, M.-A., Schwartz, N., Aitamer, N., and Bourennane, S., *Fading Reduction by Aperture Averaging and Spatial Diversity in Optical Wireless Systems.* IEEE/OSA Journal of Optical Communications and Networking, Nov. 2009. **1**(6): p. 580-593.

34. Moradi, H., Refai, H. H., LoPresti, P. G., and Atiquzzaman, M., *A PSAM-Based Estimator of Noise and Fading Statistics for Optimum Receivers of Free Space Optics Signals*, in *SPIE Photonic West*. Jan. 2010: ,San Francisco, CA, USA. p. 1-10.

35. Letzepis, N., Holland, I., and Cowley, W., *The Gaussian free space optical MIMO channel with Q-ary pulse position modulation.* IEEE Trans. Wireless Commun., 2008. **7**(5, Part1): p. 1744–1753.

36. Safari, M., Uysal, M., *Diversity gain analysis of free-space optical communication systems*, in *CCECE'08*. 2008: Niagara Falls, ON, Canada. p. 1239–1244.

37. Lee, E.J., and Chan, V. W. S., *Part 1: Optical Communication over the Clear Turbulent Atmospheric Channel Using Diversity.* IEEE Journal on selected Area in Commun., Nov. 2004. **22**(9): p. 1896-1906.

38. Bayaki, E., Schober, R., and Mallik, R. K., *Performance Analysis of MIMO Free–Space Optical Systems in Gamma–Gamma Fading.* IEEE Trans. Commun., Nov. 2009. **57**(11): p. 3415–3424.

39. Ghassemlooy, Z., Popoola, W. O., Ahmadi, V., and Leitgeb, E., *MIMO Free-Space Optical Communication Employing Subcarrier Intensity Modulation in Atmospheric Turbulence Channels*, in *EuropeComm'09*. 2009, Springer. p. 61–73.

40. Samimi, H., and Azmi, P., *Subcarrier Intensity Modulated Free-Space Optical Communications in K-Distributed Turbulence Channels.* IEEE/OSA Journal of Optical Communications and Networking, Aug. 2010. **2**(8): p. 625-632.

41. Tang, X., Rajbhandari, S., Popoola, W.O., Ghassemlooy, Z., Leitgeb, E., Muhammad, S.S., Kandus, G., *Performance of BPSK Subcarrier Intensity Modulation Free-Space Optical Communications using a Log-normal Atmospheric Turbulence Model*, in *SOPO'10*. 2010. p. 1-5.

42. Ohtsuki, T., *Multiple-subcarrier modulation in optical wireless communications.* IEEE Communications Magazine, 2003. **41**(3): p. 74-79.

43. Karp, S., Gagliardi, R. M., Moran, S. E, and Stotts, L. B., *Optical Channels*. 1988: Plenum Press.

44. Bekkali, A., Naila, C. B., Kazaura, K., Wakamori, K., Matsumoto, M., *Transmission Analysis of OFDM-Based Wireless Services Over Turbulent Radio-on-FSO Links Modeled by Gamma–Gamma Distribution.* IEEE Photonics Journal, June 2010. **2**(3): p. 510-520.

45. Wakamori, K., Kazaura, K., Matsumoto, M., *Research and Development of a Next-Generation Free-Space Optical Communication System*, in *Proc. of SPIE*. 2009: San Jose, CA, USA. p. 1-12.

46. Karout, J., Agrell, E., and Karlsson, M., *Power efficient subcarrier modulation for intensity modulated channels.* OSA Journal of Optics Express, Aug. 2010. **18**(17): p. 17913-17921.

47. Popoola, W.O., Ghassemlooy, Z., *BPSK Subcarrier Intensity Modulated Free Space Optical Communications in Atmospheric Turbulence.* IEEE/OSA Journal of Lightwave Technology, April 2009. **27**(8): p. 967-973.

48. Popoola, W.O., Ghassemlooy, Z., and Leitgeb, E., *BER and Outage Probability of DPSK Subcarrier Intensity Modulated Free Space Optics in Fully Developed Speckle.* Journal of Communication, Academy Publisher, Sep. 2009. **4**(8): p. 546-554.

49. Ben Naila, C., Bekkali, A., Kazaura, K., Wakamori, K., and Matsumoto, M., *Evaluating M-ary PSK multiple-subcarrier modulation over FSO links using aperture averaging*, in *Proc. of SPIE*. 2010.

50. Shieh, W., Djordjevic, I., *OFDM for optical communications*. 2010: Academic Publisher.

51. Djordjevic, I.B., Vasic, B., and Neifeld, M. A., *LDPC-Coded OFDM for Optical Communication Systems with Direct Detection.* IEEE Journal of Selected Topics in Quantum Electronics, Sept.-Oct. 2007. **13**(5, Part 2): p. 1446-1454.

52. Cvijetic, N., Qian, D., Wang, T., *10Gb/s Free-Space Optical Transmission using OFDM*, in *OFC/NFOEC*. 2008. p. 1-3.

53. Keiser, G., *Optical Communications Essentials*. 2003: McGraw–Hill.

54. Rorabaugh, C.B., *Simulating Wireless Communication Systems*. 2004: Prentice Hall.

55. Sandalidis, H.G., Tsiftsis, T. A., Karagiannidis, G. K., and Uysal, M., *BER Performance of FSO Links over Strong Atmospheric Turbulence Channels with Pointing Errors.* IEEE Commun. Letters, Jan. 2008. **12**(1): p. 44-46.

56. Goodman, J.W., *Introduction to Fourier Optics*. 3rd ed. 2005: Roberts & Company Publishers.

57. Harris, A., Sluss, J. J., Jr., and Refai, H. H., *Free-space optical wavelength diversity scheme for fog mitigation in a ground-to-unmannedaerial-vehicle communications link.* SPIE Journal of Optical Engineering, Aug. 2006. **45**(8): p. 1-12.

58. Arnon, S., Rotman, S. R., Norman, Kopeika, S., *Performance limitations of free-space optical communication satellite networks due to vibrations: direct detection digital mode.* SPIE Journal of Optical Engineering, Nov. 1997. **36**(11): p. 3148–3157.

59. Ho, T.H., Milner, S., and Davis, *Fully Optical Real-time Pointing, Acquisition and Tracking System for Free Space Optical Link*, in *Proceedings of SPIE*. 2005: WA, USA.

60. Shim, Y., Milner, S., and Davis, *A precise pointing technique for free space optical links and networks using kinematic GPS and local sensors.* Proc. of SPIE, 2007. **6709**.

61. Cap, G.A., Refai, H. H., and Sluss, J. J., Jr., *FSO Tracking and Auto-Alignment Transceiver System.* Proc. of SPIE, 2008. **7112**: p. 1-12.

62. Al-Akkoumi, M.K., Refai, H., and Sluss, J. J., Jr., *A Tracking System for Mobile FSO.* Proc. of SPIE, 2008. **6877**.

63. Yan, P., Sluss, J. J., Jr., Refai, H. H., LoPresti, P. G., *Enhancing mobile ad hoc networks with free-space optics.* SPIE Journal of Optical Engineering, Aug. 2007. **46**: p. 1-7.

64. Sofka, J., Nikulin, V. V., Skormin, V., A., Hughes, D. H., and Legare, D. J., *Laser Communication Between Mobile Platforms.* IEEE Trans. on Aerospace and Electronic Systems, Jan. 2009. **45**(1): p. 336-246.

65. Georges, E.S., *Evaluation of cone tracking for free-space optical communication with a retro-modulator*, in *Proc. of SPIE*. 2007.

66. Yuksel, M., Akella, J., Kalyanaraman, S., and Dutta, P., *Free-space-optical mobile ad hoc networks: Auto-configurable building blocks.* Wireless Network Journal, ACM/Springer, 2007: p. 295--312.

67. Bilgi, M., and Yuksel, M., *Multi-Element Free-Space-Optical Spherical Structures with Intermittent Connectivity Patterns*, in *IEEE Infocom'08 Workshops*. March 2008. p. 1-4.

68. Nakhkoob, B., Bilgi, M., Yuksel, M., and Hella, M., *Multi-Transceiver Optical Wireless Spherical Structures for MANETs.* IEEE Journal on Selected Areas in Communications, Dec. 2009. **27**(9): p. 1612-1622.

69. Ghosh, A.K., Kunta, S., Verma, P., and Huck, R. C., *Free-space Optics based Sensor Network Design using Angle-diversity Photodiode Arrays*, in *Proceedings of SPIE*. 2010. p. 1-7.

70. Ghosh, A.K., Kunta, S., Verma, P., and Huck, R. C., *Mobility in free-space optics based wireless sensor networks.* Proceedings of SPIE, 2010. **7814**: p. 1-7.

71. Spaunhorst, S., LoPresti, and Refai, H., *Experimental evaluation of a misalignment tolerant FSO receiver.* Proc. of SPIE, 2010. **7685**.

72. Zhou, D., Refai, H. H., LoPresti, P. G., Atiquzzaman, M., *Control algorithm development for mobile FSO node alignment*, in *28th IEEE/AIAA DASC'09*. 2009. p. 1-12.

73. Hajjarian, Z., Kavehrad, M., and Fadlullah, J., *Analysis of wireless optical communications feasibility in presence of clouds using markov chains.* IEEE Journal on selected Area in Commun., 2009. **27**(2): p. 1526-1534.

74. Kolmogorov, A., *Interpolation and extrapolation.* Bull. Acad. Sci., USSR, Ser. Math., 1941. **5**: p. 3-14.

75. Tatarski, V.I., *Wave propagation in a Turbulent Medium*. 1961: McGraw Hill Inc.

76. Andrews, A.C., Philips, R. L., Hopen, C. Y., *Laser Beam Scintillation with Applications*. 2001: SPIE Press.

77. Strohbehn, J.W., *Laser Beam Propagation in the Atmosphere*. 1978: Springer-Verlag.

78. Ishimaru, A., *Wave Propagation and Scattering in Random Media*. 2nd ed. 1997: IEEE Press.

79. Zhu, X., Kahn, J. M., *Free-Space Optical Communication Through Atmospheric Turbulence Channels.* IEEE Transactions on Commun., Aug. 2002. **50**(8): p. 1293-1300.

80. Jimenez, C.O.F., *Understanding the atmospheric turbulence structure parameter in the littoral regime*, in *Physics*. 2006, University of Puerto Rico.

81. Safari, M., Uysal, M., *Relay-Assisted Free-Space Optical Communication.* IEEE Trans. on Wireless Commun., Dec. 2008. **7**(12): p. 5441-5449.

82. Haas, S.M., *Capacity of and coding for multiple-aperture wireless optical communications*. May 2003, Massachusetts Institute of Technology.

83. Moradi, H., Refai, H. H., and LoPresti, P. G., *Thresholding-based Optimal Detection of Wireless Optical Signals.* IEEE/OSA Journal of Optical Commun. and Networking, Sep. 2010. **2**(9): p. 689–700.

84. Uysal, M., Li, J., and Yu, M., *Error rate performance analysis of coded free-space optical links over gamma-gamma atmospheric turbulence channels.* IEEE Trans. on Wireless Commun., 2006. **5**(6): p. 1229–1233.

85. Garcia-Zambrana, A., Castillo-Vazquez, C., and Castillo-Vazquez, B., *On the Capacity of FSO Links over Gamma-Gamma Atmospheric Turbulence Channels Using OOK Signaling.* EURASIP Journal on Wireless Communications and Networking, 2010. **2010**: p. 1-9.

86. Kiasaleh, K., *Performance of Coherent DPSK Free-Space Optical Communication Systems in K-Distributed Turbulence.* IEEE Trans. Commun., April 2006. **54**(4): p. 604–607.

87. Uysal, M., Navidpour, M., Li, J., *Error Rate Performance of Coded Free-Space Optical Links over Strong Turbulence Channels.* IEEE Commun. Letters, Oct. 2004. **8**(10): p. 635-637.

88. Niu, M., Cheng, J., and Holzman, J. F., and McPhail, L., *Performance Analysis of Coherent Free Space Optical Communication Systems with K-Distributed Turbulence*, in *IEEE ICC'09*. 2009. p. 1-5.

89. Zhu, X., and Kahn, J. M., *Pilot-Symbol Assisted Modulation for Correlated Turbulent Free-Space Optical Channels*, in *Proceedings of SPIE*. 2002. p. 138-145.

90. Osche, G.R., *Optical Detection Theory*. 2002: John Wiley & Sons, Inc.

91. Riediger, M.L.B., Schober, R., and Lampe, L., *Decision-Feedback Detection for Free-Space Optical Communications*, in *66th IEEE VTC'07*. Sept.-Oct. 2007. p. 1193-1197.

92. Aviv, G.D., *Laser Space Communications*. Artech House. 2006.

93. Xu, F., Khalighi, A., Caussee, P., Bourennane, S., *Channel coding and time-diversity for optical wireless links.* OSA Journal of Optics Express, 2009. **17**(2): p. 872-887.

94. Ibrahim, M.M., and Ibrahim, A. M., *Performance analysis of optical receivers with space diversity reception,* . Proc. IEE Commun., Dec. 1996. **143**(6): p. 369-372.

95. Puryear, A.L., *Optical Communication Through the Turbulent Atmosphere with Transmitter and Receiver Diversity, Wavefront Control, and Coherent Detection*. June 2011, Massachusetts Institute of Technology: Cambridge.

96. Vetelino, F.S., Young, C., Andrews, L., and Recolons, J., *Aperture averaging effects on the probability density of irradiance fluctuations in moderate-to-strong turbulence.* OSA Journal of Applied Optics, Apr. 2007. **46**(11): p. 2099–2108.

97. Chen, J., Ai, Y., *Laser Signal Intensity and Aperture Averaging Analysis in 16km Free-Space Optical Links*, in *SOPO'10*. 2010. p. 1-4.

98. Karimi, M., and Nasiri-Kenari, M., *[96] BER Analysis of Cooperative Systems in Free-Space Optical Networks.* IEEE/OSA Journal of Lightwave Technology, Dec. 2009. **27**(24): p. 5639-5647.

99. Moores, J.D., Walther, F. G., Greco, J. A., Michael, s., Wilcox, W. E., Volpicelli, A. M., Magliocco, R. J., and Henion, S. R., *Architecture overview and data summary of a 5.4 km free-space laser communication experiment*, in *Proc. of SPIE*. 2009. p. 7-9.

100. Joyner, V.M., Zhang, Y., and Zeng, J., *An area-efficient maximum-ratio-combining diversity receiver in 90 nm CMOS for free-space optical links.* Analog Integrated Circuits and Signal Processing, Springer, Dec. 2009. **64**(2): p. 115-121.

101. Moradi, H., Falahpour, M., Refai, H. H., LoPresti, P. G., and Atiquzzaman, M., *BER Analysis of Optical Wireless Signals through Lognormal Fading Channels with Perfect CSI*, in *IEEE ICT*. April 2010: Doha, Qatar. p. 493-497.

102. Popoola, W.O., Ghassemlooy, Z., Lee, C. G., and Boucouvalas, A. C., *Scintillation Effect on Intensity Modulated Laser Communication Systems—a Laboratory Demonstration.* Optics & Laser Technology, Elsevier Journal, June 2010. **42**(4): p. 682-692.

103. Hitam, S., Abdullah, M. K., Mahdi, M. A., Harun, H., Sali, A., and Fauzi, M., *Impact of increasing threshold level on higher bit rate in free space optical communications.* Journal of Optical and Fiber Communications Research, Springer, Dec. 2009. **6**(1-6): p. 22-34.

104. Kay, S.M., *Intuitive Probability and Random Processes using MATLAB*. 2006: Springer.

105. Xilinx, *Xilinx University Program Virtex-II Pro Development System*. July 21, 2009.

106. Webpage. http://www.xilinx.com/tools/sysgen.htm.

107. Webpage. http://www.xilinx.com/tools/platform.htm.

108. Le-Minh, H.G., Z. Ijaz, M. Rajbhandari, S. Adebanjo, O. Ansari, S. Leitgeb, E. , *Experimental study of bit error rate of free space optics communications in laboratory controlled turbulence*, in *GLOBECOM Workshops*. Dec. 2010: Miami, FL. p. 1072-1076

109. Kaw, A., Kalu, E. E., *Numerical Methods with Applications*. 1st ed. 2008: Autarkaw.

110. Abramowitz, M.a.S., I. A., *Handbook of Mathematical Functions with Formulas, Graphs, and Mathematical Tables*. 1964: US Department of Commerce.

111. Golub, G.H., and Van Loan, C. F., *Matrix Computations, 3rd edition*. 3rd ed. 1996: Johns Hopkins University Press.

112. Webpage. http://www.alglib.net/matrixops/symmetric/cholesky.php.

113. Jurado-Navas, A., and Puerta-Notario, A., *Generation of Correlated Scintillations on Atmospheric Optical Communication.* IEEE/OSA Journal Optical Communications and Networking, Oct. 2009. **1**(5): p. 452–462.

114. Moradi, H., Refai, H. H., and LoPresti, P. G., *Switch-and-Stay and Switch-and-Examine Dual Diversity for High Speed FSO Links.* IET Optoelectronics Journal, 2011.

115. Wang, Z., Zhong, W-D., Fu, S., and Lin, C., *Performance Comparison of Different Modulation Formats Over Free-Space Optical (FSO) Turbulence Links With Space Diversity Reception Technique.* IEEE Photonics Journal, Dec. 2009. **1**(6): p. 277–285.

116. García-Zambrana, A., Castillo-Vázquez, C., Castillo-Vázquez, B., and Hiniesta-Gómez, *Selection Transmit Diversity for FSO Links Over Strong Atmospheric Turbulence Channels.* IEEE Photonics Technology Letters, July 2009. **21**(14): p. 1017-1019.

117. Hajjarian, Z., Fadlullah, J., and Mohsen Kavehrad, *MIMO Free Space Optical Communications in Turbid and Turbulent Atmosphere.* Journal of Commun., Sep. 2009. **4**(8): p. 524-532.

118. Popoola, W.O., Ghassemlooy, Z., Allen, J. I. H., Leitgeb, E., and Gao, S., *Free-space optical communication employing subcarrier modulation and spatial diversity in atmospheric turbulence channel.* IET Optoelectron Journal, 2008. **2**(1): p. 16–23.

119. Simon, M.K., and Alouini, M. S., *Digital Communication over Fading Channels*. 2nd ed. 2005: John Wiley & Sons, Inc.

120. Abu-Dayya, A.A., and Beaulieu, N. C., *Analysis of Switched Diversity Systems on Generalized-Fading Channels.* IEEE Trans. Commun., Nov. 1994. **42**(11): p. 2259-2966.

121. Zhu, X., and Kahn, J. M., *Markov Chain Model in Maximum-Likelihood Sequence Detection for Free-Space Optical Communication Through Atmospheric Turbulence Channels.* IEEE Trans. Commun., March 2003. **51**(3): p. 509-516.

122. Moradi, H., Refai, H. H., and LoPresti, P. G., *Selection Diversity for Wireless Optical Communications with Non-CSI Non-coherent Optimal Detection*, in *IEEE Globecom'10*. Dec. 2010: Miami, FL. p. 1010-1014.

123. Anguita, J.A., Neifeld, M. A., and Vasic, B. V., *Spatial correlation and irradiance statistics in a multiple-beam terrestrial free-space optical communication link.* Journal of Applied Optics, Sep. 2007. **46**(26): p. 6561-6571.

124. Alouini, M.S., and Simon, M. K., *Dual Diversity Over Correlated Log-Normal Fading Channels.* IEEE Trans. Commun., Dec. 2002. **50**(12): p. 1946-1959

125. Ko, Y.C., Alouini, M. S., and Simon, M. K., *Analysis and Optimization of Switched Diversity Systems.* IEEE Trans. on Vehicular Tech., Sept. 2000. **49**(5): p. 1813-1831.

126. Alsaadi, F.E., and Elmirghani, J. M. H., *Adaptive mobile multicarrier code division multiple access optical wireless systems employing a beam clustering method and diversity detection.* IET Optoelectron. Journal, 2010. **4**(3): p. 95-112.

127. Moradi, H., Refai, H. H., and LoPresti, P. G., *A Switched Diversity Approach for Multi-receiving Optical Wireless Systems.* Applied Optics, Oct. 2011. **50**(29): p. 5606–5614.

128. Nam, H., and Alouini, M. S., *Optimization of Multi-Branch Switched Diversity Systems.* IEEE Trans. Commun., Oct. 2009. **57**(10): p. 2960-2970.

129. Alexandropoulos, G.C., Mathiopoulos, P. T., and Sagias, N.C., *Switch-and-Examine Diversity Over Arbitrarily Correlated Nakagami-m Fading Channels.* IEEE Trans. Vehicular Technology, May 2010. **59**(4): p. 2080-2087.

130. Cvijetic, N., Wilson, S. G., and Brandt-Pearce, M., *Performance Bounds for Free-Space Optical MIMO Systems with APD Receivers in Atmospheric Turbulence.* IEEE Journal on Selected Areas in Commun., April 2008. **26**(3): p. 2-12.

131. Popoola, W.O., Ghassemlooy, Z., Leitgeb, E., and Ahmadi, *Terrestrial Free-Space Optical Links with Temporal Diversity*, in *CSNDSP'10*. July 2010: Newcastle, UK. p. 598–603.

132. Moradi, H., Refai, H. H., and LoPresti, P. G., *Circular MIMO FSO Nodes with Transmit Selection and Receive Generalized Selection.* Submitted to IEEE Trans. on Vehicular Technology, 2011.

133. Moradi, H., Refai, H. H., LoPresti, P. G., and Atiquzzaman, M., *Mobile FSO Nodes in SIMO Setup under Transmitter Misalignment.* Wiley Wireless Communications and Mobile Computing, 2011.

134. Okorafor, U.N., and Kundur, D., *On the Relevance of Node Isolation to the K-Connectivity of Wireless Optical Sensor Networks.* IEEE Trans. on Mobile Computing, Oct. 2009. **8**(10): p. 1427-1440.

135. Alattar, J.M., and Elmirghani, J. M. H., *Optical Wireless Systems Employing Adaptive Collaborative Transmitters in an Indoor Channel.* IEEE Trans. Vehicular Technology, Jan. 2010. **59**(1): p. 63-74.

136. Spaunhorst, S., LoPresti, P. G., Pondelik, S., and Refai, H., *Evaluation of a Novel FSO Receiver for Mitigating Alignment Errors*, in *Proc. of SPIE*. 2009. p. 1-8.

137. Gray, J.E., and Addison, S. R., Characteristic functions in radar and sonar, *Characteristic functions in radar and sonar*, in *34rd SSST*. March 2002: Huntsville, AL. p. 31-35.

138. Abou-Rjeily, C., *On the Optimality of the Selection Transmit Diversity for MIMO-FSO Links with Feedback.* IEEE Commun. Letters, June 2011. **15**(6): p. 641–643.

Appendix A: Glossary of Abbreviations

APL	Additional Processing Load; the processing load induced to the diversity combiner due to branch monitoring and signal combining.
BER	Bit Error Rate
BEP	Bit Error Probability
CDF	Cumulative Distribution Function
c.i.d.	Correlated and identically distributed
c.n.d.	Correlated and non-identically distributed
CSI	Channel State Information; the knowledge of instantaneous information on the status and value of the channel gain (i.e. coefficient)
DD	Direct Detection; in this kind of detection, the detector directly converts the received optical signal power to electric signal. No local carrier signal before optical-to-electrical conversion is used at the receiver.
EGC	Equal Gain Combining
FPGA	Field-Programmable Gate Arrays
FSO	Free Space Optics
GSC	Generalized Selection Combining
IM	Intensity Modulation; the modulation technique that information is contained in the intensity of the transmitted signal; OOK, PPM and SIM are placed in this category
ISI	Inter-Symbol Interference
LD	Laser Diode
LDPC	Low Density Parity Check
LED	Light Emitting Diode
LoS	Line of Sight
LTD	Likelihood Thresholding Detection
MANET	Mobile Ad hoc Network
MGF	Moment-Generating Function

MIMO	Multiple-Input Multiple-Output; a diversity system with multi transmitter and multi receivers
MISO	Multiple-Input Single-Output; a diversity system with multi transmitters but only one receiver
ML	Maximum Likelihood
MRC	Maximum Ratio Combining
MSA	Multi-Slot Averaging
NRZ	Non-Return-to-Zero
OFDM	Orthogonal Frequency Division Multiplexing
OOK	On-Off Keying
OWC	Optical Wireless Communication
P2P	Point-to-Point
PAT	Pointing, Acquisition, and Tracking
PCD	PSAM-based Correlative Detection
PDF	Probability Distribution Function
PEP	Pairwise Error Probability; has similar concept of BER but used for M-ary digital and also when comparing samples in two sequences. For ordinary binary communication, BER=PEP.
PPM	Pulse Position Modulation
PSAM	Pilot Symbol-Assisted Modulation
PTD	PSAM-based Thresholding Detection
RF	Radio Frequency
RV	Random Variable
S-by-S	Symbol-by-Symbol
SC	Selection Combining
SDC	Switch-to-Dominant Combining
SEC	Switch-and-Examine Combining
S.I.	Scintillation Index
SSC	Switch-and-Stay Combining
SIM	Subcarrier Intensity Modulation

SIMO	Single-Input Multiple-Output; a diversity system with only one transmitter but multiple receivers
SISO	Single-Input Single-Output; a diversity system with only one transmitter and one receiver
SNR	Signal to Noise Ratio
TA	Temporal Averaging
T-GSC	Threshold Generalized Selection Combining
VLC	Visible Light Communication
WPAN	Wireless Personal Area Networks